ORNL/HTSPC-20

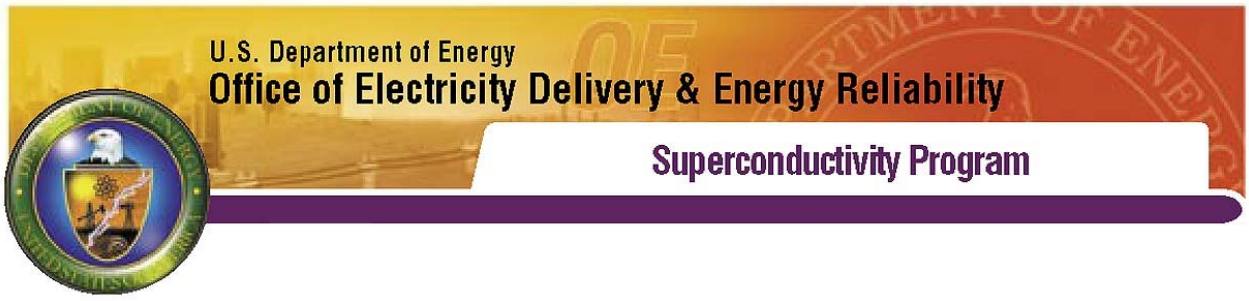

ORNL SUPERCONDUCTING TECHNOLOGY PROGRAM SUPERCONDUCTIVITY FOR ELECTRIC SYSTEMS

ANNUAL REPORT FOR FY 2007

Compiled by
Dominic F. Lee
Audrey W. Murphy

Manuscript completed: January 24, 2008

Prepared for the
Office of Electricity Delivery and Energy Reliability
U.S. DEPARTMENT OF ENERGY
(TD 5001)

Prepared by the
OAK RIDGE NATIONAL LABORATORY
P.O. Box 2008
Oak Ridge, Tennessee 37831
Managed by
UT-Battelle, LLC
for the
U.S. DEPARTMENT OF ENERGY
Under contract DE-AC05-00OR22725

OAK RIDGE NATIONAL LABORATORY
MANAGED BY UT-BATTELLE FOR THE DEPARTMENT OF ENERGY

Table of Contents

Introduction iii
Control Milestones and Status v
Significant Awards, Recognitions and Events vi

Section 1: Wire Development
ORNL – AMSC CRADA to develop RABiTS/MOD based 2G wire 1-1
ORNL – SuperPower CRADA to develop IBAD/MOCVD based 2G wire 1-7
ORNL – MetOx CRADA to characterize All-MOCVD 2G wire 1-12

Section 2: Conductor Research
Textured substrates with improved characteristics 2-1
Solution buffer development for low cost conductors 2-4
HTS processing for critical current and pinning enhancement 2-9
High performance rare-earth HTS 2-16
Substrate simplification to reduce cost 2-20
WDG: Ex situ RBCO coatings with enhanced performance and flux pinning properties 2-23

Section 3: Innovative and Enabling Technologies
HTS filamentization to reduce ac loss 3-1
Conductor design and engineering for practical HTS applications 3-11
Novel tailor-made cryogenic nano-dielectric materials 3-28

Section 4: HTS Applications
HTS Cable System R&D 4-1
Development of high-voltage HTS power transformer 4-13
Baldor Reliance Electric CRADA: HTS Industrial Motor 4-17
Fault current limiter CRADA with SuperPower 4-23
Cryogenic dielectric R&D and design rules 4-27
SPI/SPE Readiness Reviews 4-32

Section 5: Technical R&D and Support
American Superconductor Corp. 2G wire development subcontract 5-1
SuperPower Inc. 2G wire development subcontract. 5-4
NIST-Boulder electromechanical studies for superconductor development subcontract 5-9
NIST-Gaithersburg subcontract to investigate HTS phase relationships 5-12
Other Subcontracts 5-15

Appendix A A-1

Introduction

Twentieth-century power system components were based on traditional conductors–using copper and aluminum wires. The opportunity now exists to modernize and expand the nation's electricity delivery system with equipment using an emerging new capability – practical high-temperature superconductor (HTS) wires that have the potential of 100 times the capacity of conventional wires without energy loss due to electrical resistance. This breakthrough enables a new generation of reliable grid equipment with typically twice the capacity of same-sized conventional unit with only half the energy losses. Commercial versions of superconducting power cables, fault current limiters, transformers, generators, and motors are now under development and are expected to be available after 2012 – in time to accommodate expected load growth as well as to replace existing equipment – most of which will exceed their design lifetimes during the next 15 to 20 years.

Background

For full-scale commercialization of HTS electric power devices, further research and development of HTS wire, cryogenic dielectric materials, and refrigeration systems is needed. In addition, prototype or pre-commercial HTS equipment needs to be demonstrated to obtain its operation, maintenance and service reliability characteristics. This means long lengths of low cost HTS wires that can meet the demanding requirements of power applications need to be developed. While first generation (1G) HTS wire is commercial and technically adequate for prototype demonstrations, its present and projected cost is too expensive and its performance is insufficient for large-scale electric grid applications. The properties and performance of second generation (2G) HTS wire are improving rapidly but are inadequate for most commercial applications. Short samples of 2G wire, prepared under laboratory conditions, do indeed meet or exceed most requirements for commercial applications. For 2G wire to enter the marketplace, production of kilometer piece lengths that have uniform short sample properties along their entire length is needed. To achieve competitive costs, faster manufacturing processes are needed. The Department of Energy has the goal that by 2015, 2G wire will be available that can carry 100 times the amps per square centimeter of copper wire and at a price per kiloamp-meter that is comparable to copper wire.

In addition to HTS wires, research and development in other important areas are also necessary. HTS applications operate at cryogenic temperatures, typically cooled by liquid nitrogen or gaseous helium. Custom refrigeration systems are required. Refrigeration systems are needed that are reliable, highly efficient and affordable. In addition, cryostat vacuum reliability needs to be improved for long HTS cable applications. Also, there is limited industrial experience in selecting dielectrics that are proven to work well under conditions of high voltage and cryogenic temperatures. This is new territory for equipment manufacturers and electric utilities. Available cryogenic dielectric materials are limited and have not yet been fully characterized, especially in high voltage ac applications with acceptable partial discharge.

Technical Approach

To achieve the mission of applying HTS to the national effort to modernize and expand America's electricity delivery system, DOE is engaging in coordinated effort to perform Research, Development and Demonstration (RD&D) on core activities ranging from HTS wire to conductor response to cryogenic dielectrics and systems to equipment development and demonstrations. Specific activities include:

- Conductor Research
  - Development of deposition processes that will improve the mechanical and electrical properties of 2G wire and will reduce processing times and costs.
  - Extension of the ultra-high short-length electrical performance of 2G wire on scaling up to long lengths on the order of a few tens to hundreds of meters.
  - Development of 2G wires that can carry high currents in the presence of strong magnetic fields.
  - Continue support of DOD Title III Program to assure a domestic supply of 2G wires.
- Strategic Research
  - Improvement of the understanding of basic HTS issues that will lead to the tailoring of optimal properties at specified fields and temperatures.
  - Simplification of template architecture and development of new metal templates.
  - Development of innovative conductor designs to increase current carrying capability, reduce AC losses, and improve stability.
- Cryogenic Systems and Dielectrics
  - Research and development of better electrical insulating materials for high-voltage superconducting applications operating at cryogenic temperatures.
  - Development of reliable and efficient cryogenic cooling systems.
  - Development of reliable, affordable cryostats for longer HTS cable applications.
- Component Development and Prototype Testing
  - Continuation of on-going 1G-based prototype demonstration projects, including the three utility HTS cable projects, a large industrial motor, and an oil-free, easily transportable three-phase power transformer.
  - Issuance of solicitation and selection of 2G-based small (non-cable) demonstration devices.

ORNL Tasking

The proposed ORNL tasks contained in this section will draw upon the extensive expertise available at ORNL in HTS materials, dielectrics, cryogenics and applied superconductivity, and will assist DOE in achieving its mission in a coordinated manner. The proposed tasks are categorized into five areas (Agreements):

1) Wire Development 15211
2) Conductor Research 15212
3) Innovative and Enabling Technologies 15217
4) HTS Applications 15218
5) Technical R&D and Support (Sub-Contracts) 15220.

Control Milestones and Status

Control Milestone	Due Date	Status
Section 1: Wire Development.		
• Short sample RABiTS using slot-die MOD CeO_2 cap-layer with I_c of 300 A/cm.	April 30, 2007	Met Feb. 15, 2007
• Operational MOCVD system providing J_c greater than 2 MA/cm^2.	June 30, 2007	Met March 14, 2007
Section 2: Conductor Research.		
• Improve in-field performance flux-pinning factor to less than $\alpha = 0.2$.	May 31, 2007	Met Feb.6, 2007
• Deposit multi-functional epitaxial buffer that can replace at least 2 standard buffers with J_c of 2 MA/cm^2.	July 31, 2007	Met Jan.10, 2007
Section 3: Innovative and Enabling Technologies.		
• Commissioning of enhanced ac loss testing capability.	March 31, 2007	Met March 28 2007
• Obtain nano-dielectic materials with enhanced electrical and physical properties.	July 31, 2007	Met July 25, 2007
Section 4: Applied Superconductivity.		
• Develop overcurrent model for 2G wire (DC).	July 31, 2007	Met July 30, 2007
• Complete 30-in test dewar and carry out HV tests.	July 31, 2007	Met Feb. 23, 2007
Section 5: Research and Technical Support.		
• Short sample 2G wire with I_c of 750 A/cm (SuperPower)	July 31, 2007	Met July 21, 2007
• Complete delamination-strength measurements at 76 K on a total of 30 slit 2G wire samples with new geometries, fabricated by AMSC and SuperPower (NIST-Boulder).	July 31, 2007	Met July 28, 2007

Significant Awards, Recognitions and Events

ORNL HTS Program met all ten CPS Control Milestones, all major AOP Milestones and ORNL PEP Milestone.

In FY2007, ORNL HTS Program has met all ten of its CPS Control Milestones on or ahead of schedule as listed in the CPS Control Milestone table. In addition, the program has met or exceeded its Annual Operation Plan (AOP) goals and milestones as detailed in the technical section of this report. The program has also met its 2007 ORNL PEP Milestone of "Evaluate operation of the Ultera-ORNL triaxial superconducting cable installed at a substation owned by American Electric Power in suburban Columbus, Ohio against design specifications and produce draft report". The cable system experienced a peak current of 2,700 A in a hot summer day in August 2007. The system has also experienced four power-down events as well as a number of fault current events, all without damage to the HTS cable system. The cable is providing power to more than 8,600 AEP customers.

ORNL HTS researchers received awards for "World Class" performance as judged by FY 2006 DOE Annual Peer Reviewers.

Three ORNL HTS projects have received Exceptional or Outstanding Accomplishment Awards from the Office of Electricity Delivery and Energy Reliability. These awards are given to HTS projects that received "World Class" or "Excellent" ranking from the judging panels at the 2006 US DOE Superconductivity Program Annual Peer Review. ORNL projects that received these awards are:


Exceptional Accomplishment
2006 U.S. Department of Energy Superconductivity Program Peer Review
Presented this 5th day of October 2006
To
David Lindsay (Southwire Company), Jonathan Demko (ORNL)
Southwire Company, Oak Ridge National Laboratory
In recognition of their presentation:
"High Temperature Superconducting Power Cable"
This project was found to be exceptionally well-managed and to have achieved outstanding results.
Patricia Hoffman
Acting Deputy Director
Office of Electricity Delivery & Energy Reliability
James Daley
Manager
Superconductivity Program

- High Temperature Superconducting Power Cable (with Southwire Company),
- SPI Readiness Review Program (with LANL and DOE-Golden),
- ORNL-SuperPower CRADA: Development of IBAD-Based 2G Wires (with SuperPower).

In addition, Wire Development Group, of which ORNL is a participant, also received an award.

ORNL HTS projects received top rankings in two of the three FY 2007 Annual Peer Review technical sessions. Project scored second in the third session.

At the FY2007 HTS Annual Peer Review, twelve ORNL HTS talks were presented in three sessions: 1) HTS Applications, 2) 2G wire development and 3) Strategic Research. The three panels of international experts were highly complimentary on the projects, and scored ORNL-partnered projects number one in two sessions:

- High Temperature Superconducting Cable – Columbus AEP Cable (HTS Applications, 91.4/100, with Southwire Company)
- ORNL-SuperPower CRADA: Development of IBAD-Based 2G Wire (2G wire development, 98.4/100, with SuperPower)

and second in the third session:

- Engineered Columnar Defects for Coated Conductors (Strategic Research, 94.2/100)

The Southwire-ORNL HTS cable project is a consistent high achiever. This project has received top ranking 3 years in a row, and scored first in 5 out of the past 6 years. The ORNL-SuperPower CRADA project built on its 2006 ORNL Tech Transfer, 2007 R&D100 and 2007 Southeast FLC Tech Transfer awards momentum, and received top ranking with an unprecedented high score of 98.4 out of 100 points. Also note worthy is 6 of the 12 ORNL projects received "World Class" rankings of 90 points and above. The remaining 3 World Class projects are:

- ORNL-AMSC CRADA: Development of RABiTS-Based 2G Wire (2G wire development, 93.8/100)
- Performance Enhancement and Analysis of HTS Coatings (Strategic Research, 90.4/100)
- Strategic Substrate Development for Coated Conductors (Strategic Research, 90/100).

SuperPower-ORNL HTS technology wins 2007 R&D 100 and 2007 FLC Southeast Region Excellence in Technology Transfer awards,

A technology entitled "High-Performance LMO-Enabled, High Temperature Superconducting Wires" by SuperPower Inc. of Schenectady N.Y. and Oak Ridge National Laboratory (ORNL) is named a winner of the 2007 R&D 100 Award and a 2007 FLC Southeast Region Excellence in Technology Transfer Award. Based on an ORNL patented LMO buffer technology that was wholly funded by OE, this work transitioned the technology from laboratory discovery to commercial manufacturing. By fully integrating the LMO buffer technology and other innovations into its manufacturing process, SuperPower has produced long piece-lengths of second-generation HTS wires with world record long-length performances. These results make the SuperPower 2G HTS wire "one of the 100 most technologically significant products introduced into the market place over the past year." OE provided funding to ORNL (full) and SuperPower (partial) for this work as part of its strategy to accelerate the development of 2G HTS wire through partnerships with industry. In addition to these awards, this project also won the 2006 ORNL Excellence in Technology Transfer Award. The winning team members are Venkat Selvamanickam and X. Xiong of SuperPower, and M. Parans Paranthaman, Tolga Aytug, Amit Goyal and Mark Reeves of ORNL.

ORNL HTS/LDRD project named R&D Magazine's 2007 Micro/Nano 25 Award winner.

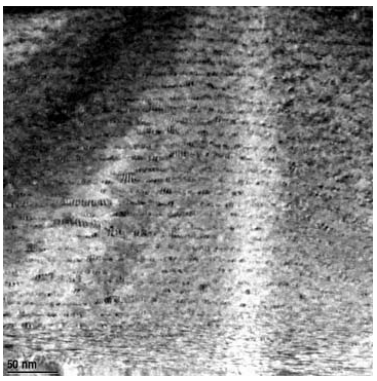

An ORNL project entitled "Nanocomposites via Epitaxial, 3-D Self-Assembly of Nanodots of One Complex Material Within Another" has been named a winner of the 2007 Micro/Nano 25 Award by R&D Magazine. Purpose of the Awards is to recognize top Micro/Nano technologies of the year. Sponsored jointly by OE and ORNL LDRD funds, this work seeks to develop fundamental scientific

understanding of self-assembled nano-heterostructure formation mechanism as well as the technique to fabricate these "designer" nanocomposites. These nano-heterostructures comprise a novel class of materials for wide-ranging applications including very high performance HTS wires. Such materials are expected to exhibit novel physical properties tunable by adjusting the overall composition, concentration, feature size, and spatial ordering of the nanodots. This project is an expansion of an existing work on "HTS Wires Enabled via 3D Self-Assembly of Insulating Nanodots', which won a 2006 Nano50 Award.

ORNL HTS Researcher wins 2007 "Pride of India" Gold Award.

Amit Goyal of ORNL has been honored with the "Pride of India" Gold Award based on his sustained achievements in the science and technology of HTS. Sponsored by the Non-Resident Indians Institute, the award recognizes people of Indian origin around the world for outstanding achievements in their chosen fields. It also recognizes public service contributions toward the economic development of India and their country of residence. Award recipients were chosen from leaders, pioneers and professionals worldwide from the fields of Technology, Medicine, Business Management, Legal, Creative Arts, Public Service, or Academia. In 2007, 24 people were selected for this award. Dr. Goyal received the award from the Deputy Chief of the Indian Mission in the U.S. Ambassador Raminder Singh Jassal, in a ceremony held on Sept. 28, 2007, which was attended by over 400 leaders in business, government, and education from all over the world.

ORNL HTS researcher receives the President's Call to Service Award.

On April 30, 2007, ORNL HTS research staff member Patrick M. Martin received the President's Call to Service Award – the highest level of recognition in the President's Volunteer Service Award Program. His is one of only 15 Call to Service Awards given to the entire DOE national laboratory system and site offices this year. In 2003, President Bush created the President's Council on Service and Civic Participation, which initiated the President's Volunteer Service Award Program as a way to thank and honor Americans who, by their demonstrated commitment and example, inspire others to engage in volunteer service. This particular award level recognizes individuals, families, and groups that have volunteered 4,000+ hours of services over the course of their lifetime. Over the past 15 years, Mr. Martin had been working with and mentoring one or more students and teachers in the science and technology of HTS during the summers. In addition, Mr. Martin had participated in numerous laboratory-sponsored outreach activities to promote HTS technology and the pursuit of an education in the sciences. Beside these professional activities, Mr. Martin was an ORNL division representative to the Knoxville Area Rescue Ministries, the provider of musical accompaniment at his church, an instructor in the East Tennessee Whitewater Club, a co-organizer of the Paddle/Discovery Festival**,** and participated in many other community activities. Mr. Martin was also a full-time foster parent of three young children.

HTS program members are recipients of UT-Battelle/ORNL Awards Night recognition.

Parans Paranthaman, Amit Goyal, and Tolga Aytug were acknowledged at the 2006 Awards Night ceremony as recipients of the Science and Technology award for "Excellence in Technology Transfer." The award recognized their contributions for the development, patenting, and transfer of high throughput buffer layer technology being commercialized by SuperPower, Inc., that enabled the achievement of world record performance in SuperPower's long-length, second generation superconducting wires.

Alvin R. Ellis, Isidor Sauers, Mark Roden, Jonathan A. Demko, Robert Duckworth, Christopher M. Rey, D. Randy James, and Michael J. Gouge, along with three employees of Southwire Company, were honored for accomplishments in "Engineering Research and Development." The team was acknowledged for its achievements in the invention, development, design, fabrication and successful testing of the world's most compact superconducting power cable.

ORNL HTS poster wins award.

An ORNL HTS outreach poster entitled "Superconducting Wires and Applications" has been named a winner of the 2007 American Inhouse Design Awards. Given by the editors of Graphic Design USA, the awards recognize graphic designs for their creativity as well as effectiveness in conveying the messages. The poster will be reproduced in a special 2007 issue of Awards Design Annual by Graphic Design USA.

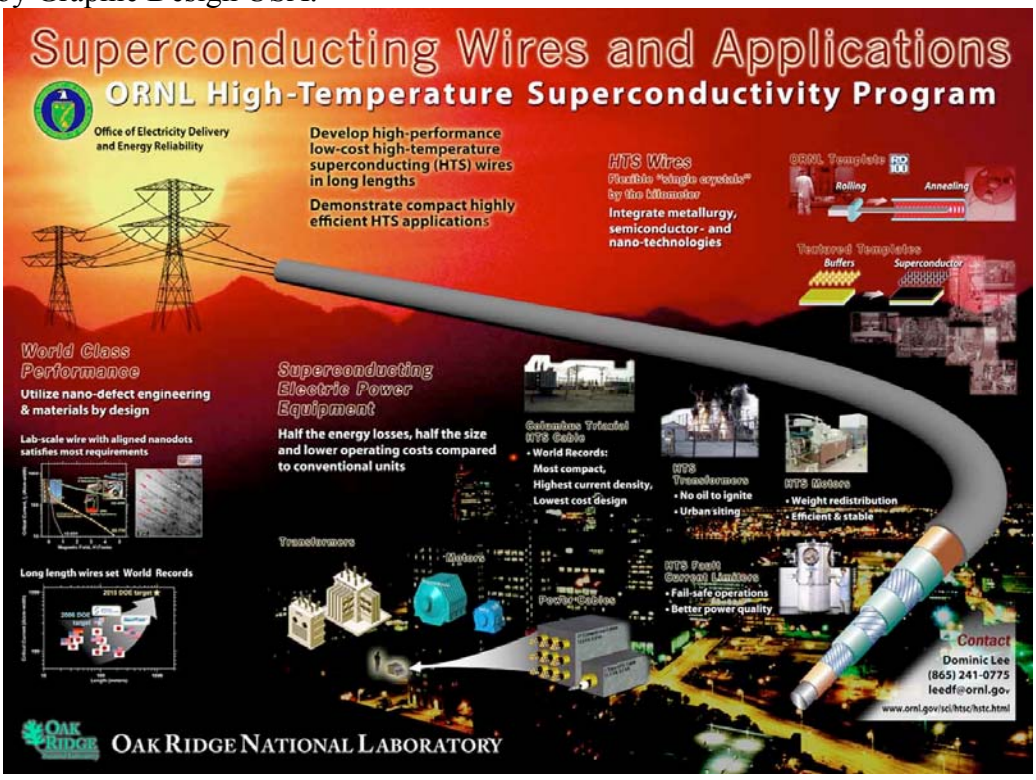

ORNL HTS researcher is elected Fellow of the American Ceramic Society.

Amit Goyal, ORNL Distinguished Scientist and Battelle Distinguished Inventor, has been elected Fellow of the American Ceramic Society. This recognition is based on Goyal's achievements in High Temperature Superconductivity (HTS) R&D, which is wholly sponsored by the DOE Office of Electricity Delivery and Energy Reliability. Goyal is also a Fellow of the American Society of Metals. the American Association for Advancement of Science, the Institute of Physics (UK) and the World Innovation Foundation (UK). His work on developing the science and technology for long-length high-performance low-cost uniform HTS wire has received other recognitions including a R&D 100 award, a Nano50 Award and an Energy 100 Award. Goyal will be formally recognized during the American Ceramic Society's 109th annual meeting at Detroit in mid-September.

ORNL HTS researcher promoted to a Distinguished Scientist.

Parans Paranthaman of the ORNL Chemical Sciences Division (CSD) has been promoted to a Distinguished Scientist level. He is also the acting group leader for the Materials Chemistry Group at CSD. The combination of a strong record of scientific accomplishment and recognition in HTS, a strong work ethic, excellent teamwork, and a strong desire to be successful has made Parans a leader at ORNL.

ORNL HTS scientist invited to join editorial boards.

Amit Goyal of the Materials Science and Technology Division (MSTD) has been invited to join the *NanoTech Briefs* Editorial Advisory Board. *NanoTech Briefs* reports on government, industry, and university nanotech innovations with real-world applications in areas such as electronics, materials, sensors, manufacturing, biomedical, optics/photonics, and aerospace/ defense. Each issue of *Nanotech Briefs* also includes a Special Report on an industry or topic of timely importance to the nanotech field, an In Person interview with a recognized leader in the nanotechnology field, a Perspective from a nano business executive, and a look inside a state-of-the-art nano research facility.

In addition, Dr. Goyal has been invited to join the Editorial Board of an upcoming, new Journal "Recent Patents on Materials Science". This journal will publish review articles written by experts in materials science summarizing recent patents on novel materials/inventions/ methods/techniques in material science, and will debut in January 2008. The journal will be

published by Bentham Science Publishers, a leading international publisher of high quality scientific journals and books. Bentham currently publishes 79 titles in 24 disciplines of science.

ORNL HTS researcher elected to the Board of Conference on Electrical Insulation and Dielectric Phenomena.

IEEE-CEIDP 2007

Enis Tuncer of the ORNL Fusion Energy Division was elected to the Conference on Electrical Insulation and Dielectric Phenomena (CEIDP) Board during the Oct. 15-18, 2006 meeting in Kansas City. Tuncer is also serving on the Nominations committee of the CEIDP. Meanwhile, Isidor Sauers, also in the Fusion Energy Division, has completed the first year of a two year term as the general chair of CEIDP. Both of them are performing research on high voltage dielectric materials. During the meeting, ORNL researchers presented four papers that covered work related to the HTS cable project and the cryogenic dielectrics initiative.

These papers were published in the 2006 Annual Report Conference on Electrical Insulation and Dielectric Phenomena, IEEE Conf. Pub. No. 06CH37829:

1. *Breakdown Statistics of Polyimide at Low Temperatures*, E. Tuncer, I. Sauers, D. R. James and A. R. Ellis and M. O. Pace.
2. *Electrical Properties of a Commercial Resin*, E. Tuncer, I. Sauers, D. R. James and A. R. Ellis.
3. *Non-Uniform Field Breakdown and Surface Flashover in Liquid Nitrogen Gaps for HTS Application*, D. R. James, I. Sauers, E. Tuncer, A. R. Ellis, K. Tekletsadik and D. W. Hazelton.
4. *Partial Discharge Measurements in a High Temperature Superconducting Tri-axial 5-m Model Cable at Liquid Nitrogen Temperature*, I. Sauers, D. R. James, E. Tuncer, A. R. Ellis.

ORNL HTS research articles featured in the 2006 *Superconductor Science and Technology* special highlights collection.

Two Oak Ridge National Laboratory (ORNL) articles, "A perspective on conducting oxide buffers for Cu-based YBCO-coated conductors" by K-H Kim et al. and "Strong flux-pinning in epitaxial $NdBa_2Cu_3O_{7-\delta}$ films with columnar defects comprised of self-assembled nanodots of $BaZrO_3$" by S-H Wee et al., are featured in the 2006 Special Collection by the journal *Superconductor Science and Technology* (SUST). Comprising 32 papers, articles in the Collection were selected for their "presentation of outstanding new research, as valuable reviews of the field, and for receiving the highest praise from the SUST international referees" In addition, the article by Kim et al. and also "'Irradiation-free, columnar defects comprised of self-assembled nanodots and nanorods resulting in strongly enhanced flux-pinning in $YBa_2Cu_3O_{7-x}$ films" by A. Goyal et

al. published in 2005 are among the most highly downloaded articles in the entire SUST journal during 2006. This is the second consecutive year that ORNL HTS research wholly funded by OE has received this distinction. These achievements reflect the high caliber and cutting-edge nature of HTS research at ORNL.
SUST 2006 Collection: http://herald.iop.org/susthighlights/m90/rsm/133375/link/562

Book on HTS co-edited by ORNL scientist slated for publication.

ORNL HTS researcher M.P. Paranthaman has co-edited a new book on HTS with V. Selvamanickam of SuperPower Inc. Entitled "Flux Pinning and AC loss Studies on YBCO Coated Conductors", the book is scheduled to be published by Nova Science Publishers Inc in 2007. Written by leading international HTS researchers including M.P. Paranthaman, R.C. Duckworth, A. Goyal, S. Kang, J. Li, T. Aytug and D.K. Christen from ORNL, this book addresses the issues related to flux pinning, AC losses and thick YBCO film growth. It presents a comprehensive review of the status, issues and fundamental materials science studies necessary for the continuing improvement of YBCO coated conductors.
https://www.novapublishers.com/catalog/product_info.php?products_id=5675

Prominent participation of ORNL HTS staff in the Materials Science and Technology 2006 Conference and Exhibition.

The Materials Science and Technology 2006 Conference and Exhibition, held October 15 -19 in Cincinnati, OH, jointly represented the American Ceramic Society, the Association for Iron and Steel Technology, ASM International, and The Minerals, Metals and Materials Society. The meeting serves as a comprehensive forum for materials science and engineering technologies. ORNL HTS researchers participated prominently in both the organization of symposia, and as invited and contributed speakers. Those involved and their activities included:

Program Organizers:

- M.P. Paranthaman and A. Goyal: *High Temperature Superconductor Wires & Tapes.*
- A. Goyal: *Microstructural and Textural Requirements for Functional Materials.*
- T. Aytug and S. Sathyamurthy: *Nanostructured Materials: Synthesis, Characterization and Applications.*

Presenters:

R. Feenstra, A. Goyal, T. Aytug, S. Sathyamurthy, M.S. Bhuiyan, S.H. Wee and M. P Paranthaman.

A. Goyal was also presented an award for the ASM-IIM Distinguished Lectureship at a Special Awards Luncheon hosted by the ASM for the ASM leadership.

ORNL researchers participated in the 19th International Symposium on Superconductivity.

Amit Goyal and Robert Duckworth presented invited talks at the ISS 2006 meeting held in Nagoya, Japan from October 30 – November 1, 2006. 693 papers, both oral and poster presentations were presented in five broad technical areas. There were 534 papers from Japan and 159 papers from foreign participants. Goyal presented an invited overview talk on flux-pinning with 3D self-assembled nanodots and co-chaired the opening session on Wires, Tapes and Characterization. Duckworth presented an invited talk on "Low ac loss geometries in YBCO coated conductors". Both talks were very well received.

HTS program members participated in DOE Wire Development and Applications Workshop.

Staff members contributed prominently, both as organizers and presenters, at the workshop held January 16-17 in Panama City, Florida, This annual workshop is sponsored by the Office of Electricity Delivery and Energy Reliability's Superconductivity Program for Electric Power Systems. The workshop, attended by about 75 participants, served as a forum to discuss the current status of the second-generation wires, electric power prototype demonstrations and possible second generation conductor engineering designs that could meet power application requirements. ORNL staff members David Christen, Michael Gouge, and Parans Paranthaman, along with five other DOE laboratory and industry representatives, served to organize the meeting and co-chair sessions. ORNL technical presentations were made by Michael Gouge, Amit Goyal, Dominic Lee, Parans Paranthaman, and Enis Tuncer.The meeting agenda and technical presentations can be accessed at http://www.energetics.com/wire07/agenda.html.

ORNL a partner in two winning "Superconducting Power Equipment" projects.

In a June 27, 2007 DOE announcement, two HTS projects with ORNL as partner were named winners in the Superconducting Power Equipment solicitation. These research demonstration projects will advance the development and application of HTS, which have the potential to alleviate congestion on an electricity grid that is experiencing increased demand from consumers. "Modernizing our congested and constrained electric grid - through the development of advanced, new technologies – is vital to delivering reliable and affordable power to the American people," Secretary Bodman said. "As demand for electricity continues to grow, we must take steps now to identify potential problems, identify solutions, and deploy new technologies to provide a secure and steady energy supply…:"

ORNL will be involved in two of the five winning projects. The two projects are:

1) *Southwire Company HTS Cable Project:* Southwire Company (Carrollton, GA) will use a 13.8-kilovolt HTS cable to connect two existing substation sites and solve a real-world electrical load problem near downtown New Orleans. The substations are owned by Entergy Corporation of New Orleans, LA, a member of Southwire's project team. The team also includes: DOE's Oak Ridge National Laboratory and nkt cables of Germany.
2) *SuperPower Inc. HTS Fault Current Limiter Project:* SuperPower Inc. (Schenectady, NY) will design, test, and demonstrate on the American Electric Power grid a 138-kilovolt HTS fault current limiter. The team also includes: Sumitomo Electric Industries

Ltd. (Osaka, Japan); Nissan Electric Co. Ltd. (Kyoto, Japan); The BOC Group Inc. (Murray Hill, NJ); American Electric Power (Gahanna, OH); and DOE's Oak Ridge National Laboratory.

ORNL HTS Program is partner in 3 SBIR/STTR Phase I awards.

ORNL HTS staff members are involved in 3 of the 5 SBIR/STTR Phase I awards announced on April 27, 2007. These projects are:

1) American Superconductor Corporation:
   Low AC Loss YBCO Coated Conductor Geometry by Direct Inkjet Printing.
2) Composite Technology Development:
   Nanocomposite Insulation for 2G Superconducting Wires.
3) Directed Vapor Technologies:
   High Rate Deposition of Epitaxial Films for Use in Superconducting Coated Conductors.

Of particular interest is the new collaboration with Composite Technology Development Inc. (CTD) of Colorado. CTD is a small business that has been involved in cryogenic dielectrics development for the high energy physics community, as well as in innovative nano-composite dielectric materials.

ORNL HTS staff participated in "Day of Science" outreach activities at ORNL that attracted 250 university students and faculty.

More than 250 students and faculty from 45 colleges and universities across the nation, including many historically black colleges and universities and minority education institutions, gathered at ORNL on Oct. 16, 2006 for the Fifth Annual Day of Science and DOE-sponsored Minority Education Technical Assistance Workshop. , Their slate included talks and presentations, one of which was HTS, and a series of pre-interviews for possible internships. Charles Greene, executive director of the White House Initiative on HBCUs and luncheon keynote speaker, discussed the importance of nurturing relationships between students, faculty and administrators at the nation's HBCUs. Greene stressed that educators and administrators must be supportive of students who wish to pursue an education in math or science, and noted that support from institutions such as ORNL is extremely helpful.

Day of Science visitors watched a demonstration of superconducting technology by the Materials S&T Division's Patrick Martin.

Patricia Hoffman, DOE-OE, visited ORNL HTS Program.

Patricia Hoffman, DOE-OE Director of R&D, visited ORNL on Oct. 26-27, 2006. As part of the OE Program, Hoffman was briefed on the FY 2006 accomplishments, capabilities and planned activities of the ORNL HTS Program. She also toured the ORNL Rolling Facility, Materials Processing Facility, Accelerated Coated Conductor Lab, Cryogenic Dielectric High Voltage Test Lab, Applied Superconductivity Lab and the Cable Test Facility. Among the many capabilities seen by Hoffman was the 3-m long, tri-axial cable with a splice in the center being set up for testing at 77 K in the ORNL HTS Cable Test Facility. The cable splice was initially tested for fault over-currents at an Ultera lab in Denmark. DC current tests at ORNL will verify that the cable was not damaged by earlier qualification testing.

Pat Hoffman and Mike Gouge look over an HTS tri-axial cable.

ORNL HTS Program hosted the Wire Development Group meeting on Sept. 26 and 27, 2007.

The Wire Development Group (WDG) meeting, which is rotated among its member sites, serves as a forum for in-depth discussion and planning of the studies of fundamental scientific issues and applied HTS materials research. Held at ORNL on Sept. 26-27, 2007, this meeting was attended by WDG members from AMSC, ANL, Florida State University, LANL, ORNL and University of Houston.

Section 1: Wire Development

Focuses on materials processing and manufacturing issues that directly impact the cost, performance, application characteristics and scale-up of commercial 2G wires.

Subtask 1.1: ORNL – American Superconductor CRADA to develop RABiTS/MOD based 2G wire.

A. Goyal, F.A. List, M.P. Paranthaman, P.M. Martin, S. Sathyamurthy, S. Cook

Objectives:

This subtask is focused on the development of the $REBa_2Cu_3O_x$ (REBCO) RABiTS-based coated conductor technology that is in the pre-commercial development stage and requires further studies. The goal of the project is to establish a low-cost, high-performance, high throughput, high yield manufacturing process for the commercial manufacturing of RABiTS-based 2G wire. To achieve this, various tasks are focused on the improved understanding of the material science related to fabrication of RABiTS templates, metal organic deposition (MOD)-based REBCO layers, and detailed characterization and correlation of 2G wire properties with the process stability. The subtask is closely coupled to AMSC's 2G scale-up program and assists AMSC in developing and implementing a robust manufacturing process.

Highlights:

1) HTS Program CPS Control Milestone Met - Short sample RABiTS using slot-die MOD CeO_2 cap-layer with I_c of 300 A/cm.

A slot-die MOD CeO_2 cap layer in a RABiTS architecture (MOD-CeO_2/sputtered-YSZ/ sputtered-Y_2O_3/Ni5%W) supported high critical current, in a 0.8 μm YBCO film, resulting in an I_c/width of over 350 A/cm-width (77K, self-field). All layers in this stack were deposited by AMSC. The challenge is to reproducibly grow MOD CeO_2 cap layer that can support high performance YBCO films. ORNL-AMSC CRADA is focused on establishing the optimum processing temperatures and gas environments for the formation of the CeO_2 films. The best CeO_2 MOD precursor will be selected for scale-up based on the processing temperature, texture, surface morphology and film density.

2) Completed technical design to increase the coverage area of ORNL slot-die coater.

ORNL is in the process of modifying its slot-die coater such that alternative 2G wire prototypes can be readily completed by AMSC's pre-pilot processing facilities for rapid testing. Previously, we have prepared 1 cm-wide samples with LZO solution buffer coated at a slot-die speed of 120 m/hr (Fig. 1). Subsequent cap layer and YBCO were completed at AMSC, with J_c's in excess of 3 MA/cm^2. These AMSC steps, however, require additional adjustments because of the substantial difference in sample-handling widths. With modification of our clot-die coater, completion of 2G wire

Fig. 1. ORNL reel-to-reel slot die coater for solution deposition.

prototypes and testing will occur more rapidly and readily. Technical design of the modification has been completed, with physical slot-die modification to follow.

3) Meters-long textured solution LZO buffer deposited on 4-cm wide templates by slot-die coater.
Several meters of 4-cm wide, slot-die coated LZO and subsequently annealed tape was fabricated (Fig. 2). The LZO was coated on a Y_2O_3 buffered Ni-5at%W substrate from AMSC. The texture of the fully converted tape was measured continuously via X-ray line-scans, and was found to track the substrate texture at all points on the tape (Fig. 3). Most significant is the reduction in annealing time; annealing residence time has been decreased from 15 minutes in FY2006 to 34 seconds in FY2007. This is an order of magnitude faster than the throughput necessary for 1,000 km/year production volume (target of Title III), and provides a realistic pathway for wire cost reduction.

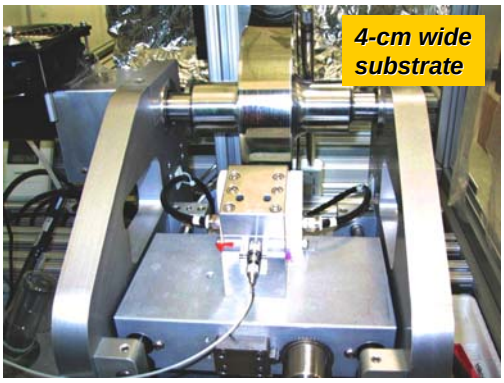

Fig. 2. Reel-to-reel slot-die coater for deposition of solution buffers on 4 cm-wide textured template.

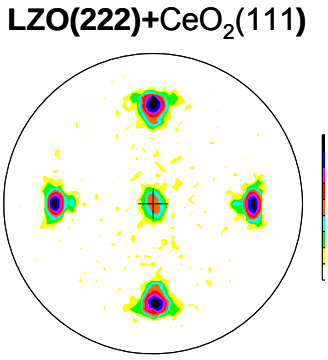

Fig. 3. (111) pole figure of LZO + CeO_2 buffers exhibiting ~99% cube texture.

4) Texture improvement in Y_2O_3 seed layers on NiW substrates understood. New understanding used to fabricate substrates with sharpest texture and with highest self-field I_c to date.
Typically some texture improvement is observed in Y_2O_3 deposited on NiW substrates by reactive sputtering at AMSC. This texture improvement is critical to obtain the high performance YBCO films that AMSC has been fabricating. However, until now this texture improvement was not understood. Moreover, in the recent past, AMSC was finding that the sharpness of texture in this layer was varying even though the texture of the NiW was constant. Solving this problem was deemed critical to scale-up activities at AMSC. , Based on recent understanding, significant progress has been made in fabrication of films with improved textures. Transport characterization of 0.8 μm MOD YBCO film gave the highest J_c obtained by AMSC so far – a J_c of 4.8-5 MA/cm^2 at 77K, self-field or an I_c corresponding to 380-400

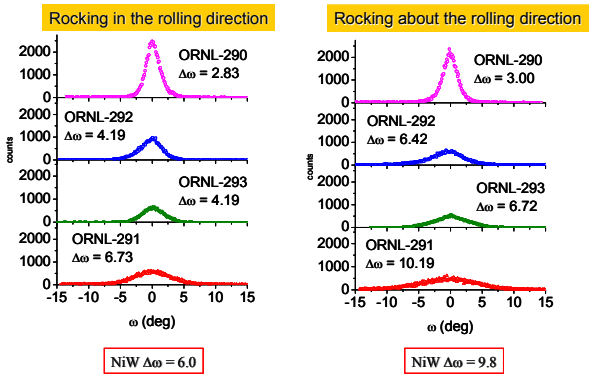

Fig. 4. Out-of-plane textures for rocking the sample in or about the rolling direction for four Y_2O_3 films grown epitaxially on NiW substrates of constant texture. Clearly a big variation in the textures of the films can be observed.

A/cm at 77K, self-field!

A series of films with different textural sharpness of Y_2O_3 layers on NiW were examined at ORNL by X-ray diffraction and TEM. Figure 4 shows that the out-of-plane textures of 4 films made under different deposition conditions. Clearly a significant difference in the full-width-half-maximum (FWHM) of the out-of-plane texture of epitaxial Y_2O_3 layers is seen on NiW of the same texture. The difference in the FWHM can vary by as much as 7 degrees! Figure 5 shows the FWHM of the out-of-plane texture plotted as a function of the tetragonal distortion. The tetragonal distortion is defined as = c/a – 1. The figure shows that the film with the broadest FWHM of the out-of-plane texture is in tension as it has a negative tetragonal distortion. The other three films are all in compression and the film with the sharpest texture is the most in compression. Prior work on epitaxial CeO_2 layers at ORNL has shown that variation of oxygen stoichiometry in the films puts the films in tension. The variation in the sharpness of texture in the epitaxial Y_2O_3 films on NiW was also attributed to variation in the oxygen stoichiometry. This information was provided back to AMSC and they devised a method to better control the oxygen stoichiometry during the deposition of Y_2O_3 films and constantly obtain sharp textures in the Y_2O_3 film.

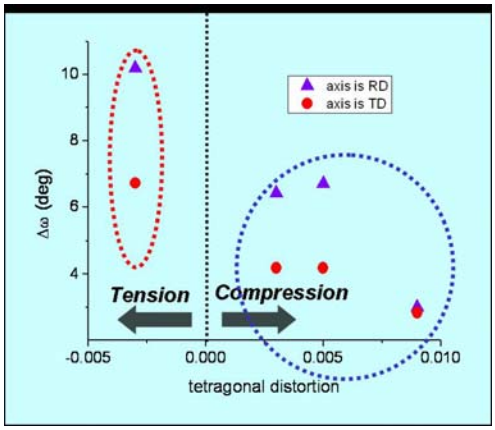

Fig.5. Out-of-plane textures as a function of the tetragonal distortion for four Y_2O_3 films grown epitaxially on NiW substrates of constant texture. The film with the broadest texture is in compression and the film with the sharpest texture has the most compressive stress.

YBCO (0.8 μm)	Δω=2.6°,2.5; Δϕ=5.1°
CeO_2 (75 nm)	Δω=2.5°,2.6°; Δϕ=5.3°
YSZ (75 nm)	Δω=2.6°,2.7°; Δϕ=5.3°
Y_2O_3 (75 nm)	Δω=2.8°,2.9°; Δϕ=4.9°
NiW 75 μm	Δω=5.6°,5.2°; Δϕ=6.6°

Fig.6. In-plane (Δω) and out-of-plane (Δϕ) textures through the stack. The very sharp texture in the Y_2O_3 seed layer is transmitted to the YBCO layer. The texture in the YBCO layer is the sharpest out-of-plane and in-plane texture obtained to date.

In keeping this summary short, details about the mechanisms of texture improvement are not being included here. However, based on theoretical analysis and cross-section TEM analysis, a large lattice mismatch between NiW and Y_2O_3 as well as incoherent growth of Y_2O_3 on NiW contributes to the sharpening with a tendency for the c-axis of the Y_2O_3 to shift towards the surface normal of the NiW substrate for films which have adequate oxygen content. Finally, based on this understanding, significant progress has been made in fabrication of films with improved textures. Y_2O_3 films with the sharpest texture to date were fabricated under appropriate conditions. Fig. 6 shows the texture of various layers in a stack of NiW/ Y_2O_3/YSZ/CeO_2/YBCO. Transport characterization of this 0.8 μm thick MOD YBCO film gave the highest J_c obtained by AMSC so far – a J_c of 4.8-5 MA/cm^2 at 77K, self-field or an I_c corresponding to 380-400 A/cm at 77K, self-field!

5) Cause of I_c non-uniformity along the width in 4-cm wide, production tapes at AMSC identified

AMSC was finding that at times some I_c non-uniformity along the width of 4-cm long tapes was observed. These tapes were sent to ORNL for evaluation, analysis and problem solving. The cause of I_c non-uniformity was traced to buffer deposition issue that originated from tilted tape.

Figure 7 shows the observed I_c non-uniformity for 4 –tapes cut along the width for a length of 25 meters. The I_c appears to be decreasing from one side of the tape width to the other with significantly lower I_c in one half of the tape along the width direction. In order to examine what was going on, it was decided that examination of the texture was important. However, in order to measure the texture along the width and length of these 4-cm wide tapes, X-ray characterization equipment at ORNL had to be modified from the 1-cm wide tape configuration to the 4-cm wide tape configuration. Also, a mechanism to translate the tape in the width direction had to be incorporated. Figure 8 shows a picture of the modified reels for the X-ray diffractometer which were put in to characterize the tape.

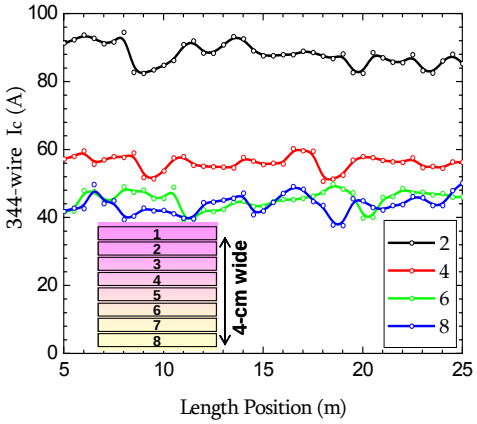

Fig. 7. I_c of 344 wires along the width of a 4-cm wide tape.

Figure 9 shows some line-scans taken using X-ray diffraction. The area of the tape along the width where the I_c was low, had a high intensity of CeO_2 (111) signal indicating incorrect texture. The curves corresponding to A and B in the figure show very high CeO_2 (111) counts. Such a region is expected to have low-I_c. Figure 10 shows that the regions with high counts of CeO_2 (111) also had peak of the YSZ (200) to lower 2theta values.

Careful examination of the data suggests that this can occur due to incomplete oxidation of the oxide layers during deposition. The variation along the width was ascribed to tilting of the tape during motion through the deposition system. Figure 11 shows this schematically. Once the fundamental problem was understood the fix was quite simple – to merely prevent tilting of the tape during motion of the tape in the deposition system.

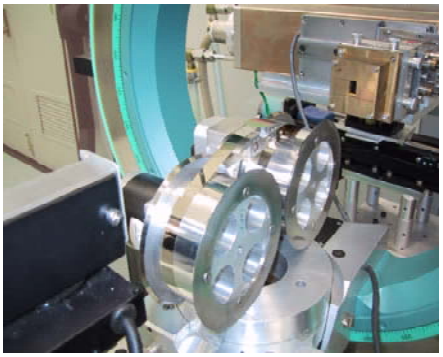

Fig.8. Modified reel-assembly in 4-circle, X-ray diffractometer.

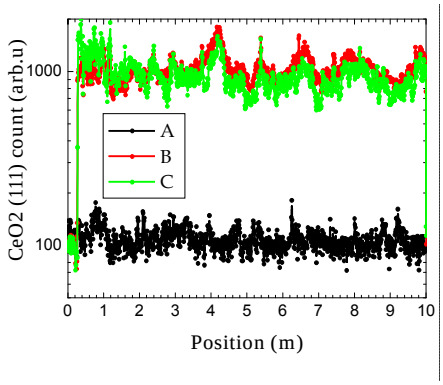

Fig.9. CeO_2 (111) signal as a function of the width and scanned along the length of the tapes. Tapes from location A and B show high CeO_2 (111) counts, which correspond to locations 2 & 6 in Fig. 1 and have low-I_c's.

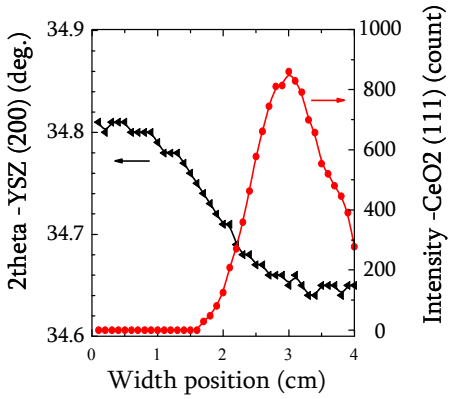

Fig.10. CeO_2 (111) signal counts and YSZ (200), 2theta as a function of the width of the tapes. Clearly a correlation of 2theta shifting to lower values results in high counts for CeO_2 (111).

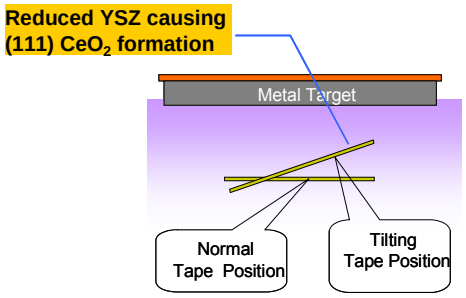

Fig.11. Schematic of sample tilting during deposition..

Technical progress:

1) Scale-up and wire performance.

ORNL continues to work closely with AMSC on scale-up and performance issues related to the development of RABiTS-based 2G HTS wire. Numerous samples have been examined for their texture characteristics. In addition, extensive testing of critical current characteristics of AMSC wires have been performed under self-field and in the presence of applied magnetic fields. Steady progress is also being made in the area of substrate improvement.

2) Processing-properties-microstructure relationship.

Work is ongoing in the CRADA to optimize the pinning characteristics of 4-cm wide YBCO conductors made by AMSC. Transport properties at 77K and 65K are being correlated with microstructural characteristics revealed by TEM as well as structural information obtained by X-ray diffraction. All of this information is then related to processing conditions in an effort to arrive at the optimal conditions for fabrication of long lengths of high performance conductors at AMSC.

3) Template development.

Work is also ongoing in the CRADA to fabricate stronger substrates with reduced magnetism. Significant progress continues to be made especially with composite substrates wherein the substrate comprises of either 2 or 3 layers of different compositions.

Status of milestones:

- Short sample RABiTS using slot-die MOD CeO_2 cap-layer with I_c of 300 A/cm. (April 30, 2007): **Met Feb 2007.**
- Fabricate MOD LZO barrier buffer with homogeneous texture and a mosaic less than 2 degrees using a slot-die coating system on 4-cm wide RABiTS. (July 31, 2007): **Met July 2007.**

- Demonstrate an I_c greater than 800 A/cm on 4-cm wide continuously processed RABiTS with a solution LZO buffer. (August 31, 2007): **Met July 2007.**

Interactions:

Interactions with AMSC included regular progress and planning teleconferences, as well as numerous and frequent sample exchanges with follow-up discussions on results. A onsite CRADA meeting was held at AMSC in March 2007. In attendance at the meeting were A. Goyal, M. Paranthaman and D. F. Lee. Technical progress made was discussed and planning for future work was done

Subtask 1.2: ORNL – SuperPower CRADA to develop IBAD/MOCVD based 2G wire.
M.P. Paranthaman, T. Aytug, R.C. Duckworth, A. Goyal, P.M. Martin, D.K. Christen

Objectives:
A critical need that was identified in the DOE Coated Conductor Roadmap is the development of a high throughput and economic deposition process for REBCO. SuperPower has demonstrated that REBCO films can be deposited by metal-organic chemical vapor deposition (MOCVD) at relatively high throughputs with world record performance. In addition to high critical current density with increased film thickness, flux pinning properties of REBCO films needs to be improved to meet the requirements for various commercial electric-power equipments. Various tasks in this project are focused on an improved understanding of the material science related to the fabrication of IBAD-MgO template, MOCVD deposition of REBCO films, and the detailed characterization and correlation of the 2G wire properties with the process stability. Another focus of this project is to investigate HTS conductor design optimization with emphasis on stability and protection issues, and ac loss measurements for SuperPower REBCO coated conductors.

Highlights:
1) ORNL established MOCVD HTS deposition capability.
With continuing development of the MOCVD REBCO process, SuperPower has produced long-length 2G wires with world record performance of length x critical current. Recently as part of the CRADA, we at ORNL have established a MOCVD HTS deposition capability by using SuperPower's MOCVD lab-scale R&D system. This reverse technology transfer of system hardware and know-how is highly unusual, and reflects the close collaboration and trust developed in the course of this CRADA. Purpose of this new task is to assist SuperPower in accelerating the performance enhancement of their 2G wire. High J_c YBCO films were successfully deposited on IBAD-MgO/LMO templates provided by SuperPower. Initial trials resulted in a short sample with high critical current of 72 A, which validated the SuperPower MOCVD approach (Fig. 1).

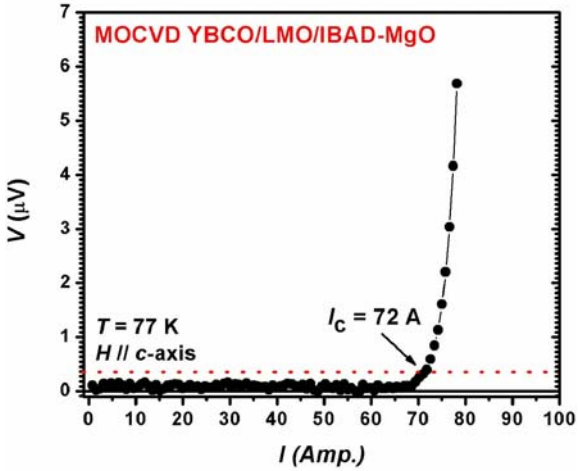

Fig. 1. I-V curve of a MOCVD YBCO film deposited on SuperPower's IBAD-MgO/LMO template.

2) HTS Program CPS Control Milestone Met - Operational MOCVD system providing J_c greater than 2 MA/cm^2.
One of the important critical needs that came out of the DOE's coated conductor workshop was to develop a high throughput and economic deposition process for YBCO. SuperPower has demonstrated that high critical current (Y,Sm)BCO films can be deposited by Metalorganic Chemical Vapor Deposition (MOCVD) at rates of 45 meters/h (135 meters/h effective speed for

4mm-wide tapes) with world record performance. In addition to enhancing high critical current density with increased film thickness, flux pinning properties needs to be improved to meet the DOE requirements for various electric-power applications. ORNL is tasked to assist SuperPower in improving thick film I_c and flux pinning using SuperPower's research MOCVD reactor, now located at ORNL. In March 2007, we have demonstrated the growth of YBCO films carrying a critical current, I_c of 216 Amps at 77 K. This translates to a critical current density, J_c of 2.25 MA/cm^2 for a film thickness of 0.8 µm. The current-voltage (I-V) curve for the same film is shown in Figure 2. Work is underway for in-field J_c enhancement through composition adjustments and doping.

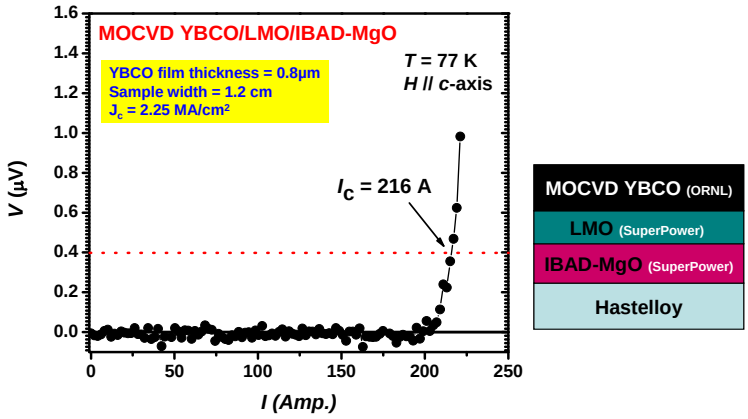

Fig. 2. I-V curve of a 0.8 micron MOCVD YBCO film with an I_c of 216 A (2.25 MA/cm^2).

3) Systematic studies of ORNL's MOCVD process conditions conducted to explore YBCO formation

One of the important critical needs for 2G wire is to develop a high throughput and economic deposition process for YBCO. SuperPower has demonstrated that high critical current (Y,Sm)BCO films can be deposited by MOCVD at rates of 45 meters/h (135 meters/h effective speed for 4mm-wide tapes) with world record performance. In addition to enhancing high critical current density with increased film thickness, flux pinning properties needs to be improved to meet the DOE requirements for various electric-power applications. ORNL is tasked to assist SuperPower in improving thick film I_c and flux pinning using SuperPower's research MOCVD reactor, now located at ORNL.

We are carrying out systematic studies of the growth of YBCO films by

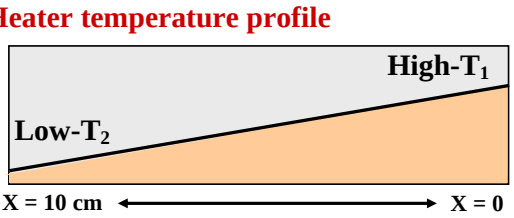

Fig. 3. Heater temperature profile of ORNL's MOCVD system

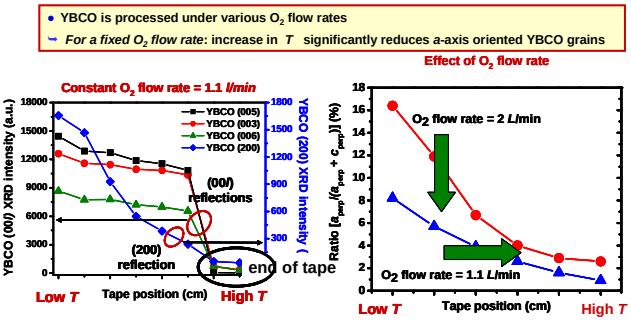

Fig. 4. XRD data of YBCO films processed at different temperatures and oxygen flow rates

optimizing deposition temperature and oxygen flow rate. In order for this study to be transparent to SuperPower operation we have kept our deposition rates similar to the scaled up version of SuperPower process rates. SuperPower's state of the art LMO/IBAD-MgO tapes were used for this study. We also initiated a new collaboration with Argonne National Laboratory (through Vic Maroni) for Raman microprobe analysis. Heater temperature profile is given in Fig. 3. YBCO growth characteristics are affected by both temperature and oxygen flow rate (number of moles of oxygen per unit time). For instance, x-ray diffraction (XRD) data along the tape length for various samples are shown in Fig. 4. Notice that the amount of unwanted *a*-axis grains are reduced by increasing the processing temperature as well as decreasing the oxygen flow rate. Following the XRD work at ORNL, tapes were sent to ANL for Raman microprobe analysis. The comparison of Raman spectra for two YBCO tapes processed at different oxygen flow rates are shown in Fig. 5. The sample processed at a higher oxygen flow rate shows more cation/oxygen disorder and more pronounced secondary phases compared to the lower oxygen flow rate processed sample. Raman analysis gives further information as to growth characteristics of the MOCVD films and well corroborates with the XRD observations. Similar work will be extended to RE modified YBCO compositions.

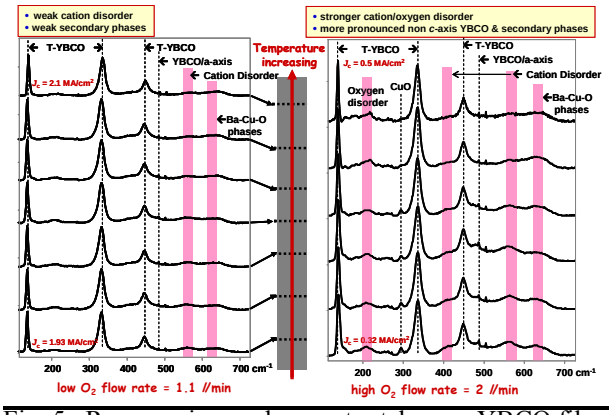

Fig. 5. Raman microprobe spectra taken on YBCO films processed at different temperatures and oxygen flow rates (Data provided by Vic Maroni, ANL)

4) Significant progress demonstrated in 2G wire and substrate using the enabling LMO technology.

ORNL-developed, LMO buffer technology is now fully integrated into SuperPower's Pilot 2G wire manufacturing operation. This enabled SuperPower to deliver nearly 10,000 m of 2G wire for the Albany Cable project. Optimization of LMO process has led to much higher throughput. This enabled SuperPower to produce world-record 2G substrates with piece length of 1,350 meters; breaking the 1 kilometer substrate threshold for the first time. In recognition of the importance of the ORNL LMO technology, an R&D100 award was won jointly by SuperPower and ORNL in 2007 for the product titled "High-performance LMOe-based HTS wire."

5) I_c retention in low applied fields increased significantly from 77% to over 95% in FY2007

Using the SuperPower's MOCVD research system, we have investigated the range of rare-earth compositions and doping levels under various deposition conditions and achieved the high I_c retention at 77 K and low fields for 0.7 µm thick single pass films.

Cable is the largest consumer of HTS wires. Magnetic field experienced by the wire in a cable is primarily parallel to the a-b plane. So

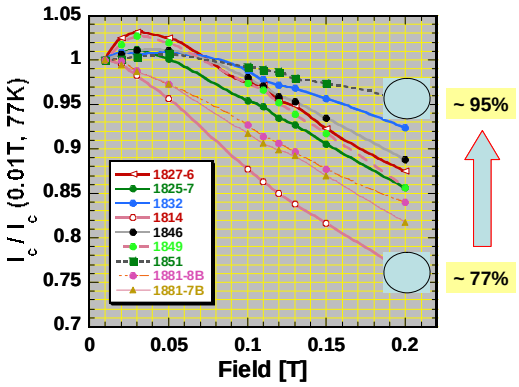

Fig. 6. Field dependence I_c at 77 K; H || ab for 0.7 µm thick RE-doped YBCO films.

far, the critical currents of present HTS cables are about a few kA resulting in relatively low self-fields. Future HTS cables, especially dc cables will be rated at significantly higher currents and accordingly the magnitude of the self-field will increase accordingly. Hence, it is valuable to study the retention of I_c of 2G wires in low-fields, parallel to the a-b plane. Through ORNL-SuperPower CRADA, we have significantly increased the I_c retention from 77 % to over 95% at 77K and low applied fields in H || ab direction. The field dependence Ic at 77 K of various RE-doped YBCO films measured at ORNL are shown in Fig. 6. As one can see, at 0.2 T, the I_c retention has been improved significantly.

6) Systematic studies of SuperPower's research MOCVD system in obtaining thick films with an I_c of 750 A/cm

The CRADA team has been investigating various means to increase I_c through thick film processing and composition modification.with a goal of achieving an I_c of 750 A/cm-width. Multilayer experiments were done for an optimal composition (Y,Gd) selected from a range of rare-earth dopants and doping levels. SuperPower has adjusted the number of layers in its research system to simulate the future deposition of thick films in a single pass in a production helix system. About 0.7 µm thick REBCO films were deposited in each single pass. The in-field superconducting transport properties from 1- 4 layers, on a 0.22 µm bridge is shown in Fig. 7. As seen in Fig. 7, the I_c at 0.01 T continue to increase with thickness. I_c also increased linearly with thickness at moderate applied fields. For a 2.8 µm thick film, an I_c of over 750 A/cm was achieved.

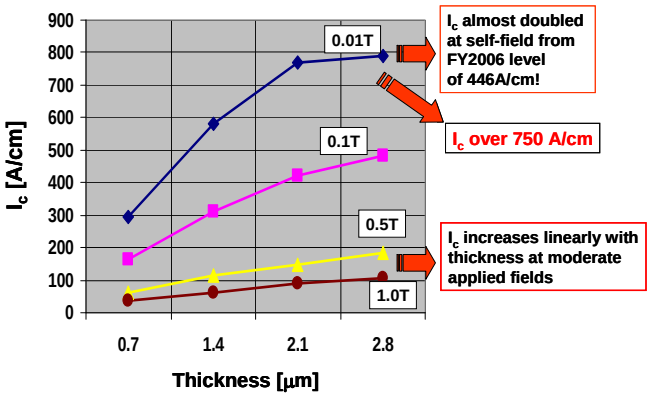

Fig. 7. I_c of MOCVD HTS on IBAD/MgO as function of thickness in the presence of various levels of applied magnetic fields.

7) Work has begun on determining wide-range temperature and field properties of SuperPower high-I_c coated conductors.

We have begun a systematic study of the magnetic field and temperature dependence of the loss-free electric currents in a series of high-current coated conductors produced in collaboration with SuperPower, Inc. Initial work is on a mixed rare-earth cuprate. In the study, both transport- and magnetically-determined critical currents will be compared, and assessments made of the detailed effects of flux creep and voltage criteria on the suitability for different applications.

For the present sample, 2.1 µm thick, the measured self-field critical current at 77K was nearly 450 A/cm-width by transport. The magnetization-derived critical current densities J_c

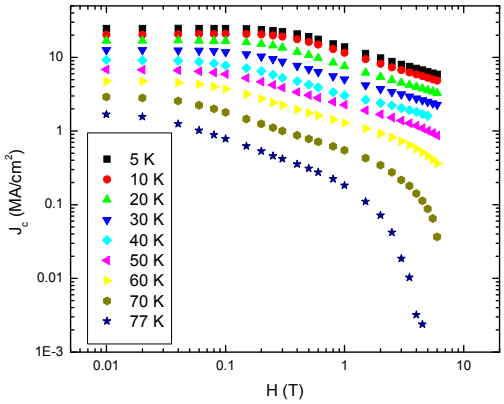

Fig. 8. Magnetization-derived J_c over a wide temperature and field range in a 2.1 µm SuperPower sample.

over a wide temperature and field range are shown in Fig. 8. For example, the values at 50 K (in principle attainable by single-stage cryocoolers) are over 1 MA/cm^2 in a field of 3 Tesla, corresponding to over 250A/cm-width - in the range required for practical high-field devices. Moreover, having been measured magnetically, the effective voltage criterion defining J_c is at the levels needed to assure sufficiently low energy dissipation. These and other practical issues will be elaborated as the studies continue.

Technical progress:

ORNL continues to collaborate closely with SuperPower on scale-up and performance issues related to the development of IBAD-MgO-based 2G HTS wire. Numerous SP samples have been examined for their critical current characteristics under self-field and in the presence of applied magnetic fields. In addition, steady progress is being made in the area of substrate improvement, and in the understanding of SP 2G wire losses and stability characteristics

Status of milestones:

- Operational MOCVD system providing J_c greater than 2 MA/cm^2. (June 30, 2007): **Met March 2007**.
- Assist SuperPower in developing highly textured and uniform 1,000 meter-class IBAD-MgO/LMO substrate. (Sept. 30,2007): **Met June 2007**.
- Assist SuperPower in obtaining high I_c thick films of 750 A/cm. (Sept. 30, 2007): **Met July 2007**.

Interactions:

Interactions with SuperPower included regular progress and planning teleconferences, as well as numerous and frequent sample exchanges with follow-up discussions on results. Also, face-to-face meetings were held as events warranted. Initiated a new collaboration with Argonne National Laboratory scientists for Raman microprobe analysis.

Subtask 1.3: ORNL – MetOx CRADA to characterize All-MOCVD 2G wires.
D.K. Christen, Y. Zhang, P.M. Martin, A Goyal, L. Heatherly

Objectives:
This work is focused on the development of RABiTS-based coated conductor technology that is in the pre-commercial development stage. MetOx is a Houston-based small business that is interested in developing and manufacturing 2G wire using an all-MOCVD process, including buffer(s) and HTS. If successful, there is a real potential that low-cost 2G wire can be produced due to the inherently high deposition rate of the MOCVD technique. It will also expand the number of domestic HTS wire suppliers to ensure a steady supply of the core component needed for HTS devices.

Highlights:
Superconducting properties of MetOx YBCO coatings have been measured and analyzed.
It is important to evaluate the progress in development of HTS coatings that have been deposited on either MetOx buffered RABiTS or on ORNL RABiTS, as MetOx seeks to become a viable third US supplier of 2G wire. We have begun to evaluate the superconductive properties of five coated conductor samples that were deposited by MetOx on both types of templates. Analysis of the data will be used by MetOx in making processing refinements.

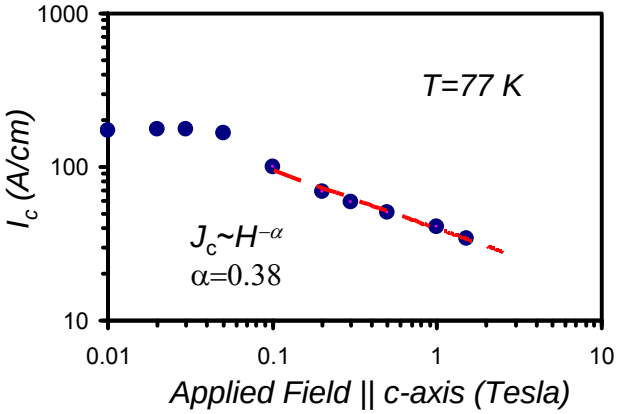

Fig. 1. The magnetic field dependence of I_c for fields aligned near the *c*-axis (⊥ to tape plane).

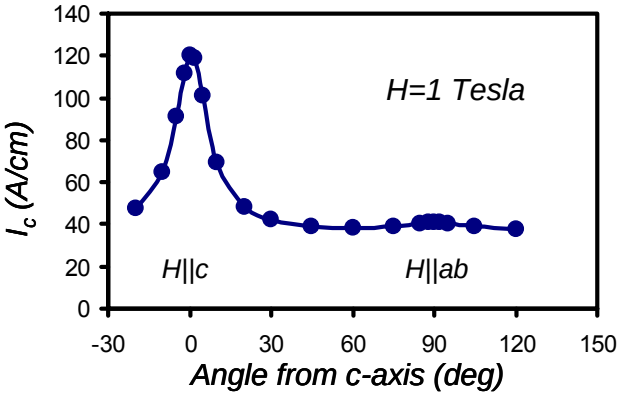

Fig. 2. The orientation dependence of I_c in a magnetic field of 1 Tesla.

ORNL conducted electrical transport measurements to determine both critical current density J_c as a function of magnetic field at 77 K, for fields parallel to the c axis, and the effects on J_c of conductor orientation in a 1 Tesla field, since in all real applications portions of the tape strands will be exposed to different field directions. Magnetic studies determined the transition temperatures T_c, which can be important for its effects on J_c is the liquid nitrogen temperature range.

- The transitions temperatures of all samples were near or just below 90 K, an indication that the MetOx MOCVD samples do not suffer from overall chemical contamination, which has been a concern due to the high processing temperatures.

- The decay of Jc with magnetic field strength is characterized by the power-law exponent a according to Jc ∝ H-a. This is an important parameter, since a low value of a sets the scale for higher Jc at operational fields. While not all the studied samples exhibited this behavior, the one with highest Ic = 175 A/cm had a value a ≅ 0.38 (shown in the Fig. 1), and the one with highest Jc = 1.4 MA/cm2 showed a ≅ 0.36. These are respectably low numbers, since predicted a values from flux pinning theories are ½ and 5/8, although very strong pinnng materials have shown values less than 1/5.

The dependence of Jc on field orientation (Fig. 2) shows little evidence of strong, correlated pinning nanostructures for H||c, which would manifest as a pronounced peak in Jc near zero angle. So the materials shows characteristics more indicative of isotropic pinning defects. The peak along H||ab is expected from both intrinsic anisotropy (supercurrent electronic effective mass) and any layered defect structure, such as intergrowths of 248 phase or a-b plane stacking faults.

Technical progress:

- A 3-metert length of ORNL textured NiW tape was supplied to MetOx for continued evaluation of their MOCVD HTS coatings. MetOx will continue to make depositions of both buffers and HTS coatings on textured templates for incremental evaluation and process development. ORNL textured tape helps enable the MetOx developmental approach.
- In addition, MetOx plans to provide ORNL with their buffered tape for ORNL to make qualifying HTS depositions. The ORNL HTS coatings should offer insight into areas of focus for MetOx processing adjustments.
- ORNL superconductive properties characterization activities will continue, with specific objective of evaluating the intra-grain vs inter-grain critical current density of MetOx HTS coatings. This is important to help MetOx identify remaining performance issues and develop processing improvements. As a part of the methodology, MetOx plans to provide ORNL with their buffered tape for ORNL to make qualifying HTS depositions. The ORNL HTS coatings should also offer insight into areas of focus for MetOx processing adjustments.
- Discussion were conducted to help MetOx advance toward self-production of textured metal template for RABiTS. We have conveyed to MetOx several details of ORNL proprietary information regarding specifications of starting metal alloys for the fabrication of textured tapes. This information is important in helping MetOx strive for independent production of their own templates.

Status of milestones:

- Deliver 10m+ textured template/RABiTS to MetOx for MOCVD buffer/HTS deposition.(Sept. 30, 2007): **Met Sept. 2007.**
- Characterize diffusion behavior of MetOx MOCVD buffer.(Sept. 30, 2007): **Ongoing.**
- Characterize MetOx MOCVD HTS in magnetic fields (Sept. 30, 2007): **Met August 2007.**

Interactions:

Interactions with MetOx have included the measurement and analysis of MetOx HTS coatings for the dependence of superconducting properties on magnetic field strength and orientation. ORNL has supplied MetOx with textured NiW alloy for the development of MetOx MOCVD buffers and HTS.

Section 2: Conductor Research

Provides underlying knowledge base needed to address the relationships between substrate and HTS performance, processing and microstructure development, and how various factors can affect current flow over long lengths. Pertinent findings to be integrated into Wire Development research.

Subtask 2.1: Textured substrates with improved characteristics.
A. Goyal, L. Heatherly

Objectives:
While textured metallic templates such as Ni-5%W have sufficient mechanical integrity for practical applications, enhancement in yield strength is preferred for handling during wire fabrication. This increased strength will enable higher manufacturing speed and therefore lower cost. Also, a low- or non-magnetic substrate will reduce the ac losses of the conductor. This project seeks to investigate innovative approaches to develop the materials science and solutions to the above stated issues.

Highlights:
Warm rolling key to obtaining cube texture in Ni-9.3% strengthened non-magnetic alloy.
Addition of high W contents to Ni reduces the magnetism of Ni and increases the strength dramatically. For Ni-9.3at%W composition, the substrate is completely non-magnetic at all temperatures and has a yield strength of ~ 300 MPa at room temperature. Unfortunately, for W contents greater than 5at%W in Ni, a texture transition occurs upon conventional rolling. We have discovered that warm rolling will circumvent this transition, resulting in cube textured substrates using Ni-9.3%W.

For W contents less than 5at%, a "Cu-type or pure metal-type" rolling texture is obtained. Fig.1 shows a typical (111) pole figure for a Cu-type rolling texture in Ni-3at%W. This rolling texture is a necessary precursor for formation of the desired cube annealing texture corresponding to {100}<100>. Beyond 5at%W a texture transition occurs and a "brass-type or an alloy-type texture" is obtained. Fig.2 shows the typical (111) pole figure for a brass-type rolling texture. This does not give the cube texture upon annealing and results innumerous high-angle boundaries and is not suitable as a substrate for growth of epitaxial HTS.

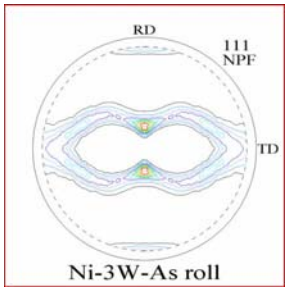

Fig. 1. (111) pole figure of 99% deformed Ni-3at%W substrate in an as-rolled condition. A typical Cu-type rolling texture is obtained.

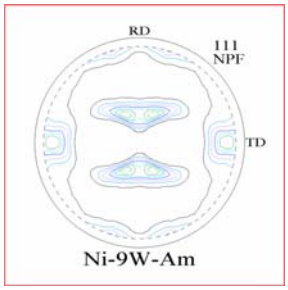

Fig 2. (111) pole figure of 99% deformed Ni-9at%W substrate in an as-rolled condition. A typical brass-type rolling texture is obtained.

In order to enable formation of cube texture in Ni-9.3at%W a processing breakthrough was necessary to reverse the texture transition mentioned above. In order to achieve this the role of stacking fault energies was examined. It was found that the texture transition referred to above comes about because of a change in stacking fault energy upon addition of higher W amounts. Since a reverse effect in stacking fault energy is obtained as one increases the temperature of deformation, Ni-9.3at%W substrate were warm-rolled at elevated temperatures as opposed to rolling at room temperature. Fig.3 shows that upon doing so, one can reverse the texture transition from brass-type to Cu-type. The above is quite significant and upon annealing under appropriate conditions, a cube texture should form.

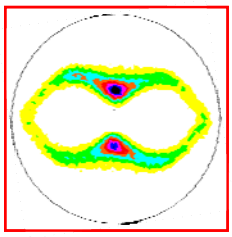

Fig. 3. (111) pole figure of 99% hot-rolled Ni-9.3at%W substrate in an as-rolled condition. A typical Cu-type rolling texture is obtained.

Here, we report on the annealing textures of as-rolled Ni-9.3at%W substrates. Figure 4 shows NiW (111) pole figures for substrates annealed at different annealing temperatures. At higher annealing temperatures, fully cube textured substrates are obtained. This is the first time that anyone has reported formation of cube texture in Ni-9.3at%W substrates. Fig. 5 ows the phi-scan for the substrate annealed at the highest temperature shown indicating a sharp in-plane texture.

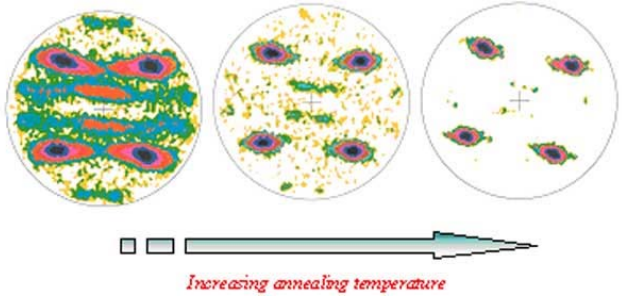

Fig.4: NiW (111) pole figures for warm-rolled Ni-9.3at%W substrates showing formation of cube texture at higher annealing temperatures.

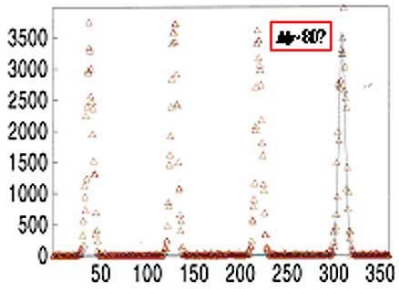

Fig.5: NiW (111) phi-scan for warm-rolled Ni-9.3at%W substrates showing a sharp cube texture with a FWHM of 8˚.

Addition of high W contents to Ni, reduces the magnetism of Ni and increases the strength dramatically. For Ni-9.3at%W composition, the substrate is completely non-magnetic at all temperatures and has a yield strength of ~ 300 MPa at room temperature. Unfortunately, for W contents greater than 5at%W in Ni, a texture transition occurs upon rolling. For W contents less than 5at%, a "Cu-type or pure metal-type" rolling texture is obtained. This rolling texture is a necessary precursor for formation of the desired cube annealing texture corresponding to {100}<100>. Beyond 5at%W a texture transition occurs and a "brass-type or an alloy-type texture" is obtained. In order to enable formation of cube texture in Ni-9.3at%W a processing breakthrough was necessary to reverse the texture transition mentioned above. As reported in the last quarterly, in order to achieve this transition, the role of stacking fault energies was examined. It was found that the texture transition referred to above comes about because of a change in stacking fault energy upon addition of higher W amounts. Since a reverse effect in

stacking fault energy is obtained as one increases the temperature of deformation, Ni-9.3at%W substrate were hot-rolled at elevated temperatures as opposed to rolling at room temperature. Upon doing so, it was found that the texture transition can be successfully reversed and one can obtain a Cu-type rolling texture for Ni-9.3at%W substrates. With this rolling texture, complete cube-texture in the substrate can be obtained upon annealing.

Status of milestones:

- Fabricate a highly strengthened, Ni-alloy based substrate with reduced magnetism using a process which can be extended to long lengths. (Sept. 30, 2007): **Met June 2007.**

Interactions:

Tasks in this base program project involve close consultations and discussions with AMSC. In addition, sample from AMSC will be included in the UHMFP process.

Subtask 2.2: Solution buffer development for low cost conductors.
M.P. Paranthaman, S. Sathyamurthy, M.S. Bhuiyan

Objectives:
Buffer layers play a key role in REBCO 2G wire technology. The purpose of the buffer layers is to provide a continuous, smooth and chemically inert surface for the growth of the HTS film, while transferring the biaxial texture from the substrate to the HTS layer. U.S. HTS wire manufacturers are now in a position to produce reasonable quality coated conductors in "pilot-scale" mode. Cost of substrate manufacturing, however, remains high because of the relative inefficiency of physical vapor deposition (PVD) method. Solution buffer approach is an inherently low cost method that combines fast deposition rate, rapid crystallizing potential and inexpensive equipment. Indeed, an all-solution approach to buffer and REBCO processing has been projected as the cheapest route to produce 2G wires. The goal of this project is to develop the materials science and technique that can result in high quality solution buffer(s) that can sustain large critical currents comparable to its PVD counterparts.

Highlights:
1) Solution technique has been successfully used to grow potential seed layers with improved out-of-plane textures.
Typically, Yttrium Oxide (Y_2O_3), Titanium Nitride (TiN), and Magnesium Oxide (MgO) buffers have been grown directly on textured Ni-W substrates using physical vapor deposition (PVD). These buffers are of particular interest because they impart improved out-of-plane textures onto the substrate. High current YBCO films have been demonstrated on these seed layers. Now, we have succeeded in growing both La_3TaO_7 (LTO) and La_3NbO_7 (LNO) seed layers with improved texture directly on Ni-W substrates using solution MOD method. These seed layers could be used for all-MOD buffer/REBCO architectures. As measured from the XRD Omega scans, both LTO and LNO textures improves by over 0.5-1° compared to the underlying Ni-W substrate texture.

Table I: Texture data for La_3NbO_7, and La_3TaO_7 films on cube textured Ni-W substrates.

Oxide Films	FWHM Values			FWHM Values of Ni-W substrates		
	Δω (004) Φ = 0° (deg.)	Δω (004) Φ = 90° (deg.)	Δφ (222) (deg.)	Δω (002) Φ = 0° (deg.)	Δω (002) Φ = 90° (deg.)	Δφ (111) (deg.)
La_3NbO_7	6.56	4.87	7.44	7.82	5.28	7.48
La_3TaO_7	3.8	3.6	7.5	7.6	5.4	7.8

2) Improvement of texture and surface morphology of Doped Ceria seed layers.
Ceria buffer plays the key role as a cap and/or seed layer in YBCO 2G wire technology. The concerning issue is to provide a continuous, smooth and chemically inert surface for the growth of the HTS film, while transferring the biaxial texture from the substrate to the HTS layer. However, the typical MOD solution ceria layer has roughness in the order of 3-4 nm that exaggerates the reactivity between HTS and ceria, and it does not improve texture from that of the metal template. Therefore, reducing the surface roughness and improving the texture can

result in better aligned HTS and lower the reactivity and thus better performance. We have employed various dopants to study the surface morphology and texture. Initial results show that appropriate dopant and processing can result in texture and roughness enhancement of solution seed layers.

Table II: Texture data for Doped Ceria Seeds grown directly on Ni-3W substrates.

Texture Comparison Data for Ceria and Doped Ceria						
	Ceria/Doped Ceria			Substrate		
Materials	Out of Plane Texture		In Plane Texture	Out of Plane Texture		In Plane Texture
	(deg.)		(deg.)	(deg.)		(deg.)
	phi-0	phi-90		phi-0	phi-90	
CeO_2	8.84	5.12	6.34	8.07	5.2	6.22
$Ce_{1-x}A_xO_2$	6.12	4.25	6.16	8.07	5.2	6.22
$Ce_{1-x}B_xO_2$	8.4	5.8	7.3	8.07	5.2	6.22
$Ce_{1-x}C_xO_2$	9.8	6.3	9.3	8.07	5.2	6.22

We have successfully demonstrated the effect of dopants in Ceria seeds on texture and surface morphology. The dopants used are identified as A, B, and C. Initial analysis from XRD and texture measurement (Table II) suggests that dopant "A" has the potential of yielding the desired properties. Therefore a comprehensive study was performed for "A" under various processing temperatures. It can be concluded that there is an increase in surface roughness with increase in process temperature. On the other hand very low temperature results in broader texture. The present study (Table III) suggests that processing the ceria film with dopant "A" at 900°C to 950°C can yield the desired characteristics of surface smoothness with improved texture.

Table III: Texture data for ceria doped with A.

Texture Comparison Data for A-Doped Ceria						
	Doped Ceria			Substrate		
Temperature	Out of Plane Texture		In Plane Texture	Out of Plane Texture		In Plane Texture
(° C)	(deg.)		(deg.)	(deg.)		(deg.)
	phi-0	phi-90		phi-0	phi-90	
900	4.5	4.36	6.56	9.6	5.72	6.68
950	3.94	3.83	6.26	9.6	5.72	6.68
1000	4.25	4.1	6.35	9.6	5.72	6.68
1050	4.36	4.25	6.63	9.6	5.72	6.68

3) Relative humidity found to have significant effect on crystallization of epitaxial solution buffers.

Ambient relative humidity (RH) during solution coating process was found to significantly influence the crystallographic texture and microstructure of the processed films. Using Y_2O_3 seeded textured-Ni-5at.%W substrates, we have determined that there is a threshold humidity level above which highly oriented lanthanum zirconium oxide (LZO) films can be processed.

However, below the threshold level, a significant portion of the film grows with a random polycrystalline orientation (Fig. 1). Using the correct processing conditions, we have demonstrated an I_c of 336 A/cm using MOD-YBCO with AMSC on these improved LZO templates with sputtered CeO_2 cap. This result indicates that with proper process controls, solution buffer with properties comparable or exceeding that of its PVD counterparts may be used in 2G wire fabrication..

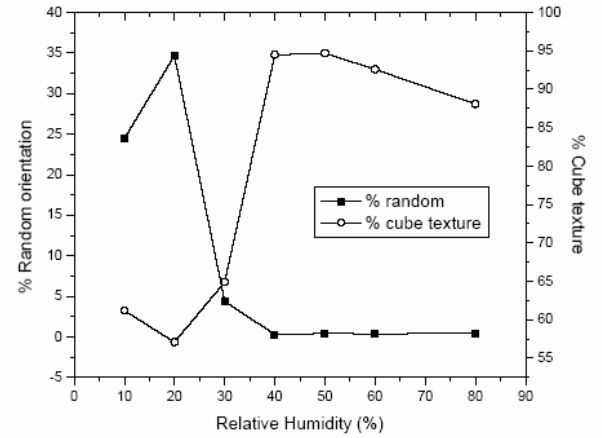

Fig. 1. Variation of percent random-oriented and cube textured LZO in the films as a function of relative humidity for samples processed at 1100 ºC for 15 min.

4) Cube texture obtained in doped-$La_2Zr_2O_7$ (LZO) solution buffer. Potential to improve diffusion barrier properties.

High I_c of 336 A/cm has previously been obtained on RABiTS with LZO solution barrier buffer layer, which exceeded the performance of its physical vapor deposited YSZ counterpart. Earlier SIMS studies have shown that there is some amount of Ni diffusion through the LZO and a film >80 nm is required for effective barrier. Also, Yttrium seed layer is found to diffuse into LZO. Hence, we are studying the effect of Y-doping on the barrier properties of LZO films. Using Y_2O_3 seeded textured substrates, we have optimized the processing conditions for a variety of doping levels (0-50%) and highly textured Y-doped LZO films have been synthesized (Fig. 2). The Ni diffusion barrier properties of these films will be compared to that of pure LZO and a correlation of the barrier properties with dopant levels will be developed in the near future.

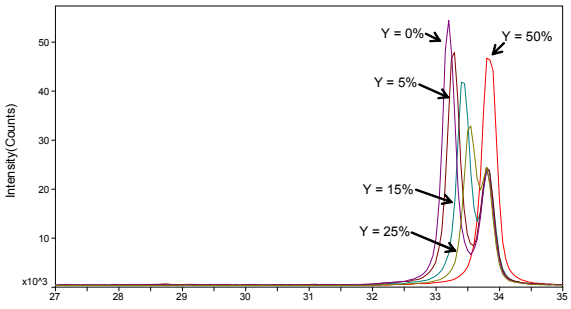

Fig. 2. X-ray diffraction patterns of Y-doped LZO films on Y_2O_3/Ni-W substrates

5) MOD LTO seeds improved the texture of MOD LZO barriers

All-solution buffer coated conductor architecture is generally agreed as one of the cheapest route to 2G wire manufacturing. In order to replace the physical vapor deposited (PVD) Y_2O_3 seed layer, however, the solution seed must offer the same advantage in texture improvement that is found in the PVD Y_2O_3 seed layer. Unfortunately, solution Y_2O_3 seeds have been found to mimic the metal template texture without any improvement. Here, we report on the development of a LTO solution seed material that is found to improve upon the template texture.

The current RABiTS architecture used by American Superconductor consists of a starting template of biaxially textured Ni-W (5 at.%) with a seed layer of 75-nm Y_2O_3, a barrier layer of 75-nm YSZ, and a cap layer of 75-nm CeO_2. In this architecture, all the buffers have been deposited by reactive sputtering. To reduce the initial investment cost for buying 2G pilot-scale production equipment, it is essential to either reduce the number of layers or to replace some of

the sputtered buffer layers with solution deposited buffers. The Metal-Organic Deposition (MOD) process offers a significant potential cost advantage over physical vapor deposition (PVD) processes. Solution coating is amenable to complex oxides and the materials utilization is almost 100%. A slot-die coating process has been chosen to scale up solution buffer layers. However, for optimizing the MOD film growth and process conditions of short samples, spin coating was used. Seed buffer layers which improve the out-of-plane texture compared to that of the substrate are of significant interest, especially in those cases when the out-of-plane texture of substrate is broad in one rocking direction. Sputtered Y_2O_3 seed layers improve the texture relative to the substrate texture. However, there is no improvement in texture when MOD LZO layers were grown directly on textured Ni-W substrates. The lattice mismatch between LZO and Ni-W substrate is about 7.9 %. We have reduced the lattice mismatch, improved the texture and also enhanced the properties of LZO by inserting a thin sputtered Y_2O_3 seed layer. Y_2O_3 seeded MOD-LZO barrier layers with sputtered-CeO_2 cap layers have matched the performance of sputtered YSZ layers using MOD YBCO films. Here, we have demonstrated the improvement of LZO texture using various LTO seeds. We have increased the surface coverage of MOD LTO seeds on Ni-5W substrates by varying the starting solution concentration. MOD LZO films were deposited on these MOD LTO seeds. As from the Table IV, one can see the texture improvement of MOD LZO from sample 1 to 4 (surface coverage of LTO increased from sample 1 to 4). These seed/barrier layers could be used for all-MOD buffer/REBCO architectures. The cross-sectional TEM image of MOD LZO/MOD LTO/Ni5W (sample 3) is shown in Fig. 3. From Fig. 3, one can clearly see the formation of MOD LTO islands. The underlying mechanism of texture improvement in these layers will be evaluated in FY 2008.

Table IV. Texture of MOD LZO on MOD-LTO seeded Ni-W substrates.

Sample #	LZO (004) Phi = 0	LZO (004) Phi = 90	LZO (222) Phi	Ni (002) Phi = 0	Ni (002) Phi = 90	Ni (111) Phi
1	8.57	6.43	8.4			
2	7.83	5.52	8			
3	6.67	5.12	7.84			
4	6.98	5.33	7.91	8.22	5.29	7.8

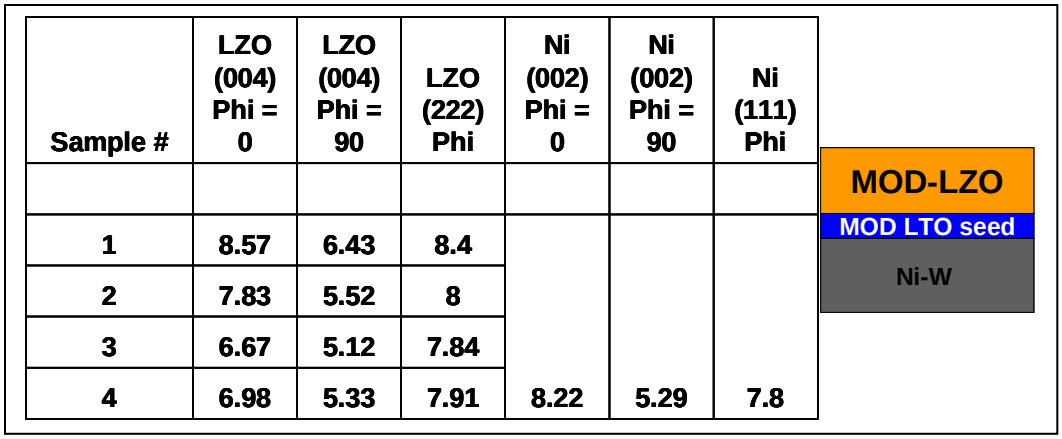

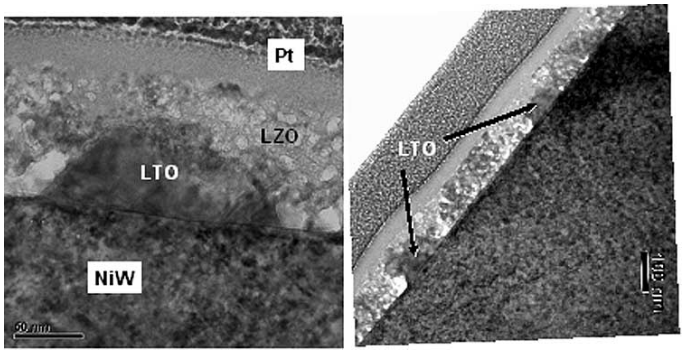

Fig. 3. TEM cross-section of MOD LZO/MOD LTO/Ni5W substrates.

6) YBCO films with a J_c of 2.6 MA/cm^2 achieved on two-layer architecture

We have demonstrated the barrier properties of MOD LZO to exceed that of PVD YSZ layers. To further improve the properties of MOD LZO, various La/Zr ratio were varied. It is possible to vary the composition from 20 to 60% La and still obtain the epitaxy. We have used modified LZO composition ($La_1Zr_3O_7$ compared to standard $La_2Zr_2O_7$) to grow directly on Ni-5W substrates and obtained good texture. American Superconductor has completed MOD-LZO/Ni05W substrates with a standard PVD CeO_2 and MOD-YBCO and achieved an I_c of 206 A/cm (J_c of 2.6 MA/cm^2) at 77 K. I-V plot for the two-layer architecture is shown in Fig. 4. With this demonstration, we have met the milestone.

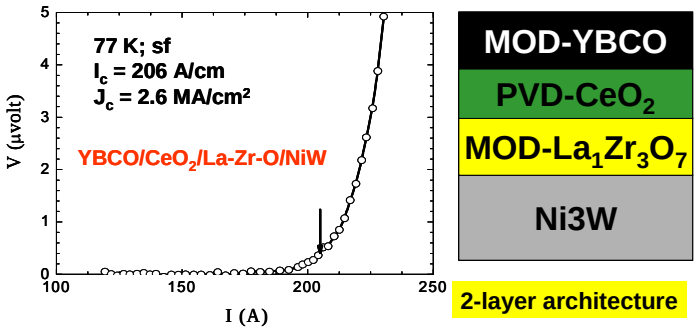

Fig.4. I-V plot for two-layer architecture.

Status of milestones:

- Develop solution precursor and processing method for epitaxial solution buffer that can replace at least two standard buffers with J_c of 2 MA/cm^2 (Sept. 30, 2007): **Met; July 2007.**

Interactions:

This base program research involves substantial interaction with AMSC on buffer evaluation using commercial HTS deposition process. There is also interaction with the Applied Superconductivity Center at the University of Wisconsin-Madison on buffer material development.

Subtask 2.3: HTS processing for critical current and pinning enhancement.

T. Aytug, M. Paranthaman, K. J. Leonard, S. Kang, P. M. Martin, L. Heatherly, A. Goyal, A. O. Ijaduola, J. R. Thompson, D. K Christen, K-H Kim, S-H Wee, R. Feenstra, Y. Zuev, O. Polat, J. Li, R. Meng, I. Rusakova, C. W. Chu

Objectives:

U.S. HTS wire manufacturers are now producing 2G wires with reasonable properties in restively long lengths. To meet the performance requirements of practical commercial applications, however, it is necessary to further improve the HTS transport properties. For example, operation of high-field equipment (motors, generators, air-core transformers) requires performance levels of J_e of 15-30kA/cm^2 at 55-65K, 2-5 Tesla. Performance optimization will require both sustained high current density with increased film thickness and improved flux pinning. Improvements in the properties of the YBCO coating require a thorough understanding of the pinning mechanisms, as well as control of a possible combination of nanostructures through extrinsic means. This work seeks to establish the limits of performance that are attainable via incorporation of controlled nanostructure defects within the HTS films and provide guidance or pathways to the ongoing work in CRADA's with US HTS wire manufacturers to further improve the HTS superconducting properties.

Highlights:

1) Substrate surface decoration by nano-particles found to enhance flux pinning in YBCO.

Recently, a collaborative team of researchers from ORNL, Univ. Tennessee and Univ. Houston have performed a study that points to a simple, economic process to increase the flux pinning and critical current density in REBCO coated conductors. The work involves YBCO films grown on both single crystal and textured metal substrate surfaces that were pretreated with 2nd -phase nano-scale particles. The nano-particles were applied using simple solution approaches and yielded growth defects in the deposited YBCO coatings. These defects contributed to prevent dissipative vortex motion, and thereby increased J_c. Compared to untreated samples, HTS on treated surfaces showed higher J_c's for all applied magnetic field angles (Fig. 1). Ultimate objective of this approach is to produce cost-effective enhancements in the properties of commercial coated conductors by a simple pretreatment applicable to all technical substrates.

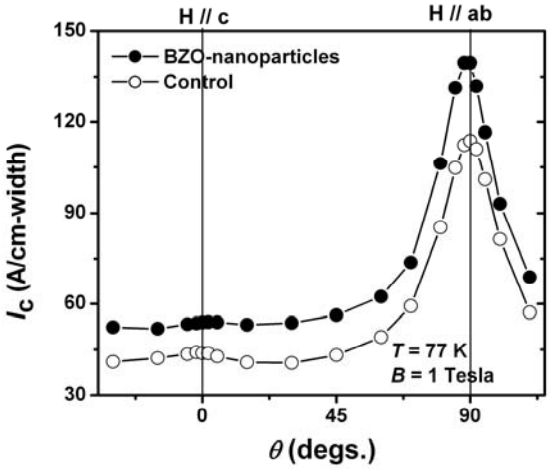

Fig. 1. Angular J_c dependencies of 3 μm-thick YBCO deposited on biaxially textured metal tapes with and without $BaZrO_3$ nano-particle modifications.

2) Pinning analyses conducted on substrate surface treated conductors.

Performance and flux-pinning analyses were conducted on YBCO films that were deposited on substrate surfaces decorated with various types of nano-particles. For example with MgO nano-

particles, magnetization J_c revealed a roughly 50% improvement at all temperatures and fields. We have observed several common features for YBCO deposited on both surface treated and untreated substrates (Fig. 2). These include a region of nearly constant J_c up to a characteristic crossover field of B^*, followed by a rollover to a power-law regime ($J_c \propto B^{-\alpha}$) at intermediate fields, and finally a precipitous decay of J_c on approaching the irreversibility field, B_{irr}. We have consistently obtained values for the power law exponent $\alpha \sim 0.5$-0.54 for both modified and control YBCO films, indicating similar field dependencies and no apparent change in pinning mechanisms. These α-values are also similar to those obtained on surfaces decorated with other nano-particles. It is believed that the pinning mechanism cannot be simply flux line shearing since TEM observations revealed no indication of c-axis extended defects, and angularly dependent data give little indication of pronounced correlated disorder near the c-axis. Rather, the dominant mechanism is likely due to uncorrelated large dilute defects with associated δT_c from non-superconducting particles and strain fields. With similar pinning mechanism, difference in performance is initially attributed to an increased pinning strength produced by nano-particles in the surface decorated samples. Much work remains to understand the influence of nano-particle size and density on the induced growth defects in HTS coatings of different thicknesses. In addition to substrate treatment, pinning modifications by aligned nano-particles as well as inclusions through composition variation / doping are also ongoing.

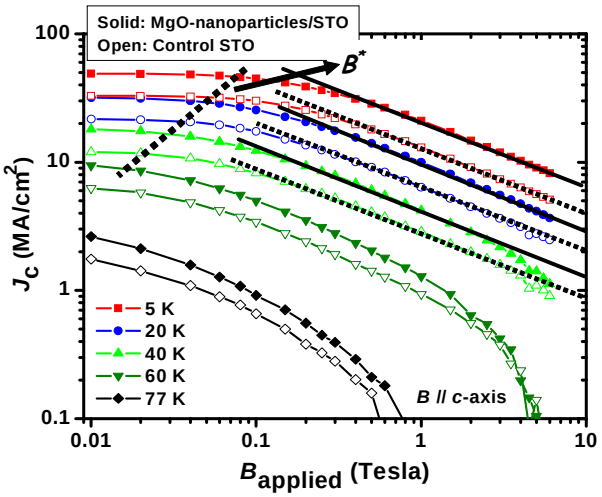

Fig. 2. Comparison of magnetic field dependence of magnetization J_c for two 0.3 μm thick YBCO films grown on substrate surfaces with MgO nano-particles (solid symbols) and without (open symbols).

3) HTS Program CPS Control Milestone met - Improve in-field performance flux-pinning factor to less than $\alpha = 0.2$.

3a) Incorporation of self-assembled nanodot columns lowers α of 0.7 μm NdBCO film to 0.17.

3-D self-assembled stacks of $BaZrO_3$ (BZO) nanodots oriented parallel to the c-axis of the film were formed in 0.7 μm thick, epitaxial $NdBa_2Cu_3O_{7-\delta}$ (NdBCO) films, deposited on IBAD-MgO templates via pulsed laser deposition. The aligned nanodot columns provide excellent pinning and lower the α to 0.17. Work is underway to develop means by which this defect

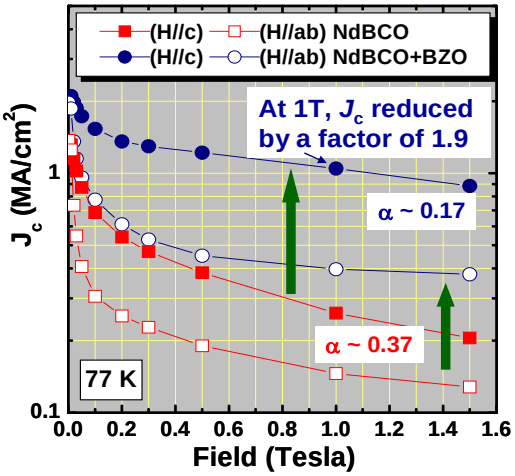

Fig. 3. J_c's of 0.7 μm NdBCO and NdBCO+BZO films on IBAD-MgO for H//a-b and H//c directions.

microstructure may be incorporated into films deposited by commercially-selected processes.

Fig. 3 shows the field dependent J_c versus applied magnetic field for 0.7 μm thick NdBCO and NdBCO+BZO films at 77 K with both field directions, the field applied perpendicular (H//ab) and parallel (H//c) to the c-axis of the film. The self-field J_c for BZO-doped films is ~2.0 MA/cm^2, ~40 % larger than J_c ~1.4 MA/cm^2 for the un-doped film. For H//c, a remarkable improvement in the in-field J_c is achieved for the NdBCO+BZO film. This can be ascribed to the c-axis oriented, columnar defects comprised of self-assembled stacks of BZO nanodots. Additional defects and strain that is formed around the interfaces between BZO nanodots and the matrix, are a possible reason for the concomitant augmentation in J_c at H//ab for NdBCO+BZO films. At a magnetic field of 1.5 T, the J_c at H//c for BZO-doped sample reduced only by a factor of 2.3 and is still over 1 MA/cm^2, more than a factor of 4 over the performance of the sample without the BZO additions. The exponent, α, in the power-law of $J_c \sim H^{-\alpha}$ was calculated by linear regression of the in-field J_c data at H//c in the power-law regime of 0.2-1.5 T. A remarkably smaller α of ~0.17 is achieved from NdBCO+BZO film, compared to α ~0.37 for pure NdBCO film.

3b) Low α of 0.2 obtained in NdBCO film deposited on surface decorated IBAD-MgO.

High performance is one of the most important requirements of a practical 2G HTS wire. In addition to self-filed J_c at 77K, high current carrying capability in the presence of a magnetic field is also essential. This is particularly true for applications such as transformers and motors. In Feb. 2007, we have demonstrated in a model-system using PLD that very good pinning can be obtained in NdBCO with nano-particle surface decoration. An α value of 0.2 has been obtained. Work is underway to develop means by which the defect structures may be introduced into HTS films deposited by commercially-selected processes.

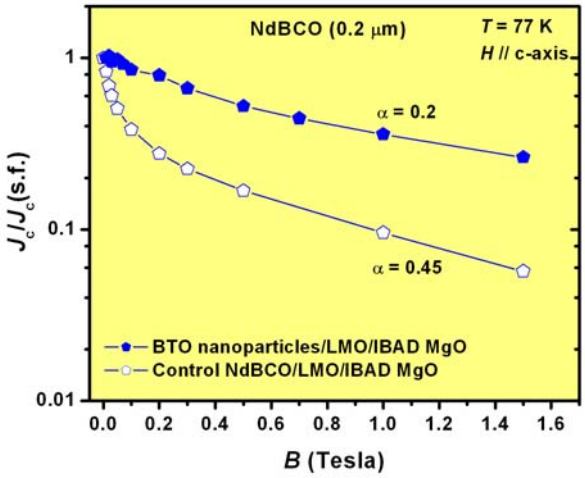

Fig. 4. J_c dependencies on magnetic field for surface modified IBAD-MgO/LMO substrate and control sample.

We have been engaging in research efforts to enhance in-field J_c through flux pinning defect engineering. A potential way to improve wire performance is by decorating substrate surfaces using preformed nanoparticles. This approach is attractive because both the formation of nanoparticles and the deposition of these particles onto substrate surfaces can be accomplished by low-cost solution techniques. In addition, different subsequent HTS deposition methods may be applicable and different type of technical substrates may be used. We have succeeded in applying preformed $BaTiO_3$ (BTO) nanoparticles to biaxially textured metal substrate surfaces using solution-based deposition technique. NdBCO films were then grown on these and on control substrates with untreated surfaces. Ability of HTS to withstand the effect of magnetic fields can generally be examined through the pinning exponent α (equation $J_c \sim B^{-\alpha}$). The lower the α, the better the pinning and in-field J_c. Transport electrical properties measurements of these samples showed substantial enhancement of flux pinning for the nanoparticle decorated sample as evidenced by the

significant enhancement of in-field J_c performance (Fig. 4), where an α-value of 0.2 is obtained. This result demonstrates the effectiveness of growth-induced defects for flux pinning in HTS films that can be produced by a relatively simple technique of nanoscale substrate surface modification.

4) An improved scientific basis for understanding flux-pinning by self-assembled nanodot columns was provided by systematic "flux creep" studies.

High-performance HTS coatings are needed for efficient and cost-effective 2G wires. Flux pinning by controlled defect structures can provide improved properties for applications in magnetic fields. Several features related to vortex pinning have been investigated for Nd-Ba-Cu-O-based coated conductors, either undoped or doped with $BaZrO_3$ particles to form self assembled columnar defect structures.

Relatively thin (0.7 μm) and thicker (2.1 μm) materials on IBAD substrates were studied, and the dependence of the critical current density J_c on temperature (5 K – T_c) and on the magnitude of magnetic field (0 – 6.5 T, applied || c-axis) was investigated. Doping with BZO reduces substantially the falloff of current density with applied magnetic field (lower α values) over the entire temperature range, with the effect most pronounced near 50-77 K. Studies of the decay with time of the current density J revealed features similar to those generated in single crystals by irradiation with heavy ions. Effective vortex pinning energies were successfully modeled with an inverse power law dependence of the form $U_{eff}(J) \sim U_0 (J_0/J)^{\mu}$, with the most notable differences between the sets of materials being the scale of current density J_0. These results help to understand the pinning of vortices and current conduction in materials with engineered defect structures, at low dissipation levels suitable for many applications

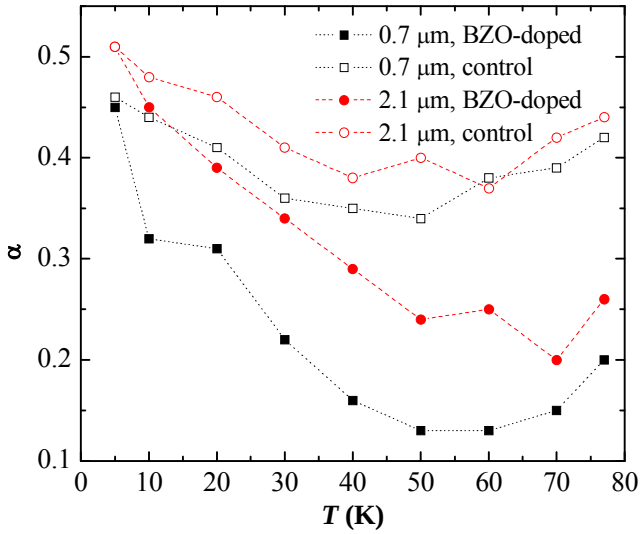

Fig. 5. The power-law exponent a describing the field-induced falloff of J_c, for several samples of undoped and BZO-doped NdBCO coatings on IBAD substrates.

5) Superconducting properties of state-of-the-art SuperPower prototype conductors were measured over a wide range of temperature, and magnetic and electric fields.

We have combined three experimental techniques to explore the voltage-current relations of the materials over a wide parameter range. This is important because the criterion used to define critical current density, J_c, by electrical transport corresponds to excessive heat generation for use in most real applications. The detailed behavior at the low dissipation levels was provided by the extended measurements using transport, magnetization field-sweep, and current decay (flux creep) techniques to map the current vs voltage over many orders of magnitude.

One relevant finding was a dependence on electric field level of the parameter, α, that characterizes the decay of J_c with magnetic field (i.e., the falloff of J_c found from transport measurements may differ from that at actual operating conditions). Additional analyses of related results show potential for feasible operation of the developing materials, for example, in superconducting solenoids cooled by single-stage cryocoolers.

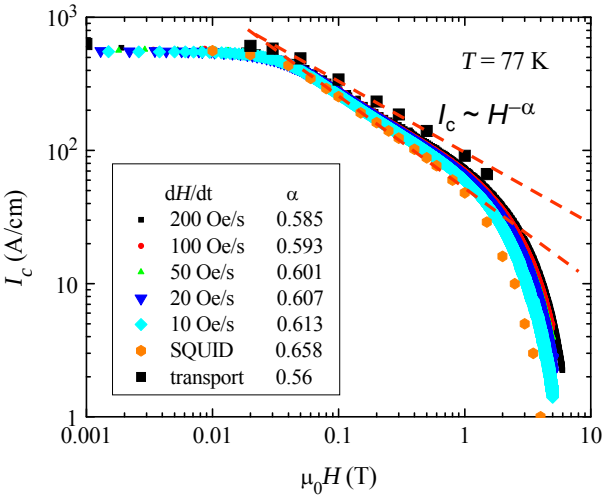

Fig. 6. Magnetic field dependence of J_c measured at different electric field levels. The power-law decay exponent shows field dependence, and is larger at the low E-fields needed for applications.

6) Analysis of wide-range temperature, and magnetic and electric field measurements of high-I_c prototype conductors.

Previously, we reported on combining three experimental techniques to explore the voltage-current relations of the materials over a wide parameter range. This is important because the criterion used to define J_c, by electrical transport would correspond to excessive heat generation for many power device applications. Generally, experimental characterization of research-size samples cannot probe the details of dissipation needed to quantify the actual current levels that are acceptable for low-level internal "index" heating (such as in a motor coil). Such details were provided by the extended measurements using transport, magnetization field-sweep, and current decay (flux creep) techniques to map the I-V over many orders of magnitude.

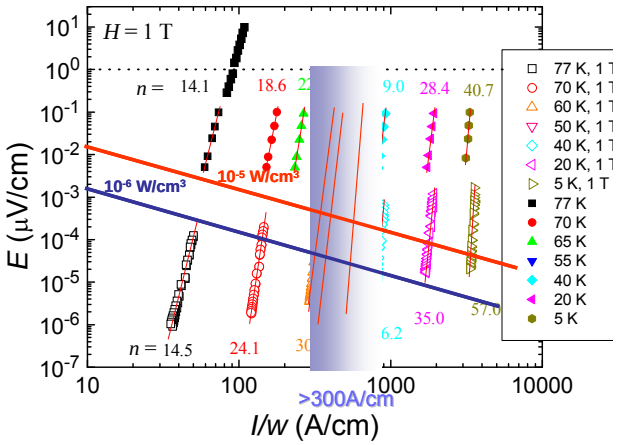

Fig. 7. Relationships between current level and generated electric field in the HTS coating, found from combinations of three experimental techniques. The range of estimated "index" heat generated per unit volume that can be tolerated within a cryocooled coil is shown. The n-values are power-law slopes of the curves

The materials studied were prototype 2G short tapes from SuperPower, with practical current levels ~750 A/cm at 77 K. Fig.7 shows results at various temperatures of measurements down to electric fields of ~10^{-6} μV/cm, six orders of magnitude below the criterion used to define transport J_c (shown as dashed line). Using the published model of Lvovsky, we have calculated the acceptable power dissipation within a cryocooled coil. The results show that the present 2G prototype could provide practical currents (<300 A/cm) at the low dissipation levels needed in the temperature range of 50 to 55 K, which can be provided by single-stage cryocoolers.

7) Observation of unique angular-dependent critical currents in strong-pinning BaZrO3-doped NdBa2Cu3Ox coated conductors.

The dependence of the critical current density J_c on material orientation in a magnetic field is an important quantity to study and understand. In real power devices, the tape conductor segments will experience a range of different magnetic field magnitudes and directions. Typically, the J_c values vary with field orientation because of anisotropy in both the intrinsic electronic properties of high-temperature superconducting (HTS) materials and possible preferential orientation of flux-pinning material nanostructures. Recently, we have found a previously unobserved phenomenon in the electrical conduction of strong-pinning $NdBa_2Cu_3O_7$ coatings that have been doped with $BaZrO_3$ to provide oriented columnar defects. By measuring the full range of J_c vs magnetic field H at several different orientations, it was found that there exists a unique field value B^* where J_c takes on a single value (i.e., the sample J_c is nearly *independent* of orientation at this field, B^*). An illustrative set of data, measured at five different temperatures, are shown in the Fig. 8.

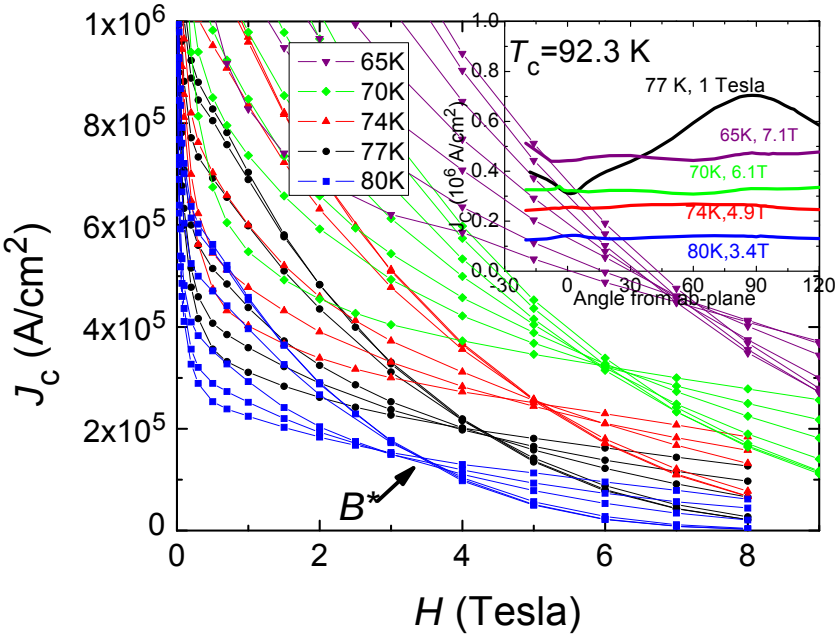

Fig. 8. Experimental transport data of J_c vs magnetic field, taken at several different orientations in the field, and at five different temperatures. At each temperature, there exists a unique field B^*, where J_c is independent of orientation. The inset shows data for J_c vs angle. Four of the curves are taken at fields near B^*, while the other (black curve) is the standard condition of 77K, 1 Tesla.

The common crossover field at each temperature is clearly evident in the main panel, while the inset shows the nearly orientation independent J_c values, taken at the crossover field B^*. For comparison, the inset also shows the "standard" angular dependence usually taken at a field of 1 Tesla at 77 K. The phenomenon has been observed in two different samples of NdBCO containing the BZO nanostructure. The effect may have important consequences for applications, because the angular dependence of J_c can be "elected," depending on the temperature and field regime of operation. Work is underway to further characterize the effect and develop a model to describe its behavior.

Status of milestones:

- Improve in-field performance flux-pinning factor to less than $\alpha = 0.2$. (July 31, 2007): **Met February 2007** (in conjunction with sub-task 2.4).
- Understand formation mechanism of columns of self-assembled nanodots. (Sept. 30, 2007): **Met September 2007**.

Interactions:

The research was performed in close coordination with SuperPower, Inc. who provided the research samples for the wide-range characterizations, and substrates for the BZO-doping studies. The results will assist SuperPower in a more quantitative assessment of their materials for potential applications. The overall understanding of J_c angular dependence will benefit all industrial partners. The ex-situ HTS research is performed in close coordination with the Wire Development Group to compliment and expand on the corporate research at AMSC. Interactions include extensive collaboration with University of Tennessee on transport characterization and pinning analysis. Results are communicated to our industry partners to assist them in process development and planning activities.

Subtask 2.4: High performance rare-earth HTS.

S-H Wee, K-H Kim, Y. Zhang, R. Feenstra, T. Aytug, P.M. Martin, Y. Zuev, A. Goyal,, H, Christen, M.P. Paranthaman, D.K. Christen

Objectives:

While performance and pinning enhancements are concentrated on YBCO, (mixed) rare-earth HTS have so far been neglected. The main reason for the emphasis on YBCO is because it is the most studied HTS 1-2-3 compound and ample results are available for comparison. Other rare-earth and mixed rare-earth HTS, however, have been shown to exhibit substantially different T_c, in-field performance, pinning behavior etc. when compared to YBCO. The main goal of this project is to establish the material science base of (mixed) rare-earth growth under various deposition/conversion conditions that are suitable for 2G wire processing. Detailed characterization of their performance and understanding of various pinning mechanisms will open up new avenues for commercial 2G wire production tailored to specific applications and needs.

Highlights:

1) New PLD chamber qualified for HTS film deposition.

Superconducting properties have been measured on YBCO films made in the new, dedicated PLD chamber described below. These samples serve as qualification prototypes to demonstrate near-optimized deposition parameters. These samples, 0.2 μm thick, yield magnetically-determined critical current density values *J*c =3 MA/cm^2 at 77K and 70 MA/cm^2 at at 5K, establishing viable conditions for systematic studies of rare-earth doped cuprates in this system.

The new system adds a third chamber to be served by the single Compex excimer laser. This chamber will be dedicated to the deposition of rare-earth substituted 123 coatings, with the aim of discovering HTS coatings with optimized properties, since previous empirical observations have indicated intrinsic, beneficial effects from rare-earth additions/substitutions.

The system has undergone substrate heater upgrades to accommodate fixed sample temperatures of up to ~900°C in oxygen. In initial testing, samples were ablated from a YBCO target onto $LaAlO_3$ single crystal substrates at temperatures of 760 and 780°C, in background oxygen pressures of 200 and 100 mTorr, respectively. The crystal structure was characterized by X-ray diffraction, and indicated that fully epitaxial YBCO films were formed, as illustrated in Fig. 1.

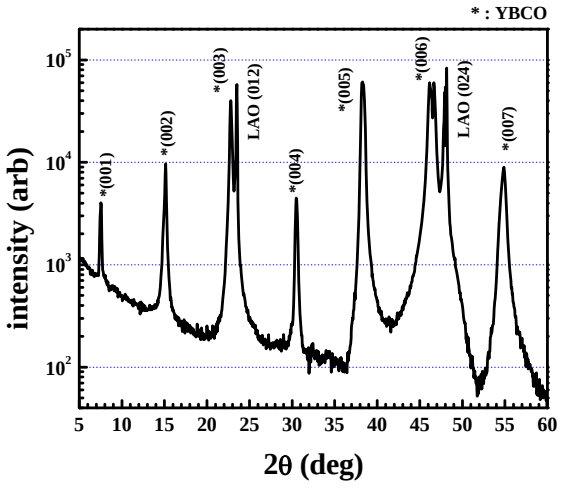

Fig. 1. XRD pattern of fully epitaxial YBCO film deposited in the new chamber,

2) Initial studies have been conducted on a series of Sm-substituted YBCO films deposited by PLD.

We have initiated a systematic study of the effects of partial Sm substitution for Y, in order to assess the possible benefits of rare-earth replacement for performance enhancement. In We have characterized the superconducting properties of these materials, deposited using the new deposition chamber and a series of ORNL-synthesized PLD targets of the compositions, $Sm_xY_{1-x}Ba_2Cu_3O_y$, for x= 0, 2.5%, 5%, and 7.5%. For the 7.5% substitution, the critical current density J_c is comparable to the optimized unsubstituted material. Here, all films depositions were conducted using parameters determined for the x=0 case, leading to the likelihood that further improvements can be achieved by optimizing deposition conditions specific to the 7.5% material.

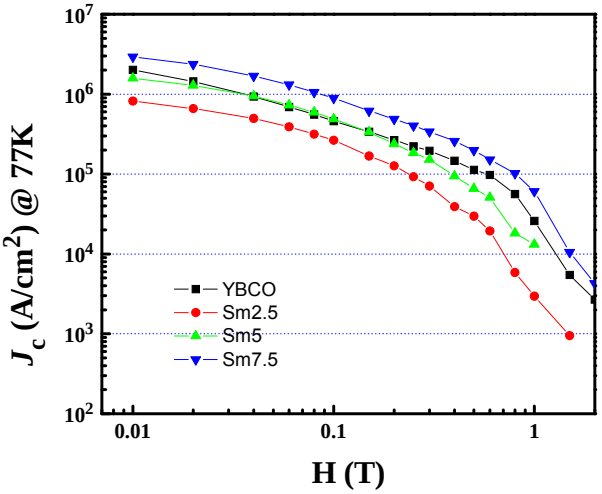

Fig. 2. Critical current density J_c measured at a low electric field criterion of 10^{-3} – 10^{-4} μV/cm, for different levels of Sm substitution in $Sm_xY_{1-x}Ba_2Cu_3O_{7-\delta}$ thin films.

3) Incorporation of self-assembled nanodots extended to NdBCO films.

Nano-scale columnar defects comprised of self-assembled BZO nanodot columns have been successfully incorporated into epitaxial NdBCO films grown on RABiTS via pulsed laser deposition (PLD). Cross-section TEM analysis showed that self-aligned BZO nanodot columns along the c-axis of the film have a dense and uniform distribution throughout the NdBCO matrix (Fig. 3). Such artificial columns resulted in remarkable enhancement in flux-pinning of NdBCO films. Compared to pure NdBCO and YBCO+BZO films, NdBCO+BZO films have significantly improved in-field properties at all field orientations. Films with such extended columnar defects exhibited a a high F_{pmax} of 9.5 GN/m^3 at 4T 77K and a H_{irr} of over 8 T.

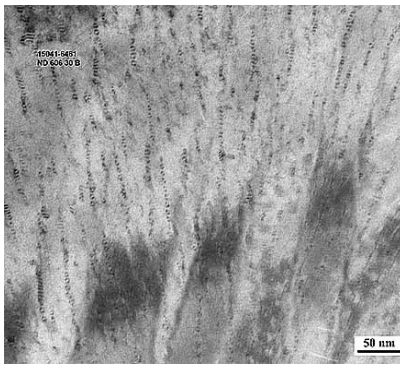

Fig. 3. Micrograph showing incorporation of BZO nanodot columns in a NdBCO film.

4) Excellent properties demonstrated in ex-situ REBCO films on RABiTS using the BaF_2 process.

Electron-beam evaporation represents a flexible and convenient method of depositing precursors of arbitrary thickness for the *ex situ* BaF_2 process. This is particularly suitable for the study of differences in the conversion among various REBCO systems. We have deposited and converted single-RE ErBCO on AMSC RABiTS. ErBCO films with a thickness of 1.2 μm were found to convert similarly to YBCO. As a preliminary result, a high critical current value of ~ 330 A/cm at 77 K (sf) was obtained. This value is comparable to that for the best YBCO films of this thickness produced by the ORNL BaF_2 process. The magnetic field dependence of J_c was

improved relative to that of recent YBCO on the same RABiTS template (Fig. 4), indicative of a higher irreversibility field H_{irr}. The latter observation hints at an improved average pinning strength.

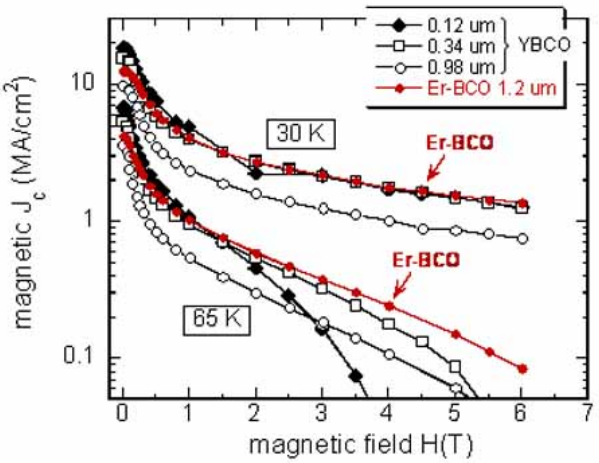

Fig. 4. Magnetic field dependencies of J_c at 65K and 30K for a 1.2 μm ErBCO ex-situ film. Also included are characteristics of YBCO films of various thicknesses.

5) Collaboration with Winnie Wong-Ng (NIST) and Tim Haugan (AFSOR) to obtain strong pinning in (Y,Sm)BCO films on coated conductors.

We have been pursuing this collaborative project with NIST and AFSOR for the last six months or so. Based on phase diagram data, NIST has fabricated 2" diameter targets of the appropriate composition $(Y_aSm_b)Ba_cCu_dO_x$. Initial data obtained shows that very significant gains in pinning can be obtained. Figure 5 shows J_c versus applied field, H, for two films. One is a Nd-123 film and the other a mixed rare-earth film of composition $(Y_aSm_b)Ba_cCu_dO_x$. The Nd-123 film has superior pinning compared to pure Y-123 films. The (Y,Sm) film clearly has better transport properties than even the Nd-123 film on IBAD. Both films were ~ 0.8 μm thick and made using PLD on IBAD substrates of configuration Hastalloy/MgO/LMO. Figure 6 shows the angular dependence data for these two films. Once again the superior pinning of the $(Y_aSm_b)Ba_cCu_dO_x$ is evident. In particular, a very strong peak for H//ab is observed. The origin of this peak is being explored.

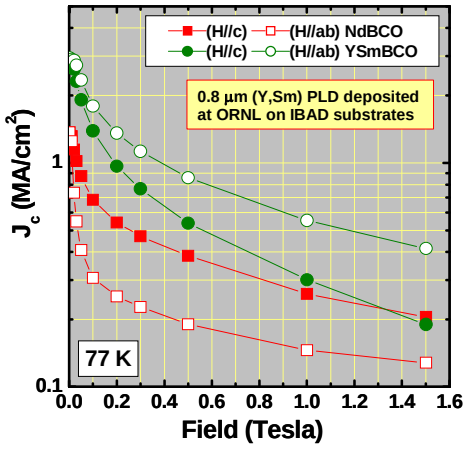

Fig.5: Critical current density, J_c as a function of applied field for a Nd-123 film and a $(Y_aSm_b)Ba_cCu_dO_x$ film on a IBAD substrate. The higher J_c for both field configurations for the $(Y_aSm_b)Ba_cCu_dO_x$ is evident.

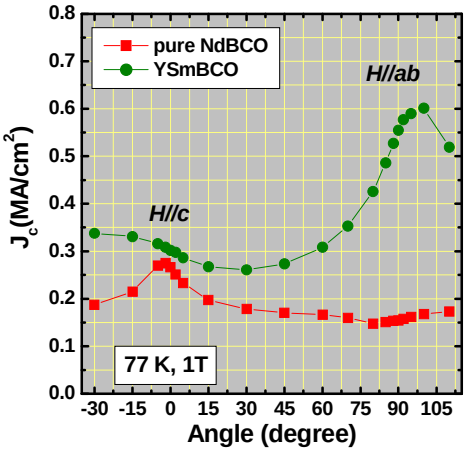

Fig.6: J_c vs angle for a Nd-123 film and a (Y, Sm) film on an IBAD substrate. A very pronounced peak for H//ab for the (Y,Sm) film is observed compared to the Nd-123 film.

Status of milestones:

- Establish the (compositions) type of effective (mixed) rare earth combinations for HTS films. (July 31, 2007): **Ongoing.**
- Improve in-field performance flux-pinning factor to less than $\alpha = 0.2$. (May 31, 2007): **Met Feb. 2007** (in conjunction with subtask 2.3).

Interactions:

Interactions include extensive collaboration with University of Tennessee on transport and magnetic characterization and pinning analysis. Interactions also include collaboration with NIST, Gathersburg and AFSOR. Results are communicated to our industry partners to assist them in process development and planning activities.

The ex-situ HTS research is performed in close coordination with the Wire Development Group to compliment and expand on the corporate research at AMSC

Subtask 2.5: Substrate simplification to reduce cost.

T. Aytug , M.P. Paranthaman, M.S. Bhuiyan, L. Heatherly, K. Kim, S-H Wee, F.A. List, S.W. Cook,

Objectives:

Buffer layers play a key role in REBCO 2G wire technology. Important buffer layer characteristics are to prevent metal diffusion from the substrate into the superconductor, as well as to act as oxygen diffusion barriers. Presently, up to 7 buffer layers are used in the standard architecture of 2G wires. To reduce cost and complexity, as well as associated mechanical and reliability concerns, it is highly desirable to reduce the number of buffer layers. This may be accomplished by utilizing multi-functional materials that can combine the tasks of various buffers into one. This project seeks to develop the materials science foundation of various candidate buffer materials suitable for a simplified substrate architecture, as well as understanding and method to improve the mechanical integrity of these substrates.

Highlights:

1) HTS Program CPS Control Milestone met - Deposit multi-functional epitaxial buffer that can replace at least 2 standard buffers with J_c of 2 MA/cm^2.

Buffer layers play a key role in YBCO 2G wire technology. The purpose of the buffer layers is to provide a continuous, smooth and chemically inert surface for the growth of the YBCO film, while transferring the biaxial texture from the substrate to the HTS layer. Important buffer layer characteristics are to prevent metal diffusion from the substrate into the superconductor, as well as, to act as oxygen diffusion barriers. In Jan. 2007, we have demonstrated in a model-system using PLD that a single $Gd_2Zr_2O_7$ layer may replace both the YSZ-barrier and CeO_2 -cap layers with J_c of 2.4 MA/cm^2. Work is underway to determine whether this high J_c can be sustained in thicker films, and whether this and other potential simplified substrate architectures are feasible for HTS deposited by commercially-selected processes.

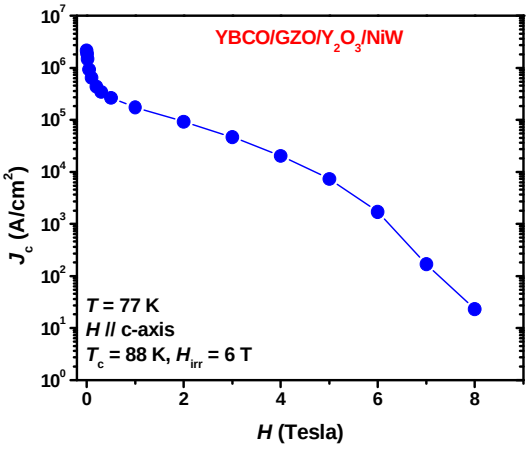

Fig. 1. Magnetic field-dependency of J_c for a 0.2 µm thick PLD-YBCO film on GZO/Y_2O_3-buffered Ni-W substrate.

The current RABiTS architecture consists of a starting template of biaxially textured Ni-W (5 at.%) with a seed layer of 75-nm Y_2O_3, a barrier layer of 75-nm YSZ, and a cap layer of 75-nm CeO_2. To achieve high throughput (increase deposition rate), both major US wire manufacturers have chosen reactive sputtering as the preferred method. Further cost savings via buffer thickness reduction and simplified buffer architecture, however, will require novel buffer materials with multi-functional properties. We have successfully deposited epitaxial films of

$Gd_2Zr_2O_7$ (GZO) on thin (10 & 75 nm) Y_2O_3 buffered Ni-W substrates. YBCO films with a J_c of 2.4 MA/cm^2 at 77 K and self-field was demonstrated on newly developed reactively sputtered GZO films using pulsed laser deposition. Field-dependence J_c for 0.2 μm thick PLD-YBCO films on GZO/Y_2O_3-buffered Ni-W substrate is shown in Fig. 1.

2) Research suggests that single solution buffer RABiTS architecture may be feasible.

The current RABiTS architecture consists of a starting template of biaxially textured Ni-W (5 at.%) with a seed layer of 75-nm Y_2O_3, a barrier layer of 75-nm YSZ, and a cap layer of 75-nm CeO_2 all deposited by physical vapor deposition (PVD) techniques. Further cost savings via buffer thickness reduction and simplified buffer architecture, however, will require novel buffer materials with multi-functional properties. We have successfully deposited solution based La_3NbO_7 (LNO) buffers directly on textured Ni-3W substrates. The powder XRD pattern for solution LNO buffers (5-coats) on Ni-W substrate is shown in Fig. 2. About 0.8 micron thick YBCO films with an I_c of 64.7 A/cm (J_c of 0.8 MA/cm^2) at 77 K and self-field was demonstrated on newly developed single solution based LNO buffers. While this performance is rather low, it shows some initial promise that thick YBCO films can be deposited on simplified buffers. Efforts are being made the study the diffusion properties of similar solution based buffers.

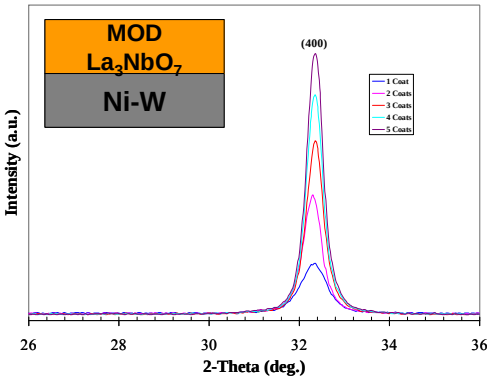

Fig. 2. Powder XRD pattern of solution LNO on Ni-3W substrate

3) Simplification of IBAD-MgO buffer architecture through the elimination of homoepi-MgO layer.

The SuperPower/ORNL High Performance LMO-enabled, High Temperature Superconducting Tape (LMOe-HTS) is a robust, high-current second-generation superconducting wire. This superconducting wire can be fabricated at high throughput rates using reel-to-reel processes. One of the key success factors which has enabled the above is the use of an epitaxial $LaMnO_3$ (LMO) buffer layer which can be deposited at high rates homogenously in long lengths. Even though the various layers can be deposited at high rates, the present SuperPower's 2G tapes still contains 5 buffer layers. To further reduce the cost of 2G wires, it is necessary to simplify the substrate. We have optimized our process conditions to sputter LMO directly on IBAD-MgO without the homo-epi MgO. The powder X-ray diffraction pattern of sputtered LMO directly on IBAD-MgO is shown in Fig. 3. C-axis aligned LMO films were obtained. In addition, LMO (110) pole figure indicate the presence of a four-fold cubic symmetry. For comparison, we also sputtered LMO on IBAD-MgO with homo-epi MgO layers. PLD YBCO films were grown on LMO films on both IBAD-MgO with/without homo-epi MgO. The field dependence J_c for both films is shown in Fig. 4. YBCO films with a comparable J_c (2.53 MA/cm^2 on IBAD-MgO without homo-epi MgO vs. 2.3 MA/cm^2 on IBAD-MgO with homo-epi MgO) was obtained on both films. Thus, we have successfully demonstrated the growth of high performance YBCO films on simplified IBAD-MgO/LMO substrates.

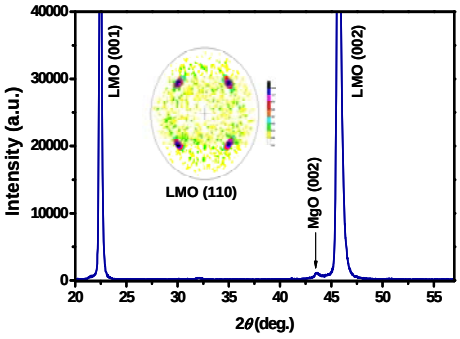

Fig. 3. Powder XRD of sputtered LMO films grown directly on IBAD-MgO. LMO (110) pole figure is shown in the insert.

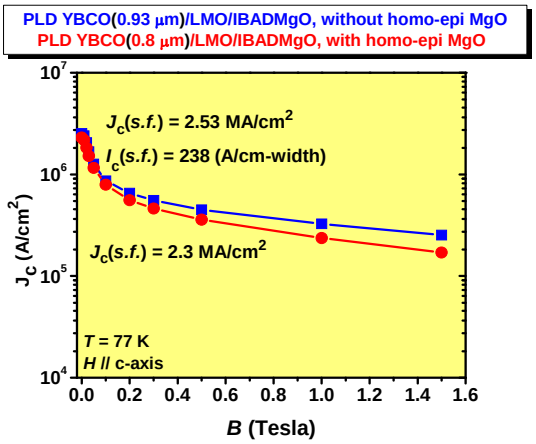

Fig.4. Field dependence J_c of YBCO films on IBAD-MgO with and without homoepi-MgO.

Status of milestones:

- Deposit multi-functional epitaxial buffer that can replace at least 2 standard buffers with J_c of 2 MA/cm^2. (July 31, 2007) **Met. Jan. 2007**.

Interactions:

Interactions include collaboration with University of Tennessee on Materials development. Results are communicated to our industry partners to assist them in process development and planning activities.

Section 2.6. Wire Development Group: Ex situ RBCO coatings with enhanced performance and flux pinning properties

R. Feenstra, F.A. List

Objectives:

The Wire Development Group (WDG) represents a multi-institution collaboration led by American Superconductor Corporation (AMSC). The primary goal is to establish a materials science basis for continued transport properties enhancement in RABiTS-2G wires featuring low-cost, ex situ $RBa_2Cu_3O_7$ coatings (RBCO; R is a rare earth or Y). Although the emphasis is on MOD-BaF_2 (TFA) processing for the RBCO layer, complimentary ex situ techniques such as PVD-BaF_2 and fluorine-free processes are also studied by the WDG. The multi-year vision presented at the 2006 Peer Review includes the reproducible achievement of wire operating at 1000 A/cm-width at 77 K, $I_c > 500$ A/cm in magnetic fields of 3 T parallel to (a,b) and 1.5 T parallel to the c-axis at temperatures ≥ 64 K, and pinning forces exceeding 20 GN/m^3 at 77 K. The WDG brings together the strengths and expertise of the collaborating institutions (LANL, ORNL, ANL, FSU, UH) to provide a framework for the necessary research and development.

Highlights:

1) Amelioration of interlayer formation in multi-coat MOD-BaF_2 precursors

To achieve large critical currents I_c in RBCO coated conductors by an MOD-BaF_2 process, AMSC has developed a multi-coat deposition process to produce precursor films of suitable total thickness. By design, the process features sub-layers which are relatively thick (0.6-1 μm), so as to minimize the number of deposition and intermediate annealing processing steps. An undesirable side effect, however, is the formation of compositional gradients though the thickness of each sub-layer. These gradients (most notably for Cu) express a dense "interlayer" of secondary phases at the interface between two stacked MOD sub-coatings during processing, affecting adversely the RBCO nucleation and growth. The severity of these effects increases with the sub-layer thickness. Building on characterization results obtained at Argonne National Laboratory (ANL) for RBCO double-coat films partially processed and quenched at AMSC, an alternative processing route ameliorating the interlayer effect was developed at ORNL.

Double-coat MOD precursors were supplied by AMSC and processed in the low-pressure conversion system described under 1). Using information provided by the real-time XRD capability, as well as post-characterization of quenched films, it was recognized that previously optimized conversion conditions induce formation of Cu_2O at the interlayer position. FIB-SEM imaging of such films (performed in close collaboration with D. J. Miller of ANL) revealed that the Cu_2O segregates into a band of nearly contiguous grains, apparently without engaging the other precursor components. By contrast, following insertion of an oxidizing processing step, the Cu can be made to oxidize to CuO, which was found to chemically react with R_2O_3 to form $R_2Cu_2O_5$. The latter oxide comprises a favorable intermediary phase in the reaction path towards RBCO.

Double-coat precursors converted using this modified process appeared structurally dense and more homogenous than counterparts converted in the presence of a Cu_2O interlayer. Magnetization measurements indicate a conservative I_c underlimit of 250 A/cm at 77 K and self-field. Although further process optimization is required to match previously reported record I_c

values, the alternative process is evidently robust. This holds promise for a reproducible route towards high-I_c values in long lengths of double-coated tape. As is customary for all work performed by the WDG, details of the processing have been transferred to AMSC who will evaluate similar approaches in their pilot production system.

2) Processing of AMSC MOD-BaF_2 precursors

One of the strengths of the WDG is the ability to incorporate out-of-the-box approaches to highlighted scientific and technological problems by synergy between the participants. As the only Laboratory participant with a hands-on thick film ex situ BaF_2 program, ORNL has taken on the task of applying their expertise in the processing of thick e-beam deposited (PVD) BaF_2 precursors towards similarly thick, multi-coat MOD precursors. Although fully processed films from PVD and MOD precursors exhibit major similarities in grain structure, grain-boundary meandering, and I_c performance, subtle differences in the precursor microstructure and fluorine chemistry mandate that subtle differences in the optimization schemes be applied. The knowledge base to simply transition between PVD and MOD precursors is presently lacking. In addition to building this knowledge base, a practical goal of MOD processing studies at ORNL is to supply an "out-of-the-box" approach to the conversion of MOD films, complementing rather than duplicating AMSC's process development.

Two furnace systems for the ex situ processing of BaF_2-type precursors are being used for this WDG research. The first is a conventional flowing-gas system (at atmospheric total pressure). High-J_c films with thickness between 0.03 and 3 μm were produced consistently with this system for films on metallic substrates converted from PVD-BaF_2 precursors. The second system is unique to ORNL and features a vacuum chamber for low-pressure conversions, resistive sample heating for fast and accurate temperature control, and real-time (in situ) XRD. This system too has been used extensively for PVD precursor processing, as well as exploratory work on MOD precursors.

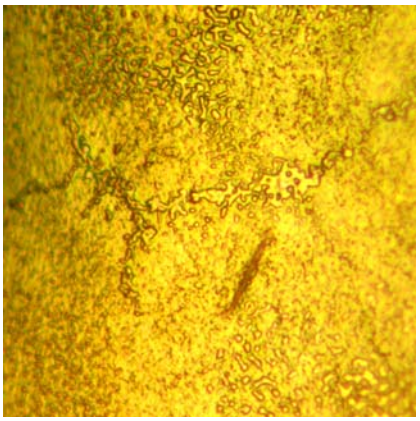
Fig. 1a.

A question of some debate is the existence and possible role of transient liquid phase(s) in the conversion BaF_2-type precursors. Although strong indications for such liquids exist, it has been difficult to prove their effect. Early experimentation with the AMSC MOD precursors in both the atmospheric and low-pressure conversion systems revealed the expulsion of large amounts of liquid to the film surface. The liquid(s) appeared in the form of droplets, puddles, as well as "eruptions". EDX analysis of the latter showed the solidified phase to be a barium-cuprate. This is consistent with the existence of low-melting phases in the Ba-Cu-O phase system. Fig. 1a shows an example of a puddle formed by coalescence of various droplets. Films with such large amounts of liquid-phase formation exhibited poor transport properties,

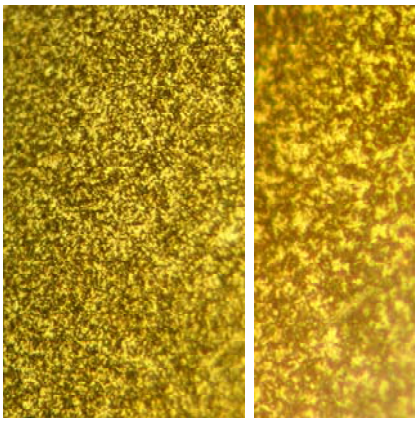
Fig. 1b

indicating the need for better control. This control may be achieved by variations in the processing conditions, most notably the ramp rate to the conversion temperature, the temperature itself, and the water partial pressure (H_2O vapor initiates the BaF_2 conversion reaction). An example of a double-coat film in which excess liquid-phase formation was successfully suppressed is shown in Fig. 1b. I_c(77 K, sf) measured by SQUID magnetometry for this film was ~240 A/cm-w. The tendency for excess liquid-phase formation was found to increase with the film thickness (i.e. number of sub-layer coatings). The direction of continuing research is to develop reproducible means to control and abate excess liquid-phase formation in the multi-coat MOD-BaF_2 films.

3) Development of a "modular" ex situ conversion process for thick, multi-coat MOD-BaF_2 precursors.

In the ex situ conversion of BaF_2-type precursors for production of $RBa_2Cu_3O_7$ (RBCO; R= rare earth or Y) coated conductors, the temperature ramp from ambient to the final reaction temperature represents a complex, yet critical part of the process. Changes in physical and chemical properties induced by the rising temperature, which precede BaF_2 decomposition and RBCO nucleation and growth, exert an *indirect* effect on critical currents and wire performance. To better understand and control the underlying dynamic events, an alternative process approach being developed at ORNL replaces the continuous temperature ramp with sequentially operated processing "modules." Each module is designed to perform a specific task and carried out under individually controlled thermodynamic conditions. The modules are linked by brief thermal ramps during which the conditions are changed. In the low-pressure conversion system available for this research, simultaneous heating (resistively) and cooling of the specimen ensures that the thermal ramps are performed fast and without overshoot. Real-time XRD feedback and high-rate quenching, furthermore, enables the generation of precursor specimens qualified to represent judiciously chosen moments of the modular process. In close collaboration with WDG co-member D. J. Miller (ANL), FIB-SEM is used for fast turnaround on the through-thickness microstructure. These unique experimental techniques provide unprecedented opportunities to derive correlations between RBCO epitaxial growth and controlling precursor parameters.

The research is performed on thick (> 1 μm), multi-coat MOD-BaF_2 precursors on RABiTS provided by AMSC. In a first iteration, processing modules are defined by comparing the MOD precursors to similarly thick PVD-BaF_2 precursors. For the latter, previous research had established the synthesis of high-J_c YBCO coatings (self-doped with excess Y_2O_3 precipitates) on AMSC-RABiTS for thickness values up to ~1.5-1.7 μm. To make thick MOD precursors resemble their PVD-BaF_2 counterparts, processing modules enabling adjustments in the F/Ba ratio (F-module) and microstructure (M-module) were successfully introduced. A useful variant of the M-module for double-coat MOD precursors, discussed also in the previous quarterly report, features the use of oxidizing processing conditions. It was discovered that microstructures resulting from oxidation prior to RBCO nucleation are favorable for amelioration of an interlayer previously found to be an obstacle for good epitaxial growth in these multi-coat precursors.

Research plans discussed at the September-2007 WDG Meeting held at ORNL call for further optimization of the presently defined processing modules on a new batch of double-coat MOD precursors supplied by AMSC to achieve I_c > 450 A/cm reproducibly. Since the modular approach is ideally suited for implementing targeted modifications to specific precursor

parameters, future research also will address presently obscure correlations between those parameters.

Status of milestones:

- Initiate conversion of MOD HTS precursor and demonstrate an initial Ic of greater than 200 A/cm. (July 31, 2007) **Met June 2007.**

Interactions:

Interactions include frequent discussions and sample exchanges with WDG members including AMSC, ANL, LANL, FSU and UH.

Section 3: Innovative and Enabling Technologies

High-impact innovative R&D that can drastically affect the performance, cost or characteristics of HTS wires. Also R&D activities in enabling technologies that are necessary for commercial applications of HTS.

Subtask 3.1 : HTS filamentization to reduce ac loss.
F.A. List, R.C. Duckworth, S.W. Cook

Objectives:
As they stand presently, as-manufactured 2G wires are approaching the performance current carrying metrics. However, these wires produce high ac losses in applied ac fields (> 1 W/m) that slow their immediate implementation into HTS applications. Creating filaments within the HTS structure presents one interesting solution that can reduce the ac loss, but further work is needed to understand and optimize filamentized 2G wires. These include filament width and geometry, filament width distribution as well as Jc distribution across the surface of the template.
This project seeks to examine and develop cost-effect means to produce filamentized 2G wire, and to understand the effects of various filament factors and geometries on ac losses.

Highlights:
1) Inkjet fabrication of filamentary conductor reveals non-uniform precursor thickness.
Inkjet printing is being evaluated as a method to produce solution precursor filaments for HTS conversion. If successful, this represents a potentially high-rate cost-effective way to manufacture 2G wires with low ac losses. Recent results of this evaluation revealed that narrow inkjet filaments exhibited substantially lower J_c than wider filaments. We have determined that inkjet filaments deposited using the present solution and conditions have non-uniform thickness profile. This variation in HTS precursor thickness may present a challenge during thermal conversion. To illustrate this, two sets of filamentary inkjet precursor samples were prepared—one with an average filament thickness 0.46 μm and the other with an average filament thickness 0.75 μm. After processing, we have determined that different optimum conversion times exist for samples of differing thicknesses (Fig. 1). These results suggest that, even for an inkjet filament that is optimally processed, the thicker regions of the filament are under-processed and the thinner regions are over-processed. This would lead to a J_c for the collective inkjet filament that is substantially lower than that if the

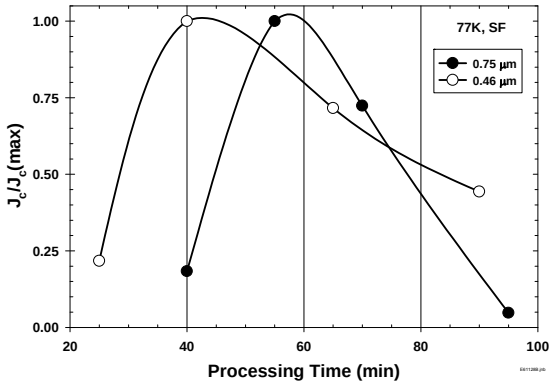

Fig. 1. Critical current density versus total processing time for inkjet precursor filaments of two different average thicknesses.

thickness were uniform. Efforts are presently underway to increase J_c for inkjet filaments by a) reducing the thickness variations of the inkjet filament and b) reducing the sensitivity of the maximum J_c on processing time and filament thickness.

2) I_c decreases with filament width in filamentized conductor produced by inkjet.

Inkjet printing is being evaluated at ORNL as a potentially low-cost, high-rate method to fabricate filamentary HTS coated conductor. The use of filamentary coated conductor in HTS applications such as motors, generators, and transformers can lead to substantial reductions in AC losses. Crack-free, HTS inkjet filaments have been successfully prepared on RABiTS substrates with a variety of filament widths ranging from ~100 μm to 1 cm. The J_c, for these inkjet filaments is found to decrease significantly and nearly linearly with decreasing filament width (see Figure 2). In contrast, the J_c for filaments prepared by laser scribing of similar HTS coated conductor is much less sensitive to filament width, especially for filament widths greater than 250 μm. The behavior of J_c with filament width for inkjet filaments is believed to be process-related and the collective result of a) a broad distribution of thickness across individual inkjet filaments and b) a strongly thickness dependent, narrow processing window for maximum J_c. Strategies to overcome these processing-related challenges are being developed and explored.

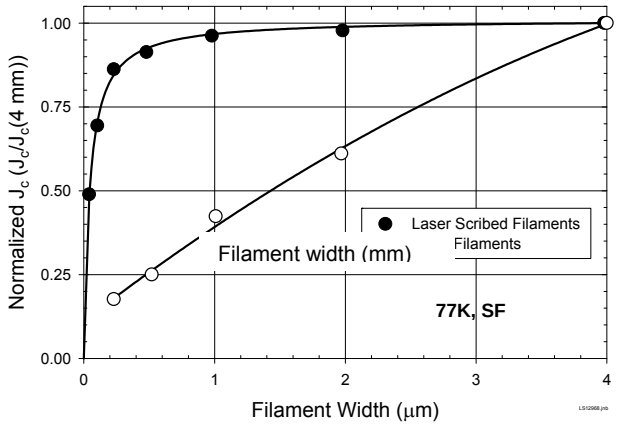

Fig. 2. Variations in I_c with filament width in conductors produced by inkjet and laser scribing.

3) Multi-filamentary inkjet-derived YBCO coated conductor reveals coupling losses.

Comparative measurements have been performed on inkjet-derived "un-filamentized" and filamentized conductors. Samples were fabricated using AMSC solution on AMSC RABiTS substrates. The un-filamentized sample was 9 mm-wide, with inkjet lines deposited without any spacing to obtain a continuous precursor layer. The filamentized sample contains spaced filaments that are 0.5 mm wide with 0.1 mm gaps. These samples were converted into HTS at AMSC, and J_c's were determined to be 2.6 and 1.0 MA/cm^2, respectively. The drop in J_c is believed to be influenced more by the slightly different conversion conditions rather than any effect of filament width to grain boundary size. AC losses were measured on companion samples as a function of field and frequency at 77 K. Curves for the estimated hysteretic loss of HTS indicate additional losses were present in the filamentary sample. When the ac losses and peak applied field are rationalized for the filamentary sample, the linear dependence of the losses indicated the presence of coupling. Despite the coupling losses still present, the intercept appears to closely match the measured critical current. Since this sample had no observable shorts, the nature of the coupling in these inkjet conductors will be investigated further through the cutting of filaments to isolate them from the substrate and magneto-optical characterization of the remaining samples.

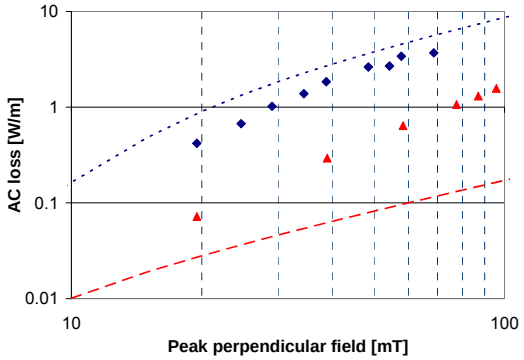

Fig. 3. Comparison of ac losses in filamentized and un-filamentized samples as a function of peak perpendicular field at a frequency of 60 Hz 77 K. Curves represent estimated hysteretic losses of HTS.

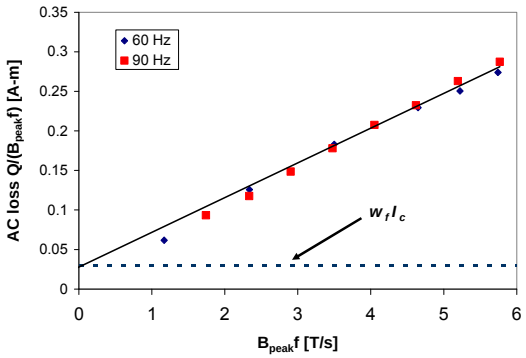

Fig. 4. AC losses rationalized with respect to peak perpendicular field and frequency for the filamentized sample at 77 K

4) Reduction of ac loss observed in YBCO filamentized samples with continuous silver stabilizer

While the reduction of ac loss in YBCO coated conductors has focused primarily on the filamentization of both YBCO and its stabilizer (copper and/or silver), a method to reduce ac loss for a continuous silver stabilizing layer has been investigated here. The use of a continuous stabilizing layer has advantages with respect to stability because current can be shared between filaments in the event of a hot-spot or filament break. However the use of a continuous stabilizer between filaments can increase the coupling losses when ac fields are applied. Through manipulation of oxygen annealing after silver is deposited on YBCO, a method to introduce barrier resistance between filaments has successfully reduced the coupling loss contribution by a factor of three in silver-coated YBCO filamentized samples.

Starting with filamentized YBCO, the YBCO surface was exposed to air for one day and then a 3 micron layer of silver was deposited onto the entire film. Once the silver deposition was completed, the samples were oxygen annealed at different temperatures for one hour, which has been shown by Ekin (1993) to impact the interface resistance between silver and YBCO. Fig. 5 shows the ac loss as a function of product of the peak applied magnetic field and its frequency. For the data shown in Fig. 15 the slope of the line indicates the level of coupling loss in the filaments; the higher the slope, the higher the coupling loss. From Fig. 5 the coupling losses decreased as the oxygen annealing temperature was dropped from 450 C to 250 C, which should coincide with an increase in interfacial resistance between the silver and YBCO. This shows that it is possible to reduce the

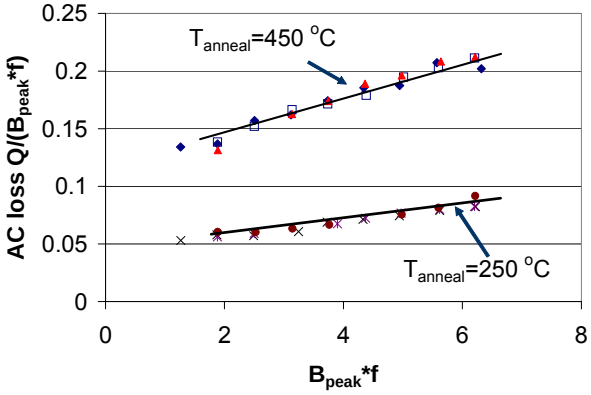

Fig. 5. Comparison of ac losses as a function of the product of the peak field and its frequency for YBCO filament samples with continuous silver stabilization that have been oxygen annealed at 250 C and 450 C for one hour.

coupling component of ac loss while maintaining on continuous stabilizing layer. Future work will focus on quantifying the contact resistance/current transfer length in this configuration and determining its impact on conductor stability.

5) eduction of ac loss by a factor of 10 in filamentized HTS conductors achieved

To establish a baseline for the work on coupling losses in continous silver stabilized YBCO filament samples described in the highlight above, the reduction in hysteretic ac loss and elimination of coupling losses between filaments needed to be established in laser etched YBCO samples. By subjecting filamentized sample to oxygen annealing to remove HTS to substrate coupling, a factor of 10 ac loss reduction was achieved.

tarting with continuous, 0.8-μm thick YBCO samples prepared in a research MOCVD SuperPower system at ORNL, a series of 1.2- cm wide, 6-cm long samples were sent out for laser scribing. The power of the laser was adjusted to remove the YBCO and buffer layers but keep the underlying substrate intact. After the samples were laser scribed, one sample was oxygen annealed at 500 °C to oxidize the electrical connection between the filaments. In previous work on laser-scribed samples, it has been shown that coupling between the substrate and the filaments was possible in laser-scribed filaments, but oxygen annealing the sample at 500 °C for 2-3 hours removes the coupling. Fig. 6shows the removal of the coupling losses for the MOCVD samples when a sample experiences a post-oxygen anneal. From the ac loss analysis for the post-oxygen annealed film, the critical current of the sample was estimated to be 181 A. When the losses in the measured sample are compared to those predicted for a continuous 1.2-cm wide YBCO sample with the same critical current (Fig. 7, a loss reduction of a factor of 10 was achieved in the filamentized YBCO sample.

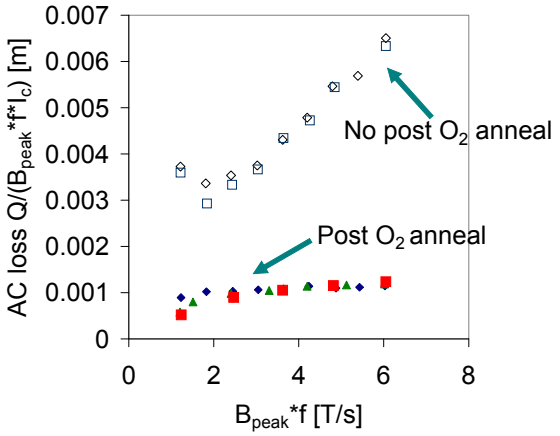

Fig. 6 Comparison of ac losses at 77 K as a function of the product of the peak perpendicular field and the frequency for a pair of laser-scribed YBCO samples--one oxygen annealed at 500 °C and the other not.

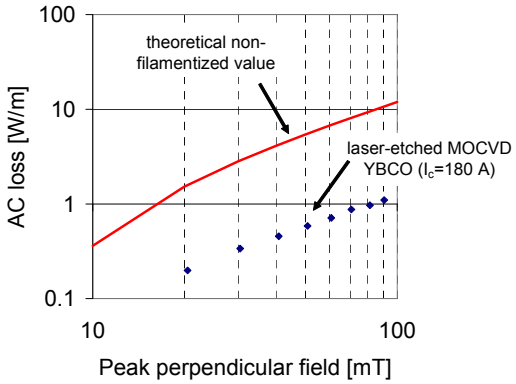

Fig. 7 Comparison of ac losses at 77 K and 60 Hz as a function of peak perpendicular field between a laser-scribed YBCO sample after oxygen anneal and theoretical ac loss for a non-filamentized YBCO sample with same critical current.

6) Preliminary ac loss and stability characterization of low ac loss geometry completed

While producing low ac loss geometries can be done in a number of different ways, the impact of these geometries on conductor stability needs to be determined so conductor stability is not sacrificed for low ac loss. With samples provided by SuperPower, experimental stability and ac loss characterization was performed on a prototype ac loss geometry where a set of striated YBCO filaments on a 4-mm wide tape were connected in series along its length via a

superconducting bridge at a center of a 25-cm long sample. When compared to a 4-mm wide non-striated YBCO coated conductor, the stability of the tape under dc conditions were similar to the YBCO striated conductor in that both tapes were damaged at 110% of the tape critical current Since damage occurred in the striated region of the sample, this supported the idea that the heating in a superconducting bridge could be considerably less than the striated YBCO regions under certain operating conditions. AC loss characterization on those sections of striated YBCO coated conductor with superconducting bridges showed that the ac loss was reduced by a factor of five for the striated YBCO coated conductor with superconducting bridges and by a factor of ten for the striated YBCO coated conductor without superconducting bridges when compared to a non-striated YBCO coated conductor with a similar critical current. This study showed how superconducting bridges impact ac loss reduction and conductor stability and provides a good starting point in order to maintain the practicality of achieving low ac loss geometries without compromising conductor stability.

As a first step to estimate the stability of Ag-coated YBCO striated samples, a constant dc current test was conducted. Each sample was mounted lengthwise onto a solid G10 mandrel and voltage taps were attached at the end of samples near the current leads. In these sets of experiments, dielectric tapes were not wound onto the G10 mandrel to isolate the tapes from the liquid nitrogen bath as was done in previous stability experiments. The omission of the dielectric tapes was due to the fact that each tape only had 3 microns of silver stabilizer and the cooling to the sample needed to be maximized in order to protect the sample from damage.

The properties of the samples are shown in Table 1. Each sample had a 3-μm thick silver cap layer, a width of 4-mm, and a length of 30-40 cm. For the sample that was striated (sample 2), there were two 12-cm long striated sections separated by a superconducting bridge 1.8-mm long as shown in figure 8. After the sample was immersed in an open liquid nitrogen bath, the critical current was measured, which was followed by constant dc current stability testing. In the constant dc current testing, the current is slowly incremented in steps until the voltage displayed a rapid, non-linear change. For all the samples tested, this non-linear change in voltage resulted in sample damage.

Table 1 – Property summary for non-striated and striated samples

	Sample 1 Non-striated	**Sample 2 Striated**
Critical current (s.f, 77 K)	147.1 A	81.5 A
n-value	30.7	21.5
Thickness of silver cap layer	3 □m	3 μm
Filament width	N/A	400μm
Filament gap	N/A	100 μm

Figure 9 shows the thermal runaway in samples 1 and 2. Even though steps were taken to increase the convection heat transfer between the sample and the liquid nitrogen bath, each sample was damaged at the operating current shown in each figure. For both samples, this damage was concentrated over a 2 to 3-cm long section of the sample and went completely through the sample. Table 2 summarizes the current and end-to-end voltage at the current where damage occurred and the previous test were the sample was still stable.

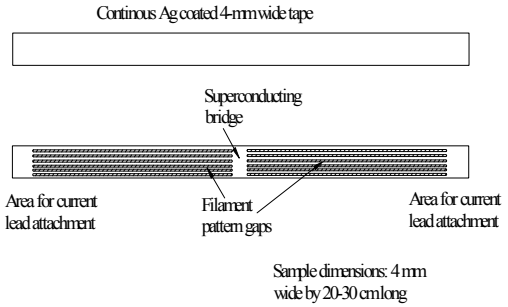

Figure 8. Comparison of striated 4-mm wide Ag-coated YBCO conductor structure to continuous 4-mm wide Ag-coated YBCO coated conductor

Averaging the heating over a 20-cm long section of the sample, the heat flux of the non-striated YBCO tape was 0.009 W/cm^2, while the striated YBCO tape had a value of 0.005 W/cm^2. While these numbers are significantly less than the critical heat flux of liquid nitrogen 20 W/cm^2, the localized damage was different between the two samples. For the striated YBCO, there were two regions of the YBCO tape where it was completely evaporated and resulted in a totally destroyed length of 3 cm, while the non-striated YBCO tape was destroyed over a 2 cm length of the sample.

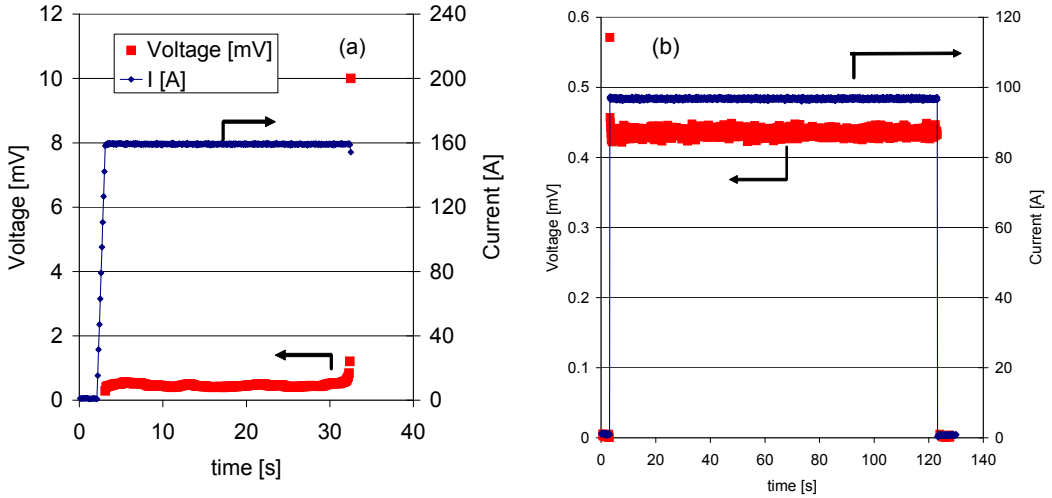

Figure 9. Constant DC current response of non-striated (a) and striated (b) YBCO coated conductors at the last stable current point before permanent damage occurred to each conductor.

Table 2 –Stability summary for non-striated and striated samples

	Sample 1 Non-striated	**Sample 2 Striated**
Critical current (s.f, 77 K)	147.1 A	81.5 A
Current at which damage occurred	159.2 A	99 A
End to end voltage at damage point	0.44 mV	>9 mV

Time to runaway	29 s	Instantaneous
Highest stable current	156.0 A	96.7 A
End to end voltage at highest stable current	0.2 mV	0.44 mV

After the stability of the striated YBCO coated conductors with superconducting bridges under constant dc current was characterized, ac loss measurements were performed on the remaining, undamaged sections of the samples. Figure 10 shows the two striation geometries that were examined. The geometry that is shown in the bottom of figure 10 was made by cutting off the superconducting bridged ends of the top geometry after the ac loss characterization was completed. It was fortunate that a section of sample with striations and superconducting sections at both ends was not damaged, because the impact of superconducting bridges and striation on ac loss could be studied together. The resultant ac loss of both geometries was compared to the ac loss in a continuous 4-mm wide silver-coated YBCO coated conductor also from SuperPower. The properties of each sample are given in Table 1.

AC losses in this conductor were measured by a thermal technique with a cernox thermometer mounted at the center of each sample and its response to the known heat input used as a calibration before ac fields were applied. The ac losses in all samples were over a field range of 20 mT to 150 mT at frequencies of 60 Hz and 90 Hz with the applied magnetic field perpendicular to the tape face. The ac loss as a function of applied perpendicular field for each sample geometry is shown in figure 11. From figure 11 it is clear that the striation of the YBCO coated conductor reduced the ac loss whether superconducting bridges were present or not. It is also evident that the lowest ac loss occurred when the superconducting bridges were removed from the striated YBCO coated conductor. This result is consistent with striated YBCO coated conductors with resistive bridges that was proposed by Ashworth where flux is allowed to penetrate periodically along the length.

Another thing to note is that the ac losses in striated YBCO coated conductor with and without superconducting bridges appear to be hysteretic. From the ac loss shown in figure 12 with the frequency of the applied perpendicular magnetic field taken into account, the ac loss for 60 Hz and 90 Hz are similar which would be consistent for hysteretic losses that depend linearly on frequency. No coupling losses were present in either geometry since there was not a linear dependence of the ac loss with respect to the product of the perpendicular magnetic field and frequency in figure 12.

While additional measurements would help better understand whether the width of the superconducting bridge impacts the ac loss, it is clear that there may be some room for conductor optimization with respect to ac loss and stability. This would only be possible if the benefits of superconducting bridges from a manufacturing and/or stability standpoint can be clearly defined.

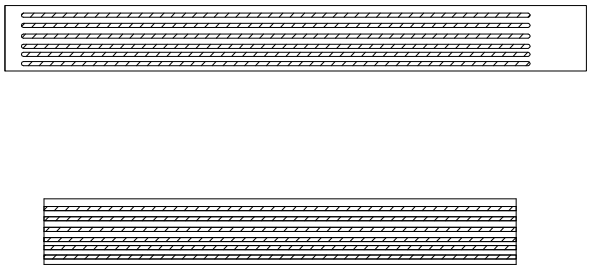

Figure 10. Geometries of undamaged, striated YBCO coated conductors that were studied with respect to ac loss. The top sketch is the striated, 4-mm wide YBCO coated conductor with superconducting bridges and the bottom is the striated YBCO coated conductor after the bridges were removed.

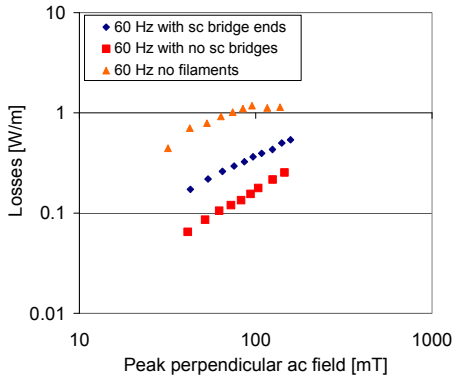

Figure 11. Comparison of ac loss in striated YBCO coated conductors with and without superconducting bridges to a non-striated YBCO coated conductor due to a 60 Hz applied perpendicular field.

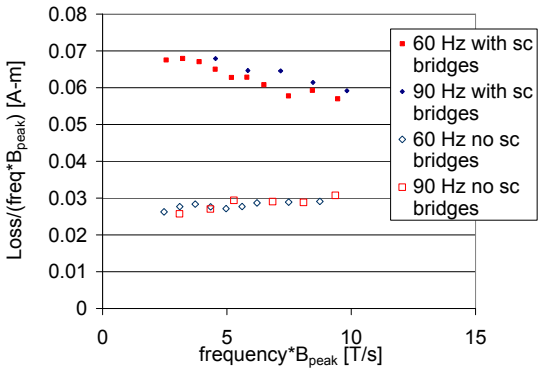

Figure 12. AC loss as a function of the product of the applied perpendicular field and its frequency for the striated YBCO coated conductor with and without superconducting bridges.

7) Alternative methods to create filament geometries explored

With filamentary geometries needed to reduce ac loss, two alternative methods to create filaments within an existing YBCO tape production process were explored where the growth of YBCO coated conductor was disrupted to create YBCO filaments separated by lines of poor growth. This interruption of YBCO growth was accomplished through the deposition/processing of YBCO inkjet filaments or low power laser-scribing of the buffered IBAD templates before YBCO MOCVD deposition in the ORNL/SuperPower MOCVD pilot center. While neither method completely removed coupling losses from the ac losses generated in applied perpendicular ac fields, the coupling losses were considerably less than that seen in inkjet filamentary structures.

To disrupt the YBCO growth and create filaments within a continuous YBCO deposition process, two methods were pursued utilizing buffered-IBAD templates from SuperPower. Figure 13 shows the inkjet disruption concept that was studied where an ORNL YBCO precursor was deposited in 250-μm wide filaments along the sample length at a spacing of 1 mm. These filaments were then converted at conditions that consistently produced non-superconducting filaments. Then YBCO MOCVD was deposited on top of the entire sample so that the non-superconducting filaments would produce isolation barriers between the filaments. When the losses were measured as a function of field and frequency and plotted in figure 14, the presence

of coupling losses indicated that the isolation was not completely successful. However, it should be pointed out that the slope of that line in figure 14, which a measure of coupling losses occurring between the filaments, was significantly less than coupling losses seen in isolated inkjet filament samples (0.015 to 0.049). The ac loss in uncoupled filaments should produce a line with a slope equal to zero when data is plotted in a manner similat to that shown in figures 14 and 16. Further optimization of the MOCVD deposition is needed to increase the sample critical current, which was less than 5 A, and determine whether inkjet disruption is a feasible method for longer lengths.

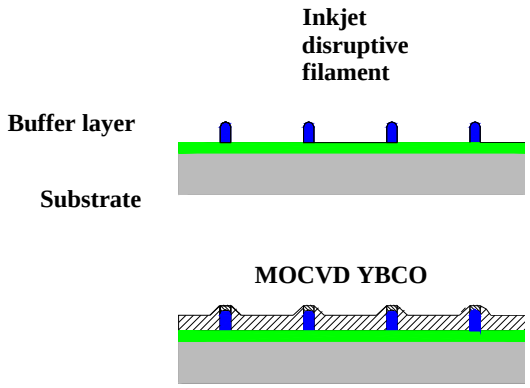

Figure 13. Schematic of inkjet disruption layer before and after MOCVD deposition

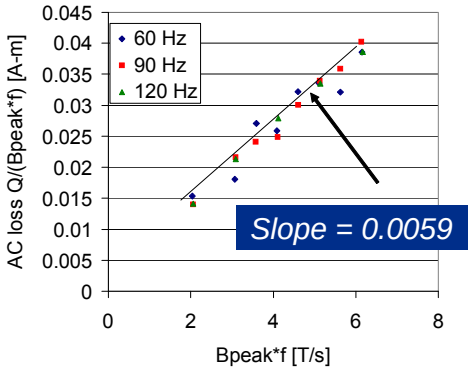

Figure 14. Comparison of ac losses at 77 K and 60 ad 90 Hz as a function of peak perpendicular field for YBCO filamentary sample made from inkjet disrupt deposition on buffered IBAD templates.

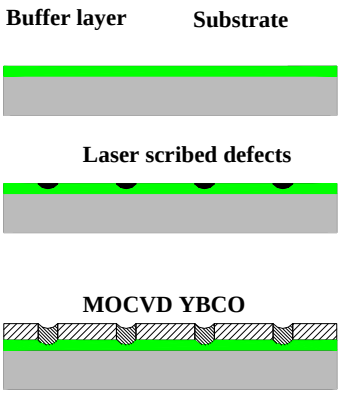

Figure 15. Schematic of laser-scribed buffer disruption inkjet disruption layer before and after MOCVD deposition

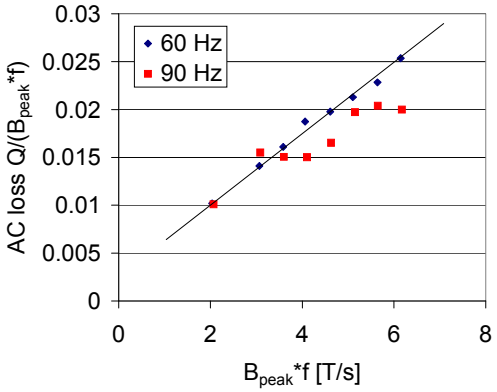

Figure 16. Comparison of ac losses at 77 K and at different frequencies as a function of peak perpendicular field for YBCO filamentary sample made from laser-scribed buffered disruption on buffered IBAD templates.

In addition to pursuing the disruption of YBCO growth via inkjet, the use of low power laser scribing was employed to disrupt YBCO growth. Starting with a buffered IBAD template, a lower power laser was used to etch away part of the buffer layer along the sample length, which would change the surface epitaxy and then disrupt the MOCVD growth as shown in figure 13.

When the ac losses were measured as a function of perpendicular field and frequency as given by figure 14, coupling losses were present in the tested films. As with the inkjet disruption layer, the coupling losses were lower than the coupling losses of direct inkjet filaments. Further research is needed to determine the nature of the coupling in disruption filaments in MOCVD filaments.

Status of milestones:

- Benchmark stability code for transient and steady state currents. (Aug. 31, 2007): **Met Sept. 2007** (for non-filamentary YBCO coated conductors).
    - This task is ongoing for filamentary samples due to lack of available long length samples with bridges from industrial suppliers to characterize.
- Reduce ac loss by 10 times with filamentized HTS conductor. (July 31, 2007): **Met June 2007.**

Interactions:

- The inkjet filamentization work is performed in close coordination with AMSC to assist in their process evaluation and planning activities.
- The filamentization work is performed in coordination with SuperPower to assist in their evaluation of low ac loss geometries from their MOCVD facilities.
- YBCO samples produced by a research SuperPower MOCVD system at ORNL were utilized. Samples were sent to Florida State University for MO imaging that will provide a better understanding of coupling losses in filamentary samples.

Subtask 3.2: Conductor design and engineering for practical HTS applications.
R.C.Duckworth, C. Rey, J. Demko, S.W. Schwenterly, M. J. Gouge

Objectives:

As long lengths of REBCO coated conductor become available from US 2G wire manufacturers, the ability to study quench and stability and ac loss in superconducting cables and coils is possible. With the emphasis of using REBCO in the SPE solicitation by DOE, quantifying these and other issues on a short sample basis and in prototype devices will be necessary to assure and accelerate the successful implementation of 2G wires into these grid applications. The goal of this project is to establish the scientific foundation to understand the behaviors of 2G wires and prototypes in the areas of ac losses, quench and stability, responses of splices, etc. Yet another purpose of this research is to develop means by which these application specific characteristics can be enhanced.

Highlights:

1) Surface preparation of HTS tape found to influence splice resistance.

Due to finite HTS wire lengths, splices will exist in most practical applications. ORNL has been investigating the splice resistance of HTS tapes as functions of: various factors, which is essential to the practical implementation of electric utility devices. Recently, we have performed a preliminary study on the "overlap resistance" (overlapping interface region) of lap joints. Tests were performed in pool boiling nitrogen at 77K. Between 50 and 100 data points were recorded in 1 power-line cycle repetition rates to determine the average values and standard deviations of series of seven (7) joints. An eighth voltage tap was connected to un-spliced region as a control mechanism.

For 1G Bi-2223 tape (I_c = 115A) with brass laminated sheath, 0.25 inch joint overlap length, Sn(60-Pb(40) solder with *no surface preparation* at 77 K, the measured splice resistance was found to increase with current (10 A, 30 A, 60 A, 90 A). At an applied current of 10 A, the standard deviation is < 10 % and decreases to < 1 % at the 90 A level.

We have compared these samples with ones made with *a paste flux in which the surface was*

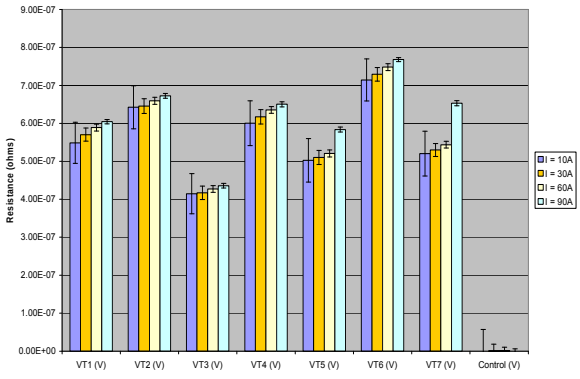

Fig. 1. Splice resistance of a Bi-2223 sample with brass lamination, 0.25 inch overlap, Sn(60)-Pb(40) solder and no surface preparation at 77 K.

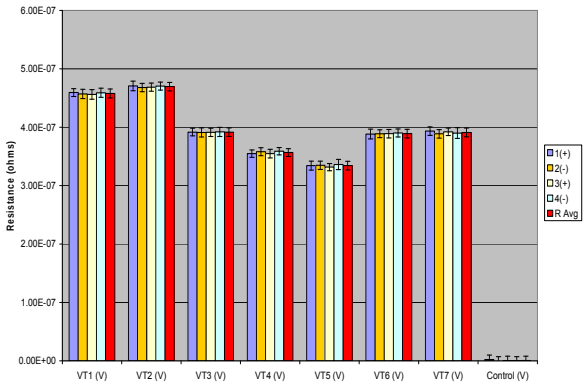

Fig. 2. Splice resistance of a Bi-2223 sample with brass lamination, 0.25 inch overlap, Sn(60)-Pb(40) solder and paste flux at 77 K with a constant current of 60 A.

clean with an ethyl alcohol wipe prior to and subsequent to ”tinning” the surface. Although the splice resistance was of similar absolute value, the consistency between successive joints is slightly improved. Understanding and controlling the variables in splice fabrication remains a key parameter for the practical implementation of HTS devices.

2) Stability measurements performed on AMSC 344 and 348 2G wires.

With increasing versatility in stabilizer lamination at AMSC, it is important to determine how the method of stabilization could impact over-current and constant current stability. A series of experiments were carried out to characterization the stability of AMSC copper laminated 344 and 348 2G wires in liquid nitrogen (77K). Major differences between the wires being the width of the copper layers and side solders. 1.1-m long 2G wires wound onto a G10 mandrel with 8 layers of dielectric thermal barrier tape were tested under constant and impulse dc current conditions; constant current mimics the operating characteristics of HTS motors whereas impulse current is more prevalent in cables and transformers.

Initial comparison of time to thermal runaway under constant current condition showed that there is some slight improvement with the 348 wire. The 348 wire was able to operate at a higher percentage of I_c. For the case of 60 seconds to runaway, the 344 wire could operate at 108% of I_c while the 348 wire could operate at 114% of I_c. As the conductor length gets longer, this difference should continue depending on the cooling conditions. For the impulse test, we were unable to identify the maximum current each wire could take before failure due to inadequate power supply and long sample length. However, we could determine the amount of energy to degrade these wires from the integrated current voltage product. As seen in the table, Initial results showed that 344 wire is slightly better than 348 in retaining I_c over length at higher energies. It should be noted, however, the current drops associated with 344 wire was greater. Further testing on shorter lengths of conductor is necessary to confirm this differential and determine the amount of current that is being utilized in each stabilization configuration.

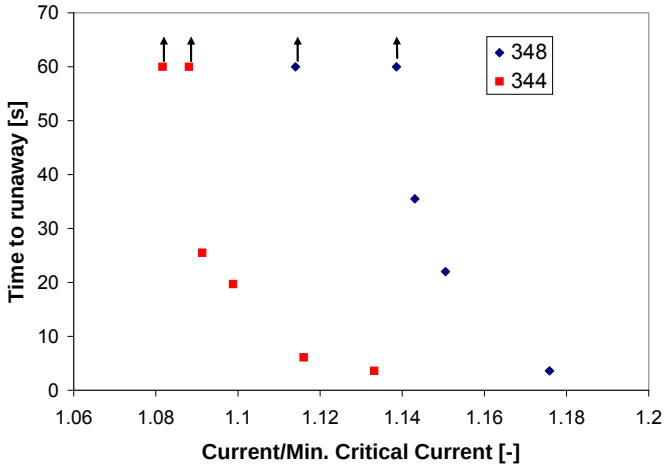

Fig. 3. Time to thermal runaway as function of the ratio of operating current to minimum Ic for the 344 and 348 wires.

Summary of impulse results for 344 and 348 superconductors.

	344 superconductor	348 superconductor
Amount of energy to degrade conductor	1524 J/cm^3	1032 J/cm^3
Percentage of degraded conductor	10%	30%

3) Modeling of stability in potentially low ac loss 2G conductor design.

One potential way to reduce the ac losses is through the introduction of periodic non-superconducting bridges in the HTS wire. Careful consideration, however, is needed to ensure that the conductor stability is not compromised. A model is being developed to determine the

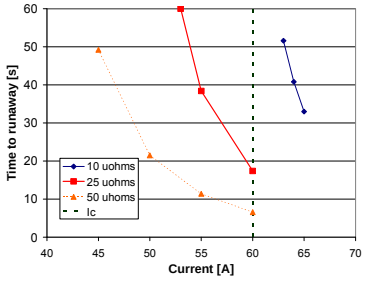

Fig. 4. Effect of bridge resistance on the dependence of time to thermal runaway with respect to current for a filamentary YBCO sample with 4 bridges at a spacing of 25 cm, an I_c of 60 A, and 3 μm of silver stabilization.

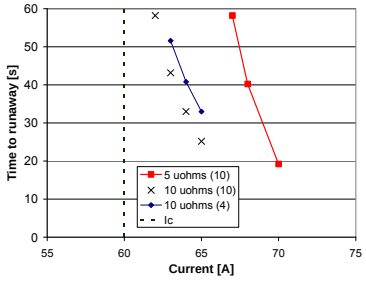

Fig. 5. Impact of number of bridges and resistance on the time to thermal runaway as a function of current for a filamentary YBCO sample with an I_c of 60 A and 3 μm of silver stabilization.

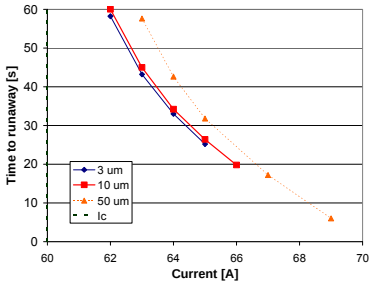

Fig. 6. Time to thermal runaway as a function of current for different amounts of silver stabilization for a filamentary YBCO sample with an I_c of 60 A and 10 μΩ bridges spaced every 10 cm.

effects of a given resistance on conductor stability. This model assumes a filamentary wire with n-value of 20, width of 4-mm, length of 1-m, I_c of 60 A at 77 K, and T_c of 90 K with stabilization coming only from the silver cap layer. Using this model, time to thermal runaway for different non-superconducting bridge resistance, number of bridges and the stabilizer thickness can be estimated. In a sample calculation, we found that the current at which runaway occurs drops below the sample I_c of 60 A when the bridge resistance is above 10 μΩ. This factor appears to affect the stability the most as changes to the number of bridges only affects stability by 10%. Also increasing the silver thickness will only provide slightly higher runaway currents.

4) Modeling of stability in as-manufactured copper stabilized 2G wires.

Localization of heating can contribute greatly to conductor stability depending on the amount and type of stabilizer. A model is being developed to better understand the formation of resistive zones in as-manufactured samples, and to facilitate fundamental investigation of properties that influence conductor stability. For a 60s constant current test case of a 30-cm long 2G wire, thermal runaway was calculated to occur when the transient voltage reaches 1 mV/s, which is consistent with experimental values. A dominant parameter was found to be the n-value of the conductor; as the n-value is increased, the voltage in the superconductor forces more current through the stabilizer and the time to runaway is much shorter. Another dominant factor is I_c uniformity along the wire length. When a slight defect (lower I_c) was purposely introduced, the time to runaway was decreased. This influence suggests that the specification of the wire I_c along a given length could greatly impact conductor stability. Comparison between numerical and experimental results is underway to determine the necessary I_c resolution for stability prediction.

5) HTS Program CPS Control Milestone met - Commissioning of enhanced ac loss testing capability.

In order to better understand ac loss in HTS coated conductors, a new test facility was commissioned and successfully brought on line in March 2007. The first operation and sample

measurements were completed in the new ac loss test facility on commercially available superconducting materials. The test facility, which is shown in Fig. 7, is a double racetrack resistive copper magnet immersed in liquid nitrogen that provides an ac background field up to 170 mT. This field is 70% higher than previous ac background coils used at ORNL. Additionally, the sample length and field orientation allow for the angle dependence characterization of longer superconducting samples. This hardware provides a valuable diagnostic tool that will address the best methods to reduce ac loss in advanced conductor geometries without having to remove the sample to adjust the field angle.

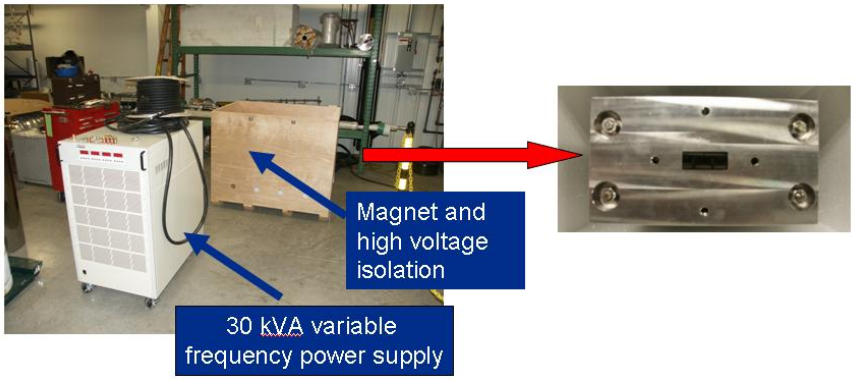

Fig. 7. AC loss test facility with 30-kVA, variable frequency ac power supply. Close-up of double-racetrack, resistive coil is shown to the right.

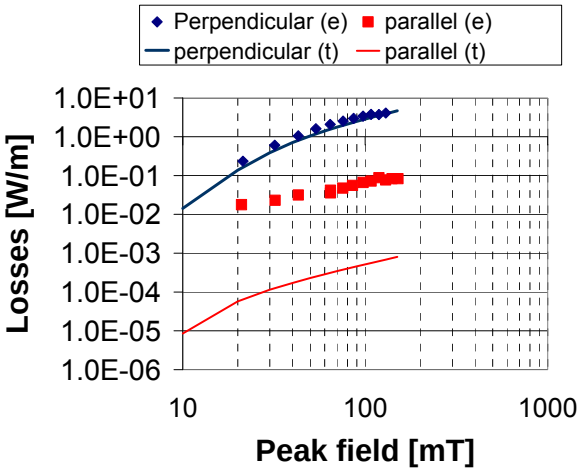

Fig. 8. AC loss at 77 K and 60 Hz in applied ac fields for an AMSC 344 superconductor with a critical current of 150 A with applied ac field perpendicular and parallel to the tape face. The Brandt model for hysteretic loss in the superconductor is shown by solid

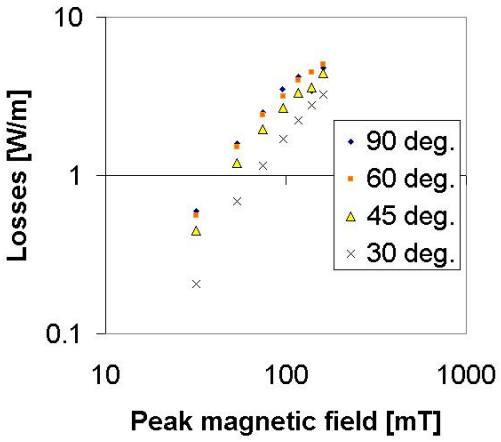

Fig. 9. AC loss at 77 K and 60 Hz in applied ac field as a function of angle for an AMSC 344 superconductor with a critical current of 150 A.

The first sample measurements were conducted on an as-manufactured YBCO coated conductor from American Superconductor (AMSC). The superconductor was a 344 superconductor with a critical current of 150 A at 77 K. This superconductor has a 4-mm wide, 75-µm thick Ni-5at%W buffered substrate with a ~ 1-µm thick YBCO superconducting layer that is laminated between two 4.4-mm wide, 50-µm thick copper stabilizing layers. The sample

was outfitted with a heater and thermometer to calibrate the thermal response of the sample to a known heat input so that when the external ac field was applied, the change in temperature was used to measure the generated ac loss. Figure 8 shows the ac losses for this sample as a function of applied ac field when the field was perpendicular (higher losses) and parallel to the tape face. An angle dependent scan of the ac loss is shown in fig. 9. While the experimental ac losses as a function of field was in agreement with the Brandt theory for perpendicular field, there was a discrepancy between the experiment and theory for the parallel fields. This discrepancy is consistent with the influence of the ferromagnetic Ni-5at%W substrate on the ac loss that has been reported elsewhere.

6) Experiment initiated to characterize the current distribution in YBCO tapes.

With YBCO having a preferred orientation for splices, it should follow that in the presence of resistive zones or faults, the copper stabilization nearest to the substrate should carry less current than the copper stabilization nearest to the YBCO. For superconducting coils, this means that this part of the stabilization decreases the engineering current density with only a possibly modest impact on conductor stability. The copper would still function as either a thermal stabilizer or a means to electrically connect the substrate to the YBCO layer. Initial results, however, suggest that stability of 2G conductors may not be orientation dependent.

To examine the stability effect, two current leads were attached to both sides of conductor as shown in Fig. 10. The copper that was soldered to each side of the conductor was identical in length and thickness and the area of solder joint was the same to prevent the resistance of the current leads from impacting the measurement. Voltage taps were attached to each current lead to measure the voltage drop across each lead. After the sample measurement was completed, the sample was removed and the current leads were calibrated through the measurement of the voltage drop as a function of current. The only common point of electrical contact during sample characterization was where the dc power source connected to the current leads. The sample and leads were held in place on a G10 sample holder and the YBCO sample was insulated with dielectric tape to isolate it in the open liquid nitrogen bath.

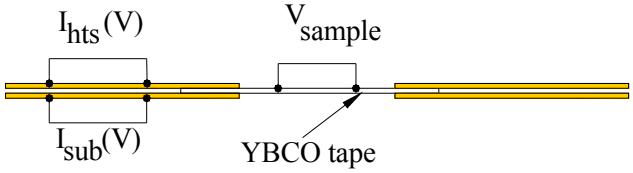

Fig. 10. Schematic of dual current lead setup.

Samples that were examined were as-manufactured YBCO coated conductors from American Superconductor (AMSC) and SuperPower (SP). From AMSC, the YBCO coated conductor was a 344-superconductor with a total width of 4.4-mm and thickness of 0.15 mm. Two 50-μm thick layers of copper were laminated with solder to the 4.0-mm wide YBCO tape, which had a critical current of 104 A and an n-value of 15 at 77 K. The YBCO coated conductor from SP was 4.0-mm wide and had copper surround stabilizer thickness of 38 μm on each side. Its critical current was 68 A and the n-value was 22. The current distribution was measured during conductor characterization (V-I curves) and for short duration, dc current impulse measurements. Figures 11 and 12 showed that during V-I measurements, the percentage of current flowing to the copper in contact with the YBCO (*Ihts%*) and the copper in contact with the substrate (*Isub%*) divided evenly as the current increased. This nearly equal distribution was

also present during the impulse measurements as pictured in Figs. 13 and 14. These results would suggest that the stability of the conductor is not orientation dependent, but further measurements of the current transfer is needed to determine whether these results are sensitive to current lead length or other factors that may artificially influence the results.

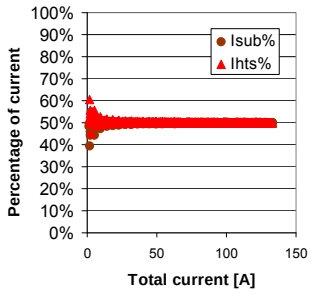

Fig. 11. Current distribution during V-I measurement of AMSC 344-superconductor at 77 K with a critical current of 104 A.

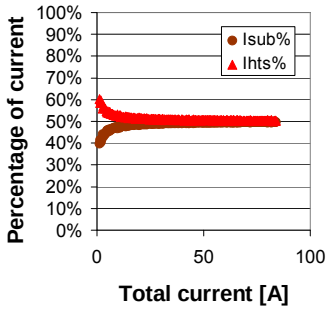

Fig. 12. Current distribution during V-I measurement of SP YBCO coated conductor with 38 μm of surround stabilizer and a critical current of 104 A at 77 K.

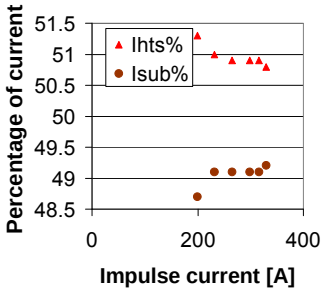

Fig. 13. Current distribution in AMSC 344 superconductor as a function of dc impulse currents.

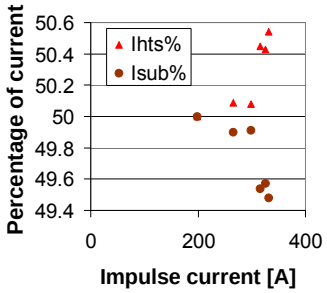

Fig. 14. Current distribution in SP YBCO coated conductor as a function of dc impulse currents.

7) Initial analyses suggest that n-value strongly influences the modeling of thermal runaway in YBCO coated conductors.

The finite difference model that was used to understand the role of critical current uniformity on conductor runway was utilized to analyze previous measurements of SuperPower YBCO tapes with different amounts of copper stabilization. Initial analyses suggest that the n-value strongly affects the modeling.

Figure 15 shows the experimental thermal runaway time as a function of current (normalized to I_c) for a set of YBCO tapes with different amounts of copper stabilization. Utilizing the thermal and electrical properties of the conductor and assuming a uniform critical current and n-value over the conductor length, figure 16 shows that the model prediction underestimated the thermal runaway time for the copper-stabilized YBCO coated conductors, while it overestimated the thermal runaway time for the YBCO coated conductor with only silver stabilization.

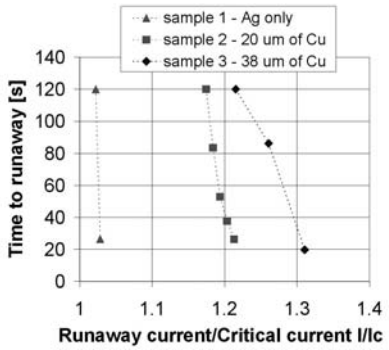

Fig. 15. Time to runaway as a function of the ratio of the runaway current to end-to-end critical current. The amount of copper-surround stabilizer is indicated for each sample. Lines shown are meant as visual guides and not trends in the experimental results.

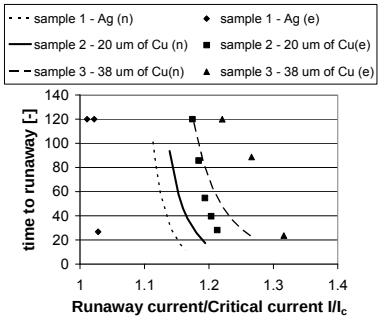

Fig. 16. Comparison between numerical (n) and experimental (e) results for the time to thermal runaway as a function of the ratio of current to critical current for samples 1, 2, and 3.

The differences in figure 16 are strongly influenced by the n-value of each conductor. The numerical simulation results that are shown in figure 17 for samples 2 and 3 (20 μm and 38 μm of surround copper stabilizer respectively) indicated the jump in thermal runaway has more to do with n-value than the amount of copper stabilization. Since the thermal runaway is a balance between resistance of the superconductor and the resistance of the metal layers, the YBCO coated conductor with only silver stabilization may have had a region of localized high n-value, which could explain the difference in numerical and experimental results for the sample with only silver stabilization.

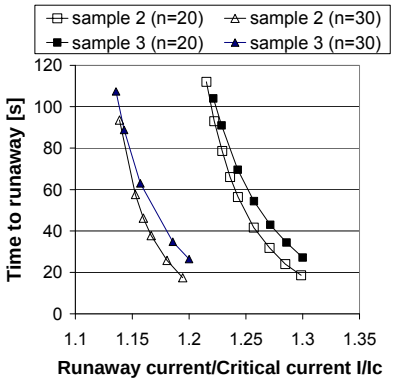

Fig. 17. Numerical prediction of time to runaway as a function of current for samples 2 and 3 with selected n-values

8) Experimental ac loss measurements completed in YBCO prototype cables.

To help with the successful implementation of YBCO coated conductors in future superconducting cable projects, two single-phase, 1.25-m long YBCO cables were successfully design, fabricated, and tested. These high temperature superconducting cables were constructed to determine differences, if any, in YBCO cable construction and performance when compared to BSCCO-based superconducting cables. In addition, these YBCO cables allowed for the investigation of YBCO coated conductors from both American Superconductor and SuperPower, which could give us some insight how the different tape architectures affect cable performance. While these tapes have widths of approximately 4 mm, the method of copper stabilization affects the tape stiffness and thickness and could impact the installation and performance of a YBCO

cable. We have found that normalized ac losses of the two cables converge at higher I_{peak}/I_c ratios, indicating that increasing the I_c is an effective way to reduce transport losses.

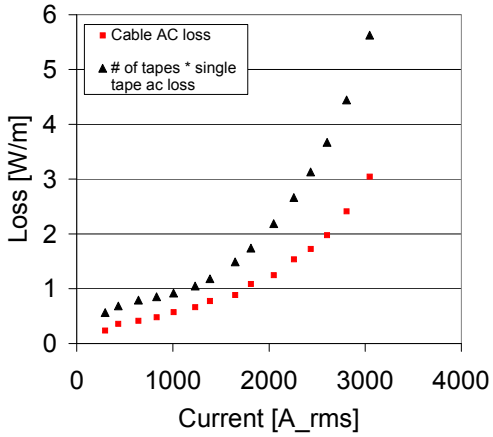

Fig. 18. AC loss at 77 K for AMSC cable as a function of ac current. The single tape results that is shown above is the ac transport loss on an individual AMSC YBCO tape multiplied by the number of tapes in the cable.

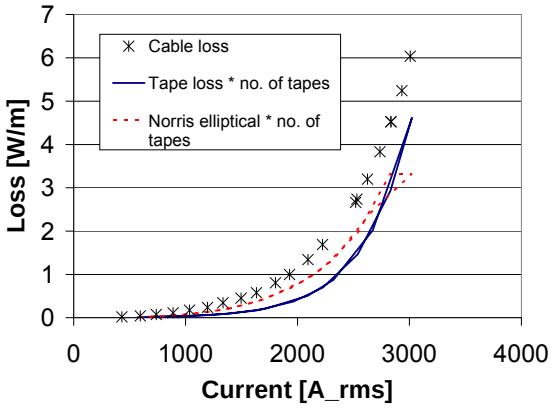

Fig. 19. AC loss at 77 K for SP cable as a function of ac current. The single tape result that is shown above is the ac transport loss on an individual AMSC YBCO tape multiplied by the number of tapes in the cable.

Each cable consisted of two layers of YBCO tapes wound on an insulated 1.5" former. These tapes were wound at opposing +/- 20 angles which allowed the current distribution to be similar as current distribution in long length cables. Based on the single tape specifications that were provided by AMSC and SuperPower, the critical current of both cables at 77 K was greater than 95% of the single tape values. The critical current in the AMSC cable was 5380 A and 4300 A for the SP cable; both values are almost twice the critical current in other YBCO cables that have been reported publicly. Fig. 18 and 19 show the ac loss as a function of current for both cables and each cable was compared to the single tape ac transport loss multiplied by the number of tapes. While the functional dependence for the ac loss in the AMSC cable was similar to the single tape values, this was not the case in the SP cable. Despite this difference, there is some common functionality between the two when the critical current is taken into account as is done in Fig. 20. While the ferromagnetic substrate of AMSC causes a divergence at low currents, the convergence of the ac loss of the two cables indicate the increasing the cable critical current is an effective means of reducing ac loss in YBCO cables. Additional modeling is underway to better understand the source of the ac loss in the cable, which will meet the HTS milestone for minimization of ac loss in cable by the end of September.

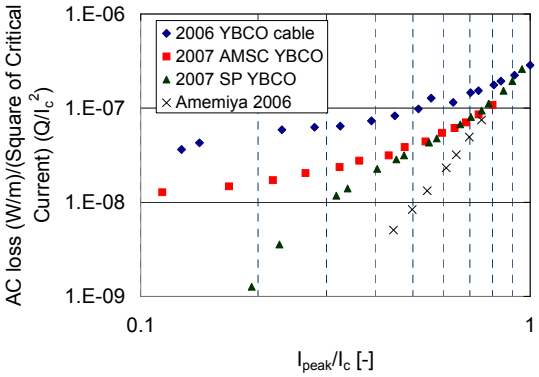

Fig. 20. AC losses in AMSC and SP prototype YBCO cables divided by the square of the critical current as a function of the ratio of the peak current to the critical current.

9) New test facility used to study ac loss in spliced YBCO coated conductor geometries

Building on the successful commissioning of our new ac loss test facility, the reduction of ac loss was examined in assembled geometries using as-manufactured YBCO coated conductors. The use of as-manufactured YBCO is being considered as an alternative in the event that the cost increase that is associated with the filamentization of YBCO is significantly higher than the project tape cost.

During the last year, it was observed that spliced stacks of YBCO coated conductors reduced ac loss when compared to the non-spliced stacks of YBCO coated conductors as shown in Fig. 21. A spliced stack of YBCO, which is shown in Fig. 22, consists of two 2-mm wide YBCO coated conductors, which are soldered together and a break is added to a single tape to create a low resistance joint. On a longer sample, the two 2-mm wide YBCO conductors would have periodic breaks in opposing layers to introduce low resistance joints along the length. However based on the previous result it was not clear whether the break was the source of the ac loss reduction or the second superconducting tape.

By expanding the available sample area exposed to a given field in the new test facility, a new set of samples were made were just a simple copper splice was placed in the center of a 4-mm wide YBCO and compared to a continuous 4-mm wide YBCO tape with approximately the same critical current. From Fig. 23, there is a reduction observed for the copper spliced YBCO sample, but it was not of the same order as was seen previously in Fig. 22. While the resistive break may have helped, its influence on ac loss reduction may be secondary to the presence of the second YBCO tape. Further testing of 2-mm and 4-mm wide YBCO samples will confirm this possibility.

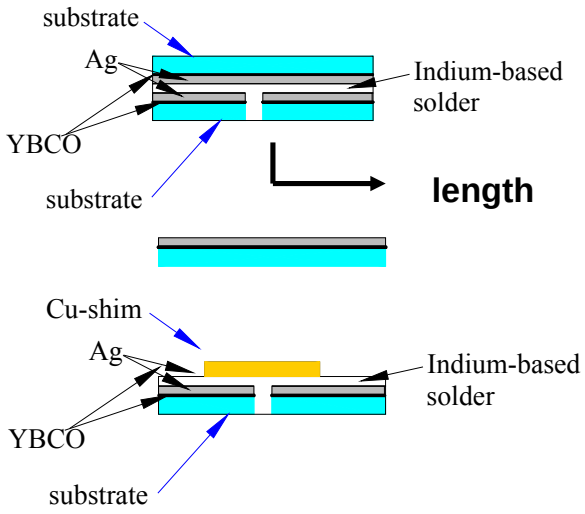

Fig. 21. Schematic of splice stack of 2-mm wide YBCO tapes (top) and of single YBCO tape with

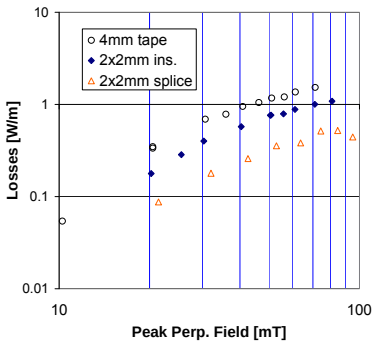

Fig. 22. AC loss at 77 K and 60 Hz as a function of peak perpendicular field for a 4-mm wide YBCO (Ic=60 A), an insulated 2x2-mm wide YBCO tape stack, and a spliced 2x2-mm wide YBCO tape stack.

10) Splice measurements on YBCO coated conductors show orientation dependence, solder material secondary

Splices are an essential part of the construction of all superconducting devices. If the splice resistance is too high in a given device such as a transformer, motor, or cable, then additional heating could limit the operational limits of the device. Building on previous results of splices with BSCCO, a series of splices were made with 344-superconductor from American Superconductor and copper-surround stabilized YBCO from SuperPower to determine best practices for splices with a focus on solder material, splice length, and sample orientation. Sample orientation refers to whether the copper closest to the YBCO in the first sample is soldered to the copper closet to the YBCO in the second sample (H-H) or soldered to the copper closest to the substrate (H-S).

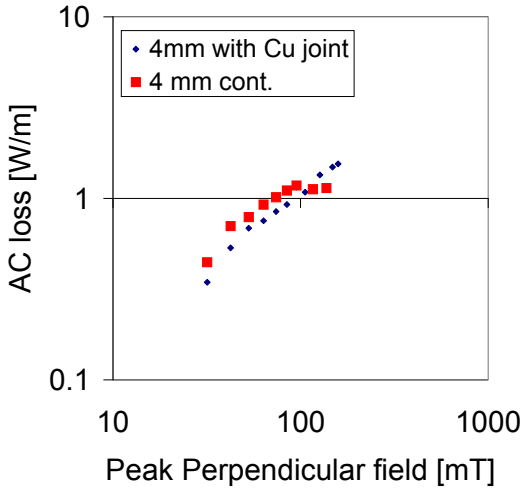

Fig. 23. Comparion of the ac loss at 77 K and 60 Hz for a copper-spliced 4-mm wide YBCO coated conductor and a non-spliced 4-mm wide YBCO coated conductor.

For each sample run, seven different splices are made for a given splice length, material, and orientation. The voltages are measured as a function of current for each splice as well as a control section of the YBCO tape, which makes sure the voltage that is measured, is below the critical current of the sample. A schematic of the sample and sample test setup is shown in Fig. 24

Fig. 25 shows the splice resistance as a function of splice length for both AMSC and SP tapes for different solder materials and orientations. For similar solders, there was no real difference between AMSC and SP tapes and the splice resistance. However for similar tapes and solders, the splice resistance increased by an order of magnitude. While the resistance is still below 1 μohm, the orientation may become an issue as the operating current increases for a given application.

Fig. 24. Experimental setup for splice measurement of YBCO coated conductors and schematic of series of splice joints that was wound on the anodized aluminum mandrel.

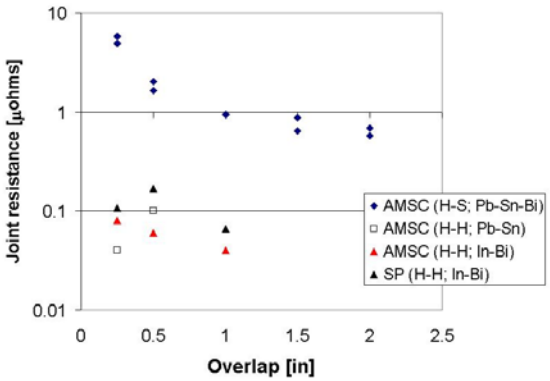

Fig. 25. Splice resistance as a function of splice length for different YBCO tapes, orientation, and solder materials

11) AOP milestone met for "Establish the level of stability in spliced YBCO samples".
For HTS electric devices such as cables and transformers, superconducting splices or joints between YBCO coated conductors are needed to connect shorter lengths of YBCO coated conductors when longer tapes are not available or when localized damage necessitates repair. Because YBCO has a different tape geometry than BSCCO, the orientation of the YBCO tapes within a splice could result in a higher joint resistance and impact the stability of the device. To gain understanding as to the impact of joint resistance on stability at the tape level, a test was conducted where the long-length, dc constant current stability of a spliced YBCO coated conductor was compared to the stability of the same YBCO coated conductor without a splice in an open liquid nitrogen bath. It was found that there was little difference in the stability between a non-spliced YBCO coated conductor and a YBCO coated conductor with a 8.9 μΩ splice. This splice resistance represents a worst case splice scenario since the copper near the YBCO is attached to the copper nearest the substrate and shows that, on a single tape basis, conductor stability in a liquid nitrogen bath is not compromised.

The stability of spliced YBCO samples was measured through the monitoring of the voltages along a 1-m length of 344 superconductor provided by American Superconductor. This 344-superconductor consisted of a 4-mm wide, YBCO silver coated tape that is laminated between two 50 μm thick pieces of copper. In the center of the 1-m length, a 1" long splice was fabricated with the copper side closest to the YBCO soldered to the copper side closest to the substrate. This orientation typically results in the highest splice resistance assuming the solder type and solder conditions are comparable. The 1-m long YBCO sample is secured to a solid G10 rod and then insulated with dielectric tape to impede heat transfer from the liquid nitrogen bath to the tape, which simulates the cooling geometry frequently seen in transformers and cables. After the sample was cooled down, the splice resistance and sample critical currents were measured at 77 K and then the dc current held at different constant current values to determine the current where the stability of the YBCO coated conductor is compromised. Figure 26 shows examples of runaway in the non-spliced and spliced YBCO coated conductors. A non-zero voltage contribution in the spliced YBCO coated conductor (V5) was observed but it did not lead to runaway in the tape. When comparing to the time to runaway and the critical currents for each case as given by figure 27, the current at which runaway occurred were comparable.

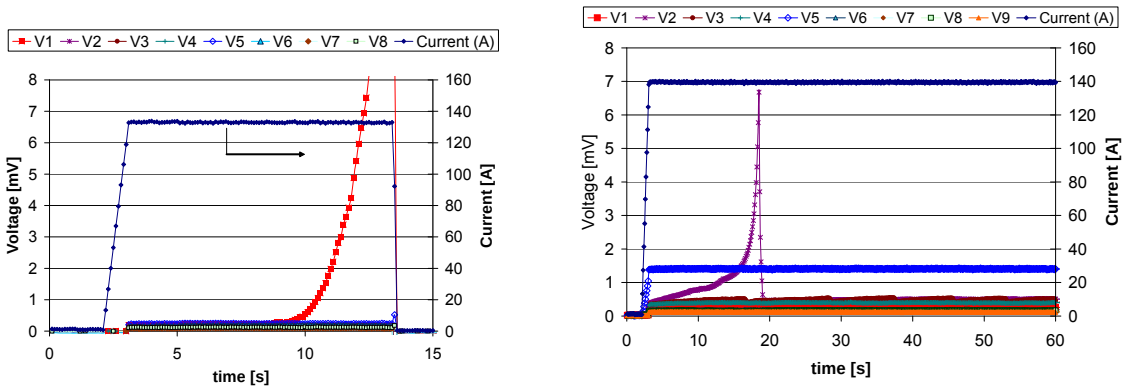

Figure 26. Comparison of observed voltages when a constant dc current is applied to a non-spliced YBCO coated conductor (top) and a spliced YBCO coated conductor with a 8.9 μΩ splice (bottom). The YBCO coated conductor used in both cases was a 344 superconductor from American Superconductor with the self field critical currents at 77 K of 120 A for the non-spliced YBCO coated conductor and 131 A for the spliced YBCO coated conductor

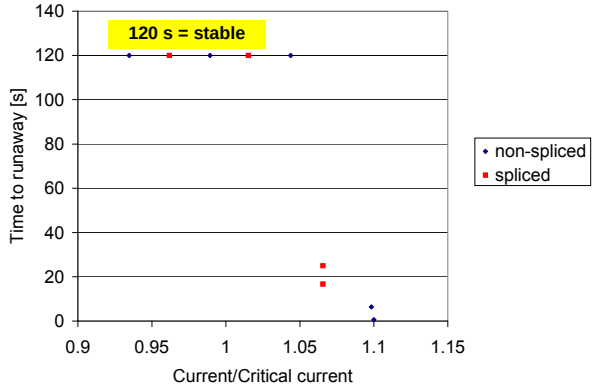

Figure 27. Comparison of time to runaway as a function of the ratio of current to critical current for the non-spliced and spliced YBCO coated conductors.

12) AC losses measured in stacks of twisted YBCO coated conductors

As currently configured, ac losses that are generated by applied ac fields in as-manufactured YBCO coated conductors are high enough that it makes HTS applications such as transformers and some fault current limiter designs challenging. While a considerable effort worldwide is looking at ways to create low ac loss filamentary YBCO coated conductors, assembled geometries present a possible alternative to reduce ac loss if the pathways to filamentization add considerable cost or complexity to the conductor. To determine the effectiveness of assembled geometries, a set of 2-mm wide YBCO coated conductors were stacked and then twisted at different twist pitches to see how the transposition of tapes affected the ac loss in an applied ac field. While there was a slight reduction observed when the twisted tapes are compared to a non-twisted stack of 2-mm wide YBCO tapes, the reduction in ac loss could be explained by averaging the ac loss of the non-twisted, 2-mm wide stack of YBCO coated conductors at the angle between the tape face and applied ac field. This twisting resulted in ac loss that was almost invariant to the orientation of the tape face to the applied ac field.

AC losses were measured in a series of stacked 2-mm wide YBCO coated conductors that had been twisted at different twist pitches. Each sample was prepared by taking two 2-mm wide YBCO coated conductors that were provided by SuperPower and putting them face to face with a thin insulating layer between them. With one end fixed, the stack of conductors is twisted to the desired twist pitch and then epoxy potted with a heater and thin platinum wire to hold the twist pitch during measurement. The single tape critical current at 77 K, self field is between 25 A and 30 A. The use of two 2-mm wide tape is motivated by seeing if there is an advantage gained from an ac loss perspective in this configuration when compared to a single 4-mm wide YBCO tape with the same total critical current, which in this case would be about 60 A.

Figures 28 and 29 show the ac loss as a function of angle at 60 Hz for non-twisted 2-mm wide stack of YBCO coated conductors and a twisted 2-mm wide stack of YBCO coated conductors respectively. The non-twisted 2-mm wide stack of YBCO shows the typical angular dependence on ac loss with the lowest ac loss for the case when the applied field is parallel with the tape surface (0^0). However it is interesting to note that the angular dependence on the ac loss in the twisted YBCO tape is not strong. While there is slight reduction in ac loss in perpendicular fields and a larger increase in ac loss in parallel fields in twisted YBCO coated conductors, the small change in ac loss with field angle could be advantageous in that the ac loss for a given coil

configuration could be calculated by the magnitude of the field and not this orientation to the conductor. Further work will be guided to determine the impact of electrical connection on twisted stacks of YBCO coated conductors, which is important from a current sharing and stability standpoint in large sample lengths.

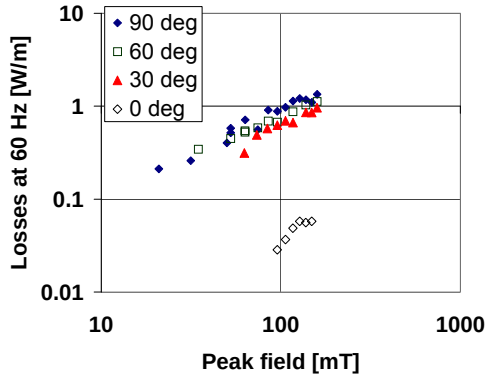

Figure 28. AC loss at 60 Hz and 77 K as a function of applied field and its orientation for an insulated, non-twisted stack of two 2-mm wide YBCO coated conductors with critical currents of 27 A each.

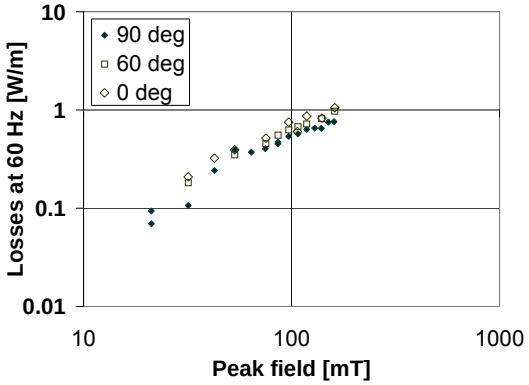

Figure 29. AC loss at 60 Hz and 77 K as a function of applied field and its orientation for an insulated, twisted stack of two 2-mm wide YBCO coated conductors with critical currents of 27 A each and a twist pitch of 12-cm.

13) Methodology of ac loss minimization in YBCO cables proposed

With the proposed number of YBCO cable projects increasing significantly over the next few years, recommendations as to best method to reduce ac loss in YBCO cables are needed. Previous models of ac loss in HTS cables are difficult to apply because YBCO layers are approximately 200 times thinner than BSCCO, which results in different field penetration in the tapes when current is applied to the cable. The basis for the recommendations for low ac loss in YBCO cables was obtained from the successful testing and analysis of two 1.25-m prototype cables with similar cable construction but with different YBCO tapes (one with AMSC and the other with SP 2G tapes) and after a review of data from other YBCO test cables and models that have been done worldwide. Table 1 summarizes the cable dimensions and parameters for the YBCO cables made from AMSC and SP 2G conductor as well as the dimensions for a hypothetical BSCCO cable on the same diameter former. Based on the experimental data, increasing the cable critical current appears to be the most effective means at reducing ac loss for an given operating current. While the removal of the ferromagnetic material in AMSC 2G tape would decrease ac loss further at low operating currents (I_{peak}~0.1-0.5 of I_c), the ac loss in the higher operating current range is dominated by hysteresis loss in the HTS material. The similarities in the ac loss observed in each cable were in contrast to expected differences in the ac losses due to tape-to-tape spacing and spacing between tape layers that have been predicted by several numerical models. Since each YBCO cable produced a unique configuration with respect to the space between adjacent tapes and the space between the tape layers, additional testing on longer length cables is needed to determine whether these physical parameters are primary or secondary factors in the ac loss of cables.

The ac losses in the AMSC and SP YBCO cables were different in that the AMSC cable ac loss was approximately 50% of the single tape ac transport current loss multiplied over the number of tapes and the SP cable ac loss was approximately two to four times of the sum of the

ac transport current loss in the individual tapes when plotted as a function of ratio of the peak current to the critical current as shown in figures 30 and 31. However when the critical current is taken into account by dividing the ac loss by the square of the critical current as shown in figure 32, the ac losses in the two cables begin to converge as the peak to critical current ratio approached one. The monoblock model was used to represent the ac loss in the BSCCO cable that is shown in figure 32 since the monoblock model has been used successfully in the past to predict ac loss in BSCCO cables.

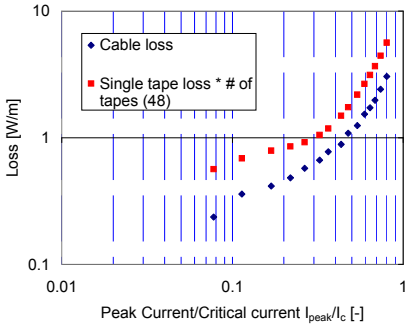

Figure 30. AC loss as a function of peak current ratio for a 1.25-m long AMSC YBCO model cable with a critical current of 5380 A. The ac loss of the cable is compared to the transport current ac loss of a single tape multiplied by the number of tapes in the cable.

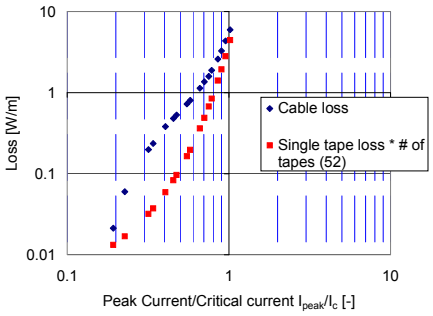

Figure 31. AC loss as a function of peak current ratio for a 1.25-m long SP YBCO model cable with a critical current of 4300 A. The ac loss of the cable is compared to the transport current ac loss of a single tape multiplied by the number of tapes in the cable.

The physical parameters listed in Table 1 are shown in figure 33 to better understand how the distance between adjacent tapes, $d_{buttgap}$, and the distance between layers, d_{layer}, and the thickness of the superconducting layers relate to each other. The distance, $d_{buttgap}$, is the separation between two adjacent tapes in the same layer and the distance, d_{layer}, is the separation between the superconducting materials in each layer.

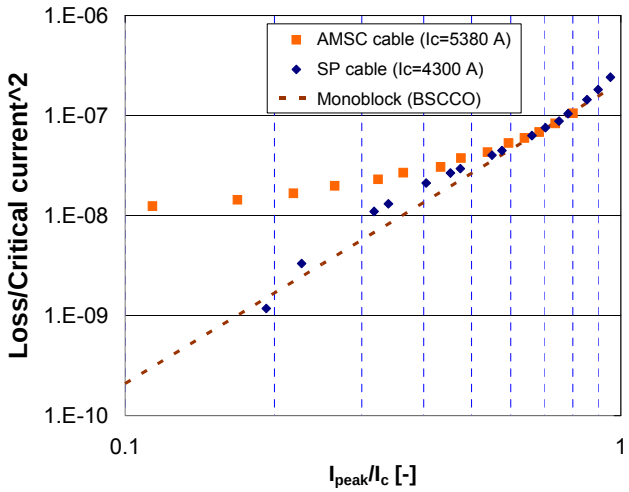

Figure 32. AC loss divided by the square of the cable critical current as a function of peak current ratio for the two YBCO cables. Monoblock model shown is for a BSCCO cable with the same former diameter.

From figure 33 and table 1, it should be observed that relative thickness of the superconducting layer to separation between the layers, d_{layer}, is smaller for the YBCO cables than the BSCCO cable. This distance changes how the field generated by the current in the cable penetrates the superconductor. This distance, which is the result of the change in thickness of the superconductor, changes how the field generated by the current in the cable penetrations in the superconductor. This difference in field penetration should influence how the ac loss is produced in the YBCO cables. In BSCCO cables, the ac loss from the field parallel to the tape is the primary source of ac loss due to the thickness of the tape. However because of the reduction in the superconducting thickness in YBCO cable, the perpendicular field generated within the buttgap space between two adjacent tapes in a given layer becomes more important. With the differences in $d_{buttgap}$ between the AMSC and SP YBCO cables, it was expected that the ac loss as a function of current would be functionally different over all currents. This was not the case as the ac losses of the two cables were very similar as the I_{peak}/I_c approached 1. The only way that this could be possible is if the field penetration of ferromagnetic AMSC tape with the larger $d_{buttgap}$ is similar to non-ferromagnetic SP tape with smaller $d_{buttgap}$. This is different than from what has been proposed by ac loss finite element modeling that has been done by other groups, which has shown that as $d_{buttgap}$ increases the ac loss in the cable approaches the sum of the transport current ac loss of the individual tapes. The difference between these models and the experimental results indicates that careful systematic testing is needed to determine the significance of the physical parameters of the cable.

Table 1. Parameters of 1.25-m long YBCO prototype cables made from AMSC and SP tapes and a hypothetical BSCCO cable that will be used for ac loss comparison through the monoblock model.

Cable	AMSC YBCO	SP YBCO	BSCCO
Cable critical current	5380 A	4300 A	5500 A
n-value	22	28	15
Former diameter, D_{former}	38.1 mm	38.1 mm	38.1 mm
Inner diameter, D_{inner}	38.23 mm	38.18 mm	38.22 mm
Outer diameter, D_{outer}	38.72 mm	38.44 mm	38.66 mm
No. of layers	2	2	2
No. of tapes per layer	24	26	24
Width of tape	4.4 mm	4.0 mm	4.4 mm
Thickness of tape	0.2 mm	0.126 mm	0.31 mm
Avg $d_{buttgap}$	0.4 mm	0.1 mm	0.4 mm
Average d_{layer}	0.24 mm	0.13 mm	0.132 mm

As was mentioned earlier, the monoblock model was used to determine how the ac loss in a BSCCO with the same former diameter would compare with the ac loss in the YBCO cables. From figure 32, good agreement at high I_{peak}/I_c between the monoblock model and the YBCO cables is shown, which is unexpected given the fact that the ac loss of the monoblock model is generated by the field parallel to the tape face and the ac loss generated by the YBCO tapes is

due to the perpendicular fields within the butt gaps. This coincidence needs to be put in the perspective in that this is the first time that the monoblock model matched an experimental result for ac loss in a YBCO cable. Additional work is needed to come up with an engineering formulation to predict ac loss in YBCO cables. Until then, increasing the cable critical current is the easiest way to reduce ac loss in a YBCO cable at a fixed ac operating current.

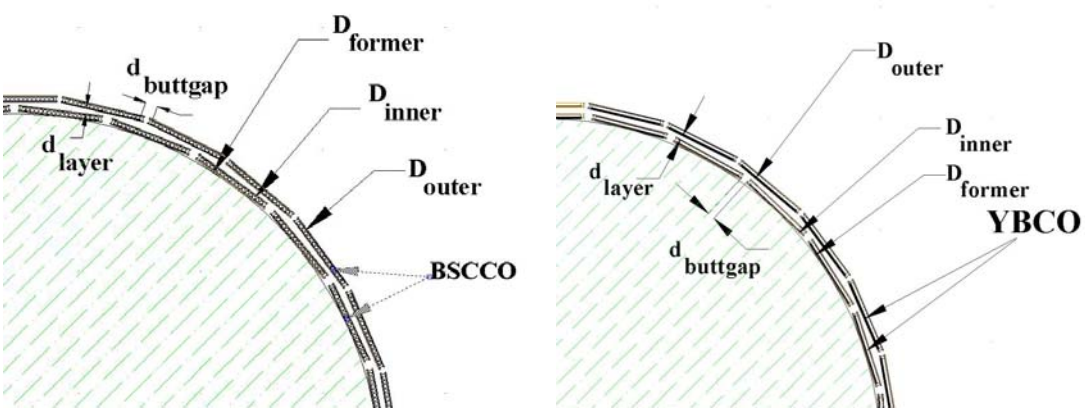

Figure 33. Dimensions of layer spacing and tape spacing as shown on a schematic of a BSCCO (left) and YBCO cable (right).

14) Control milestone met with over-current model for 2G wire

An over-current model for YBCO coated conductors has been developed and successfully benchmarked against experimental measurements of YBCO coated conductors from SuperPower and American Superconductor. This 1-D finite difference model, which calculates the currents in the superconducting and stabilizing layers of the composite conductor through an iterative solver, calculated conductor temperatures and voltages in a 1-m long section of 344 superconductor that was tested in December 2006. Using only the end-to-end critical current and n-value of 97 A and 26 respectively, the model voltages match well with experimental voltages as shown in figure 34. This model will be used in future over-current simulations and experimental measurements of YBCO cables to help understand concepts such as peak temperature and cable recovery times.

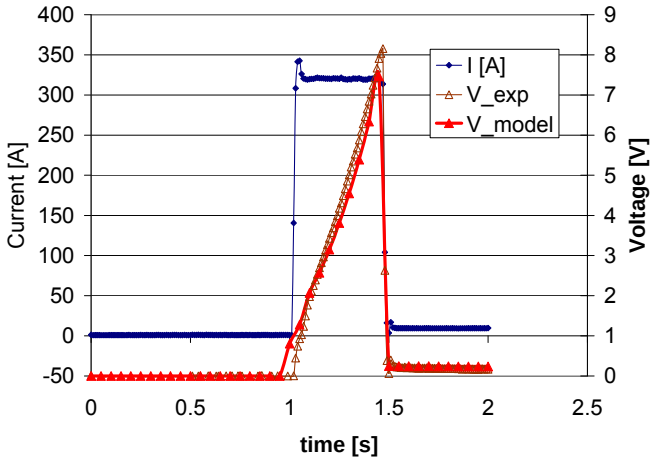

Figure 34. Comparison of voltage from an over-current model for YBCO coated conductors to experimental measurement of 320 A, 0.5 s long over-current pulse on a 1-m long 344 superconductor that had an critical current of 90 A and n-value of 26.

Status Status of milestones:

- Commissioning of enhanced ac loss testing capability. (March 31, 2007): **Met March 2007**.
- Establish the level of stability in spliced YBCO samples. (Sept. 30, 2007): **Met Sept. 2007.**.
- Develop theoretical methodology for ac loss minimization in YBCO cables. (Sept. 30, 2007): **Met Sept. 2007.**
- Characterize ac loss and stability of YBCO coils as a function of cooling conditions and coil geometry. (Sept. 30, 2007): **Not met due to coil damage during testing**.

Interactions:

AC loss measurements were conducted on as-manufactured 2-mm wide YBCO tapes from SuperPower. Representative YBCO splices with three different candidate solders on AMSC 344 YBCO superconductor were fabricated and sent to NIST-Boulder for electrical and mechanical characterization.

Subtask 3.3: Novel tailor-made cryogenic nano-dielectric materials.
E. Tuncer, I. Sauers, D. R. James, A. R. Ellis, M.P. Paranthaman, K. More and A. Goyal

Objectives:
In general, dielectric materials currently used in HTS grid applications (cable, transformers, fault current limiters) are essentially "off the shelf" and have not been developed specifically for cryogenic applications. Nano composite dielectrics represent a new class of materials with the potential for tailoring to the application by using base materials that operate well at low temperatures and adding nano-particles that improve specific targeted physical properties such as thermal conductivity, mechanical strength, thermal compatibility (i.e. contraction) and permittivity. Objectives of this project are to develop scientific understanding of novel cryogenic dielectric materials, identify materials and their processing to affect targeted properties while maintaining or improving the cryogenic dielectric characteristics, and correlate modeling with experimental data to facilitate the discovery of effective materials.

Highlights:

1) Micrograph of novel nano-dielectric material featured on cover of Nanotechnology.

An investigation on the dielectric properties and influence of particle size on breakdown strength of nano-composite dielectrics was recently published in *Nanotechnology* (Enis Tuncer et al., *Nanotechnology*, volume 18, 2007); see the following link (http://stacks.iop.org/0957-4484/18/025703). One of the figures (Fig. 4c) in the paper was selected for the cover for *Nanotechnology* volume 18, issue 2 and the article was featured in this issue.

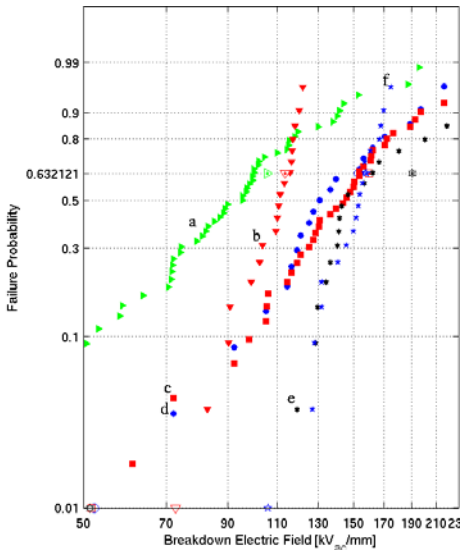

Fig. 1. Weibull probability plot of breakdown in various polymers/mixtures: a:PVA, b:PPLP, c & d: PMMA toluene, e: PMMA acetic acid and f:Cryoflex.

2) Dielectric breakdown strength affected by PMMA solvents.

Preparation of polymeric materials plays an important role in their electrical properties. To investigate this we have prepared PMMA with three different solvents, acetone, toluene and acetic acid. The acetone dissolves the PMMA quickly, but it is very volatile and did not form nice smooth PMMA films. The other two on the other hand form excellent PMMA films. Breakdown strength is found to be affected by the solvents.

PMMA mixed with acetic acid is found to exhibit very high dielectric strength.

The breakdown tests performed on these samples are shown in figure 1. The values are compared to other materials tested. The labels denote different materials as follows, a:PVA, b:PPLP, c & d: PMMA toluene, e: PMMA acetic acid and f:Cryoflex. PMMA prepared with acetic acid has very high dielectric strength at 77 K.

3) PMMA filled with magnetic nano-particles show effect on dielectric properties.

Magnetic nano-particles obtained from Adam Rondinone (CNMS & CSD) were dispersed in PMMA. Both the PMMA and particles were diluted in toluene solutions. Dielectric measurements show that properties are affected by the magnetic nano-particles in various ways.

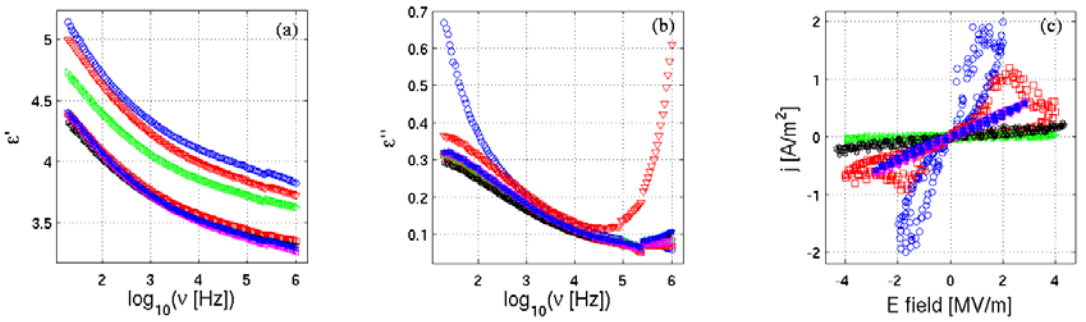

Fig. 2. (a) real and (b) imaginary parts of dielectric permittivity for unfilled and magnetic nano-particles filled PMMA. (c) Dielectric polarization in unfilled and filled samples. The unfilled PMMA is plotted by open circles.

Dielectric measurements (Fig. 2) at room temperature were performed with impedance and polarization methods. It was observed that small amounts of particles added to the PMMA decreased the dielectric permittivity of the base polymer. However, the sample with the highest particle concentration had very similar dielectric permittivity to the base material at a broad frequency range. Addition of particles decreases the dielectric loss in the material as well. The polarization measurements revealed the actual physical mechanism that caused the decrease in the permittivity even with inclusion of metallic particles. Notice that the pure PMMA illustrated a hysteresis with high polarization and plausibly ionic conductivity. Samples with low amounts of nano-particles modified the electrical properties and decreased the polarization effects in the polymer, such that they restricted the polarizing units. The breakdown data (Fig. 3) of the samples did not show significant changes for unfilled and filled materials at 77 K. The filled samples had higher 63% breakdown values than the unfilled PMMA except for the sample with the highest nano-particle concentration. The data spread on a broad range. Breakdown values at 63% were between 140 and 160 kV/mm.

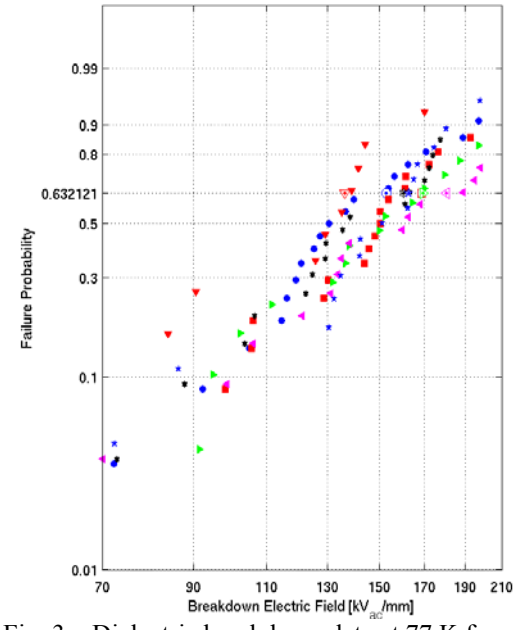

Fig. 3. Dielectric breakdown data at 77 K for unfilled and magnetic nano-particles filled PMMA.

4) New computer program developed for the dielectric characterization of materials.

A new measurement program in Labview was written for the dielectric characterization of materials. The program controls the Keithley 6517A and reads out the current with varied voltage inputs. The voltage is taken to be a saw tooth with a given low frequency period as shown in Figure 4. To test the program and the measurement setup, a sample composed of polyvinyl alcohol which is filled with nanometer-size, ferroelectric, barium titanate particles was fabricated. The barium titanate concentration is 10 wt % in the sample. The nonlinear behavior of the composite was observed as a hysteresis in the current-voltage diagram as seen in Figure 5. Similarly the behavior is also significant in the voltage and current versus time plots in Figure 4. In the figures responses at the end of the measurement cycle are presented.

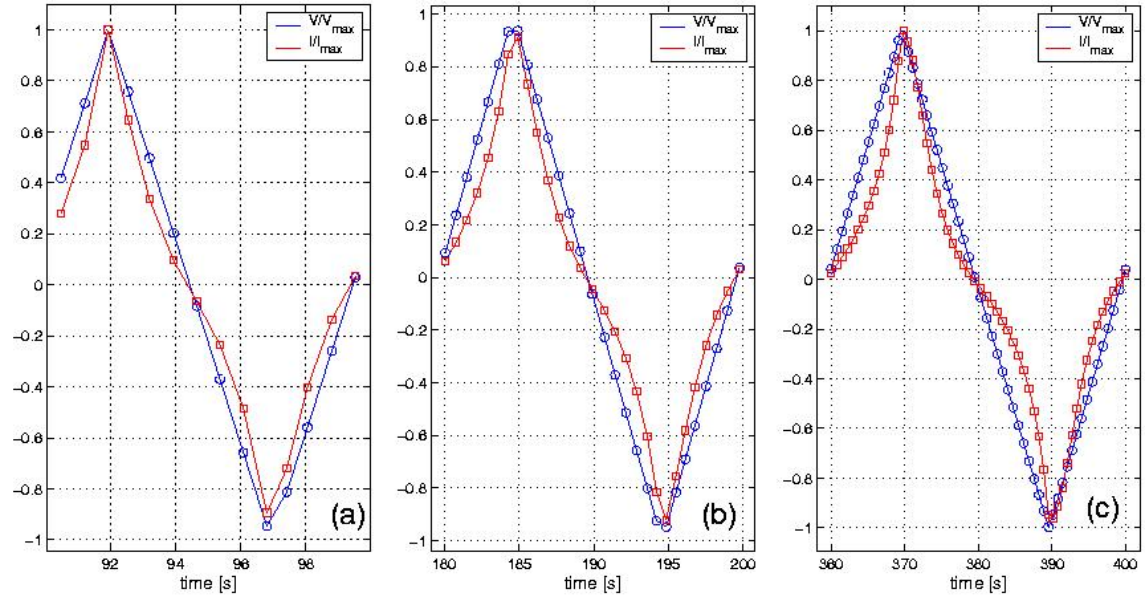

Fig.41. Voltage and current shapes as a function of time. The period of the oscillation is varied (a) 10 s, (b) 20 s and (c) 40 s.

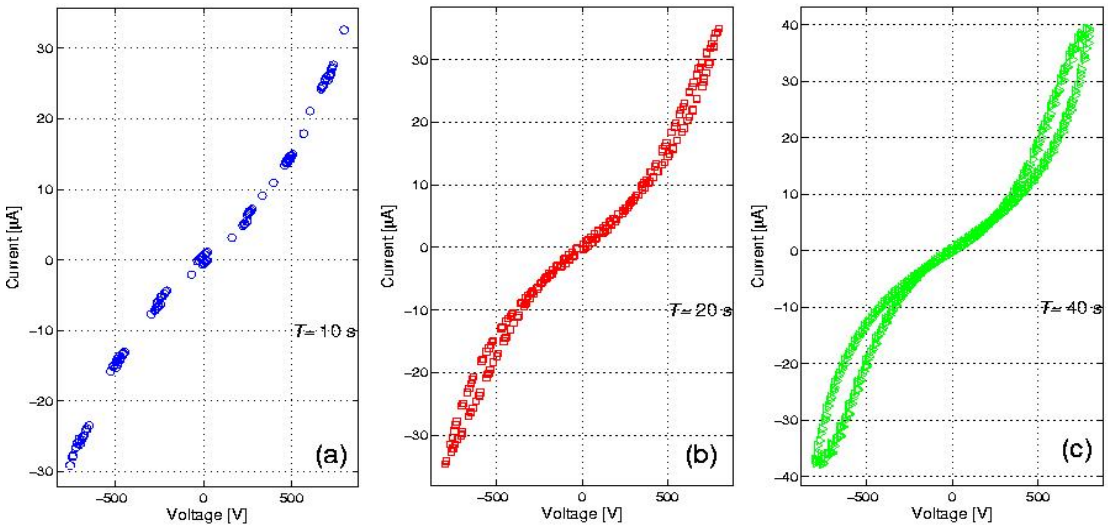

Fig. 5. Nonlinear behavior of barium titanate-filled polyvinyl alcohol. The period of the input voltage is varied (a) 10 a, (b) 20 s and (c) 40 s.

Nonlinear behavior of this composite can be used in field grading applications, where high electric regions in an insulation system can be covered with this material to distribute the electrical stress. Further investigations on the subject are needed. Samples with different wt % of barium titanate will be fabricated. The temperature dependence of the nonlinear behavior as well as the dielectric permittivity of the samples will be measured.

5) Measurement setup to determine thermal properties of cryogenic dielectrics has been completed and tested.

A new experimental setup was constructed using the existing cryorefrigerator chamber. A measuring program was written to record the transient time response of materials to an applied constant-heat-input. The setup will be employed to characterize the thermal properties of both commercial and developed dielectric materials. Thermal conductivity of materials is needed in cryogenic system design.

6) ORNL obtained nanodielectric composite with enhanced thermal property without electrical degradation.

Solid dielectric materials are needed for low temperature application as spacers between high and low voltage nodes in an apparatus. Unfilled resins do not have desired mechanical properties for cryogenic applications due to cracking in a temperature cycle. Therefore they are mainly loaded with particles or fibers to enhance the mechanical integrity of the material. Although desired mechanical strength can be obtained with micron size particulate fillers, the electrical properties of the matrix degrade. It has been shown previously that nanometer size fillers do not degrade the breakdown strength of matrix resin previously. Unfilled and 10wt% barium titanate filled resin samples were prepared using the centrifugal mixer, and no difference in dielectric strength of the unfilled and filled samples was observed. Thermal property measurement performed with the new experimental setup indicated that the filled samples have better thermal conduction compared to unfilled ones. Resin-nanoparticle composites can be implemented in HTS grid applications when materials for mechanical support as well as for cryogen-free-designs are of importance.

7) Selected candidate polymeric materials for cryogenic application have been characterized.

Performance of dielectric materials and their compatibility determine the size of electrical insulation systems. Electrical properties of polymeric materials are needed for cryogenic applications. Several polymeric materials, polyvinyl alcohol, poly(methyl methacrylate) and polyvinyl butyral resin were selected and characterized using the dielectric spectroscopy technique. The permittivity of polymers are between 3-4 at cryogenic temperatures. Their 63% breakdown values are between 100-300 kV/mm. These materials are potential candidates to be implemented in nanodielectric composites as matrix media in equipment and apparatus designed for HTS grid applications. The properties of these materials can be further improved with addition of nanometer size inclusions.

8) Selected commercially available insulating films have been characterized.

To utilize commercial electrical insulation films, which are employed in room temperature applications, in cryogenic power applications, it is needed to know the dielectric behavior of such films at low temperatures. In addition acquiring dielectric properties of such films draw a baseline for material development efforts in our laboratory such that scientists look for

improvement by comparison. In addition, equipment designers can select the appropriate novel materials over these already existing films. Three dielectric films, porous high density polyethylene (Tyvek®), polypropylene laminated paper (PPLP®) and polyimide (Kapton ®), were selected and characterized. It was observed that all three materials have different dielectric breakdown strength behavior. Polyimide has the highest breakdown strength of all with 63% failure probability of 300kV/mm. PPLP® and Tyvek® have their 63% failure probability at 113kV/mm 44kV/mm respectively. Tyvek® has very low dielectric permittivity that is close to liquid nitrogen. A database is needed for cryogenic physical properties of commercially available materials for cryogenic power apparatus designers. A web-based database is in progress.

9) Established electrical and physical improvement in one of the nanodielectric materials.

Mechanical properties, yield strength and Young's modulus of titanium oxide/polyvinyl alcohol, nano-dielectric system were investigated at room temperature. Samples with thicknesses around 250 micron were fabricated and delivered to NIST for the measurements. It was observed that the Young's modulus of nano-particle-filled PVA increased. Similarly the yield strength of the material was also increased. These results are shown in figure 6.

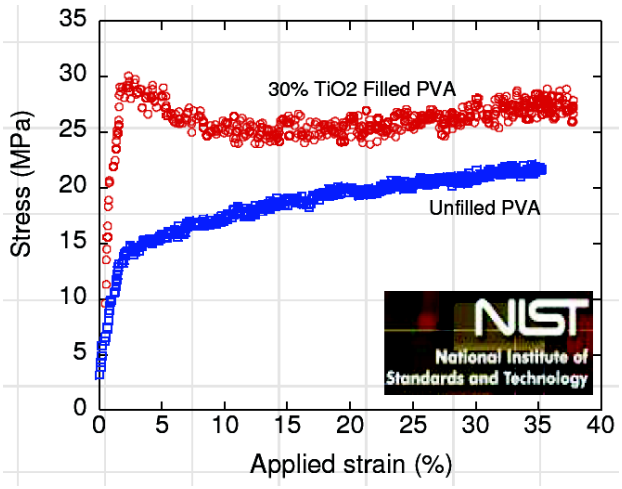

Figure 6. Stress-Strain curve for unfilled and titanate filled PVA.

10) Characterized pure polymeric materials to be used as matrix media in nano-dielectrics

Three different polymeric materials and one commercially available film were considered. The polymers were polyvinyl alcohol (PVA), poly(methyl methacrylate) (PMMA), and polyvinyl butyral resin (PVB). PVA and PMMA were supplied from Sigma-Aldrich. PVB was supplied from Sekisui Chemical Co., Ltd., BL-X is the trade name. Polymers were dissolved in different solvents: PVA in water; PMMA in toluene (PMMAt) and acetic acid (PMMAa); and PVB in toluene. The polymeric samples were cast on glass slides; their thicknesses were less than 50 micron. Polyimide (PI) is a commercially available film with the trademark name Kapton® having 25-micron thickness.

In Fig. 7, the real and the imaginary part of the dielectric permittivities of the samples are shown at room temperature. PVA has the highest permittivity and losses of all. Both PMMAt and PMMAa indicate high losses, however, PMMAt has lower dielectric permittivity than PMMAa. This could be due to structural differences between the two cast films due to employed solvents. Solvents might have changed the morphology of the polymer. Similar behavior is observed when acetone was used as a solvent for PMMA The cast films were not transparent due to volatility of acetone. PI (Kapton®) has the lowest loss among the tested samples; no dipolar polarization is visible over the measured frequency window. PVB is similar to PI which also shows a flat dielectric loss in the frequency response. However, it has a higher permittivity than PI.

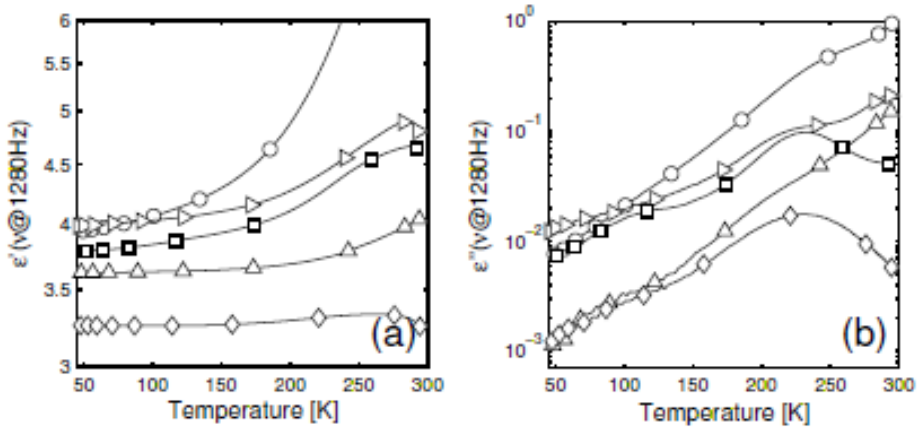

Figure 7 (a) The real and (b) the imaginary part of the complex dielectric permittivity for the investigated polymers as a function of temperature at frequency 1280 Hz, (circles:PVA), (up triangles:PMMAt), (right triangles:PMMAa),(squares:PVB) and (diamonds:PI).

In Fig. 8 average breakdown values with error bars (open symbols) and failure probabilities at 63% are summarized for the samples. PI (Kapton®) has triple the average breakdown values of PVA and PVB. The two PMMA samples prepared with different solvents indicate slightly different breakdown characteristics. PMMAa has approximately a 20% higher average breakdown than PMMAt. PVB and PI have significantly high b values, which yield small error bars in Fig. 8. Although PI has superior dielectric properties to other materials tested, it is mechanically inflexible. PVA is the most flexible among the materials reported here.

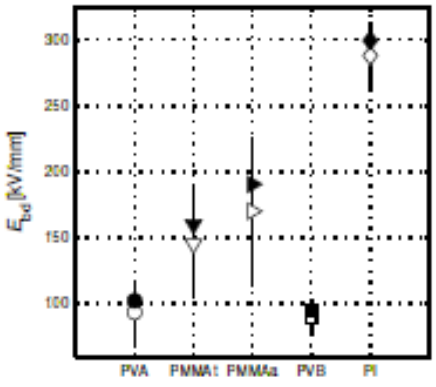

Figure 8. Mean (open symbols) and 63% failure probability (filled symbols) of dielectric breakdown strength values, E_{bd}, for the polymers investigated. Error bars represent the standard deviation. The measurements were performed in a liquid nitrogen bath at atmospheric pressure.

Status of milestones:

- Develop nano-dielectic materials with enhanced electrical and physical properties. (August 31, 2007): **Met July 2007**
- Build and test an apparatus for measuring thermal conductivity as a function of temperature in the range 20-300K. (Aug. 31, 2007): **Met June 2007**

Interactions:

Results are communicated to the appropriate industry partners. NIST-Boulder has been engaged to collaborate in the area of mechanical testing. Also, potential areas of collaboration are being discussed with the Center for Advanced Power Systems (CAPS) as well as a dielectric company.

Section 4: HTS Applications

Work with industry to perform generic R&D on issues related to the practical application of HTS. Also work in the design, operation, reliability and efficiency of prototype HTS demonstrations.

Subtask 4.1: HTS Cable System R&D.

J. Demko, M. J. Gouge, C. Rey, Robert C. Duckworth, D. R. James, I. Sauers, A. R. Ellis, Tim Kadri

Objectives:

HTS cable systems have been demonstrated which can carry several times the current (2-5x), and hence several time the power, of conventional cable systems of the same physical size. In order for HTS cables to be commercial, however, many issues remain to be solved. Objective of this project is to perform generic research on remaining issues that are critical to the development of HTS cables systems of arbitrary lengths that will lead to the successful commercialization of HTS cables. These include the development of system components associated with high voltages, cryogenic systems for long cables, and analytical models to simulate the behaviors of wires and cables during operation.

Highlights:

1) Superconducting cable at AEP Bixby Substation operating reliably.

The cable has been on line since August 8, 2006. The AEP HTS cable continues to operate reliably according to design specifications, and is providing services to more than 8,600 customers.. The plot below shows the substation load in amps at 13.2 kV for the three cable superconducting phases (magenta, blue and yellow) and the concentric neutral (red) over a 24-hour period in October 2006. The phase current peaked at 1,800 A which is lower then summer levels when air conditioning loads were significant. The lower red curve is the shield current which is near zero as the three ac phases are nearly balanced. During a 24 hour period on the coldest winter day in December (December 8, 2006, a low of -10 C or 14 F) in Columbus OH,

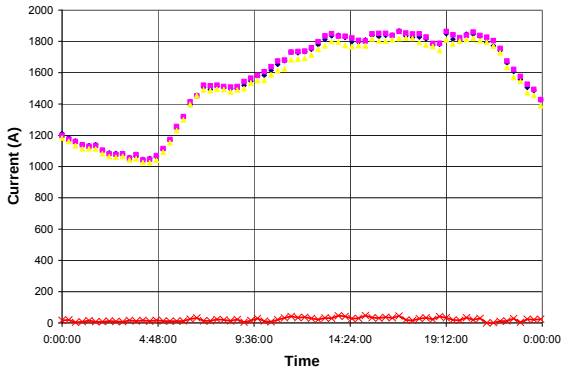

Fig. 1. Load current on the HTS cable over 24-hour period.

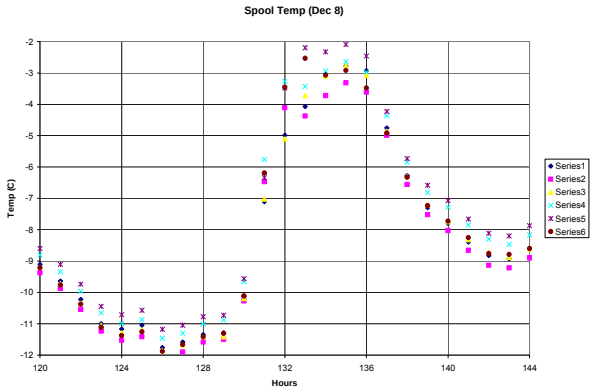

Fig. 2. HTS cable spool temperatures for coldest day in December 2006.

the cable spool temperatures (on each phase) ranged from -12 C to -2 C. This is a key parameter in that it indicates the design features are intact to provide good cable integrity.

The cable operated through the Ohio winter season after some external bushing temperature sensor settings were reduced to be consistent with low ambient temperatures on the coldest winter evenings. While the HTS cable continues to provide power to more than 8,600 residential, commercial and light industrial customers, two events have occurred in this quarter. These events triggered programmed responses without damaging the cable, and demonstrate the value of real-world testing necessary for broad commercial adoption of the HTS technology.

On January 3, the unintentional loss of the station battery system while troubleshooting a ground caused a breaker to open which removed input power to the cable cryogenic system. As a result, the HTS cable was taken offline according to the control strategy. The cryogenic system and HTS cable were restored shortly after the initial incident was resolved. In addition, there was a brief cable system outage on February 15th due to some leaking sensor line isolation valves on the cryogenic skid that were replaced. These unplanned real-world occurrences demonstrate the robust design margin of the HTS cable system, and provide valuable operational data. Thus far, the cable system has experienced four power-down events – three unplanned events and one planned maintenance – all without damage to the cable system. In addition, the cable has withstood a number of fault current events, again without damage to the cable system. The operation experience and gathered data are very valuable to the industry.

Recently, the cable was warmed up due to maintenance on the Praxair cryogenic system. After completion of the repairs, the cable was successfully cooled down and placed back into service providing power to 8,600+ residential, commercial, and light industrial customers. A plot of the temperatures measured during the cooldown, which took place September 10-11, 2007, are shown in Fig. 3. From a warm state it took about one day to cool the cable back to its operating condition. The operational experience and gathered data are very valuable to the team.

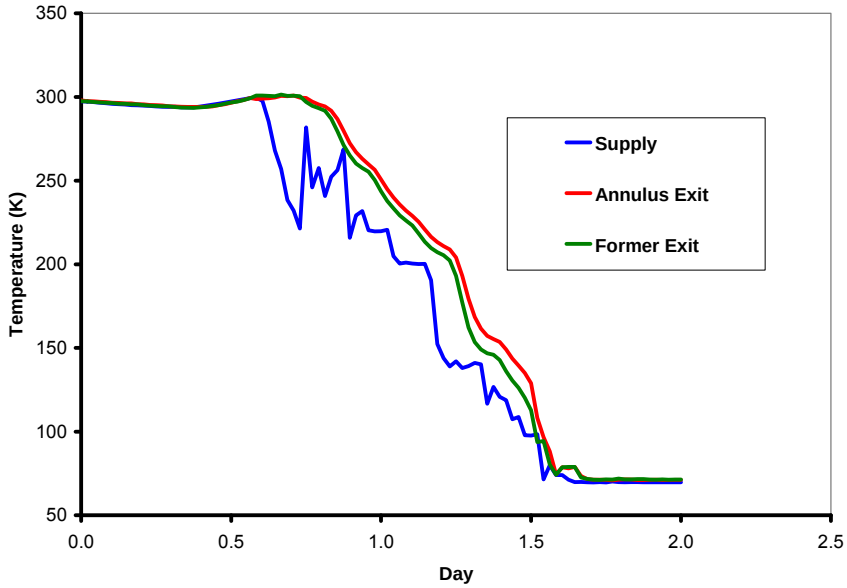

Fig. 3. . Cooldown of the AEP Triaxial HTS cable in Spetember 2007.

2) DC test performed on a 3-meter tri-axial cable splice.

DC testing was conducted on a 3-meter long section of a tri-axial HTS cable splice. The section had previously undergone design over-current testing to simulate fault currents by Ultera-Denmark). Results from dc tests showed that this cable exhibits I_cs in the 6,100-8,200 A range at 77 K. These values are comparable to dc I_cs of 7,000-8,000 A for a similar 5-m long tri-axial cable tested at ORNL in 2005. The HTS tri-axial cable at the AEP Bixby substation operates under ac conditions at rms/peak currents below 3,000/4,230 A and thus there is a substantial margin between the ac peak and dc critical current, which minimizes the ac hysteretic losses.

Two sets of dc testing were performed on the cable. The first round of testing was conducted on all three phases using jumpers. In this arrangement, the current flowing in phase 1 (innermost) and phase 3 (outermost) is in the same direction but opposite to phase 2 (middle). A second series of measurements were performed on individual phases. The measured voltage-current (VI) curves are compared in the following plots for the three phases under these two measurement conditions. The measurements show that the net magnetic field developed from the application of current to all three phases results in a slight decrease in the critical current of phase 1, the innermost phase. There was no measurable change in the outer two phases.

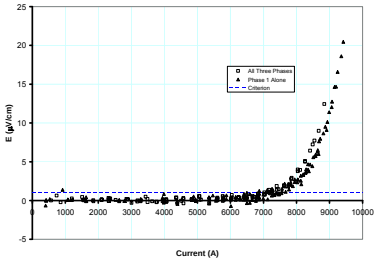

Fig. 4a. DC V-I characteristics for phase 1 alone and during simultaneous three-phase testing.

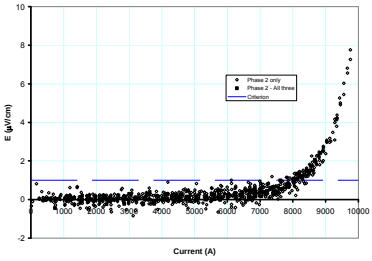

Fig. 4b. DC V-I characteristics for phase 2 alone and during simultaneous three-phase testing.

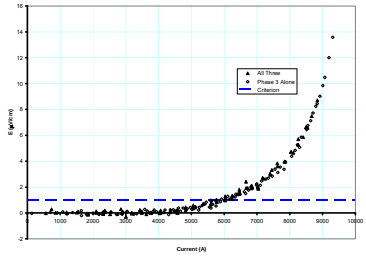

Fig. 4c. DC V-I characteristics for phase 3 alone and during simultaneous three-phase testing.

An additional measurement of the dc V-I characteristics was conducted on phases 1 and 2 with current applied in the same direction in both phases. The fields produced when the neighboring phase is energized cause a decrease in the I_c and an increase in the n-value.

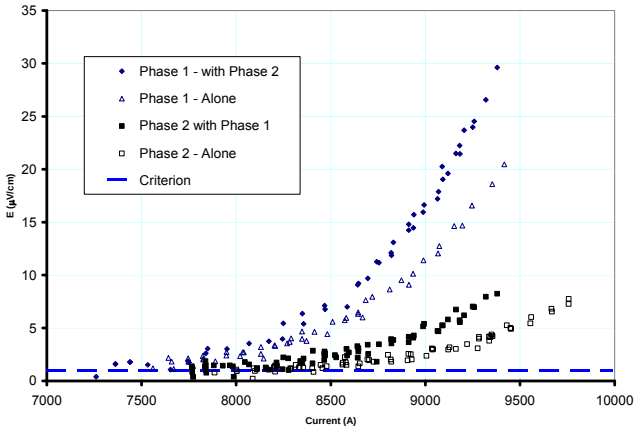

Fig. 5. V-I curve of phase 3 for high currents.

3) Work begins on the evaluation of thermal-hydraulic effects in long cable cryostats.

ORNL began working with Southwire staff (Mark Roden) on a test to evaluate thermal-hydraulic effects in long cables/cryostats. An existing 50-m vacuum-jacketed cryostat that was used for an earlier Bixby cable prototype will be used for a pressure drop test in the field. In parallel, efforts are ongoing to develop a model to simulate this test so the experimental results can be correlated with the model. Based on this, a realistic thermal-hydraulic model for the proposed longer SPE cable can be developed. The thermal

effects are due to heat in-leak and ac losses which change the properties of the liquid nitrogen along the cable length. ORNL completed preliminary calculations for determining flow required to cool the long cable. This will be used to optimize the cable former diameter and the cryostat inner diameter.

4) Feasibility of thermal ac loss measurement in superconducting cables demonstrated.
Based on discrepancy between the thermal and electrical ac loss measurements for a YBCO cable that was measured in July 2006 and in preparation for the measurement of two new YBCO cables, an investigation was carried out to determine the source of the discrepancy and suggest a possible alternative method to measure the ac loss thermally. This alternative method uses the V-I product for dc heating when the operating current is slightly greater than the critical current in the cable. This method resulted in uniform heating down the entire length of the cable and this known heat source was used to calibrate the platinum resistance temperature detector (RTDs) on the cable.

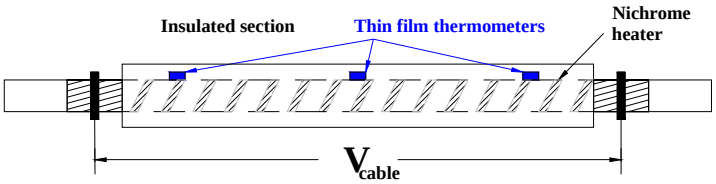

Fig. 6. Diagram of thermal ac loss measurement setup for the YBCO cable

The HTS prototype cable that was measured was a two-layer, 1.25-m long YBCO cable that was wound on a 25.4 mm diameter G10 former with the 344-superconductor produced by American Superconductor (AMSC). Each layer consisted of sixteen YBCO tapes that were wound at ± 20° pitch angles on the former and were attached to solid copper end plugs with a Sn-42 Bi-58 solder. This solder was chosen as a compromise between the recommend solder 52In 48Sn with a melting point of 118 C and the solder used in the copper lamination which has a melting point of 179 C. A set of thermometers and a nichrome heater were wound to the exterior of the cable and then covered with sixteen layers of PPLP insulation. This insulation isolated the thermometers from the liquid nitrogen bath and allowed for measurement of the ac loss. While the use of the local heater has been previously used to estimate ac loss, the difference between the electrical and thermal ac loss measurements suggested that an alternative method was needed. The alternative method for measuring the ac loss thermally was found through adaptation of a successfully demonstrated method used for single HTS tapes. When the dc current exceeded the cable critical current, the product of the current and the voltage drop across the insulated section produced uniform heat generation along the length of the cable. This known heat load is used to calibrate the platinum thermometers that

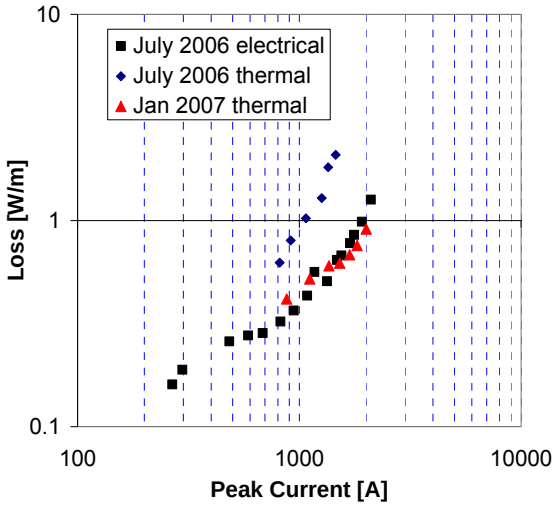

Fig. 7. Comparison of electrical and thermal ac loss measurements made in July 2006 to the thermal ac loss measurements in January 2007 on the same 25.4 mm diameter, 1.25-m long YBCO cable.

were positioned along the length of the cable as shown in figure 6. Then, the change in temperature is measured when ac current is applied to the cable and the ac loss as a function of ac current is found. It appeared that the thermal method using the nichrome heater overestimated the change in temperature due to a known heat input. When the new thermal method was compared to the previous measurements shown in figure 7, the agreement between the thermal and electrical data has improved greatly.

5) Work begins on the evaluation of thermal-hydraulic effects in long cable cryostats.

ORNL began working with Southwire staff (Mark Roden) on a test to evaluate thermal-hydraulic effects in long cables/cryostats. An existing 50-m vacuum-jacketed cryostat that was used for an earlier Bixby cable prototype will be used for a pressure drop test in the field. It was decided to drop the surrogate fluid test and test only with liquid nitrogen. One major concern is that the SPE cable is proposing to use a counterflow configuration. This has been shown to be limited in length to maybe a few hundred meters for most practical sizes (see J. A. Demko, et. al. "Practical AC Loss and Thermal Considerations for HTS Power Transmission Cable Systems", IEEE Transactions on Applied Superconductivity, Volume: 11 Issue: 1 Part: 2 , March 2001 Page(s): 1789 –1792).

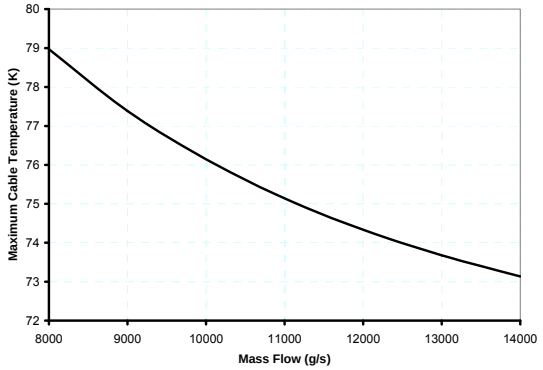

Fig. 8. Preliminary calculations of a 1700-meter long counterflow cable similar to the proposed SPE configuration

Preliminary analysis results, which are given in Fig. 8, show that for a 1700-meter long cable using the same dimensions as the existing triaxial HTS cable design require very high flow rates (~10000 g/s to limit the maximum temperature to 76 K in the cable) compared to other installations such as AEP Bixby substation (~300 to 500 g/s). The higher flows are attributed to axial and inter-stream thermal conductance effects which become exacerbated in very long length cable systems. The pressure drop scales approximately with the mass flow squared, so the system pressure drop could increase by 500 times the existing cable system. Methods to reduce these flow requirements through modifications to the triax cable design are being investigated.

An accurate thermal-hydraulic model for the proposed longer SPE cable can be developed but a cryogenic test loop is required to validate the calculations. This is proposed to be designed and installed next year depending on funding, to provide additional data needed to calibrate analysis of long length cables. The thermal effects are due to heat in-leak and ac losses which change the properties of the liquid nitrogen along the cable length. ORNL completed preliminary calculations for determining flow required to cool the long cable. The model in conjunction with the test loop results will be used to optimize the cable former diameter and the cryostat inner diameter.

6) Work continues on the evaluation of thermal-hydraulic effects in long cable cryostats.

ORNL collaborated with Southwire Co. staff (Mark Roden, Jerry Tolbert) on a test to characterize the pressure drop in long cables/cryostats. An existing 50-m vacuum-jacketed cryostat was used with a dummy cable inserted to measure the pressure drop for the annular flow

between the dummy cable and the inner wall of the cryostat. The two cooling flow paths are shown in Fig. 9. A solid rod of nearly the same diameter as the triaxial HTS cable was used for this test so there is no flow through the former. The test was conducted using the cryogenic system from the Southwire Co. 30-meter HTS cable site to supply the flowing liquid nitrogen. The characterization of the pressure drop is very important for long length cables such as the Entergy project. Correct estimates are needed to provide sufficient flow to cool the cable system, but over-prediction can result in costly over-design.

In Fig. 10 is a comparison between the pressure drop measurements as a function of flow with calculations using different characteristics of the cryostat and dummy cable. A generalized one-dimensional flow calculation with friction and heat transfer was performed given the cryostat inner diameter, corrugation height, nominal diameter of the dummy cable and a measured minimum diameter (about 2 mm smaller). The relative roughness (RR) is based on the cryostat dimensions. There was a significant decrease in the pressure drop for the calculations based on the smaller diameter. By increasing the relative roughness the smaller diameter calculations can be shown to correlate with the measurements. There is some uncertainty in the dummy cable diameter, which may vary along its length. No conclusion has been made to which parameters to use for an accurate calculation or on the friction factor that applies.

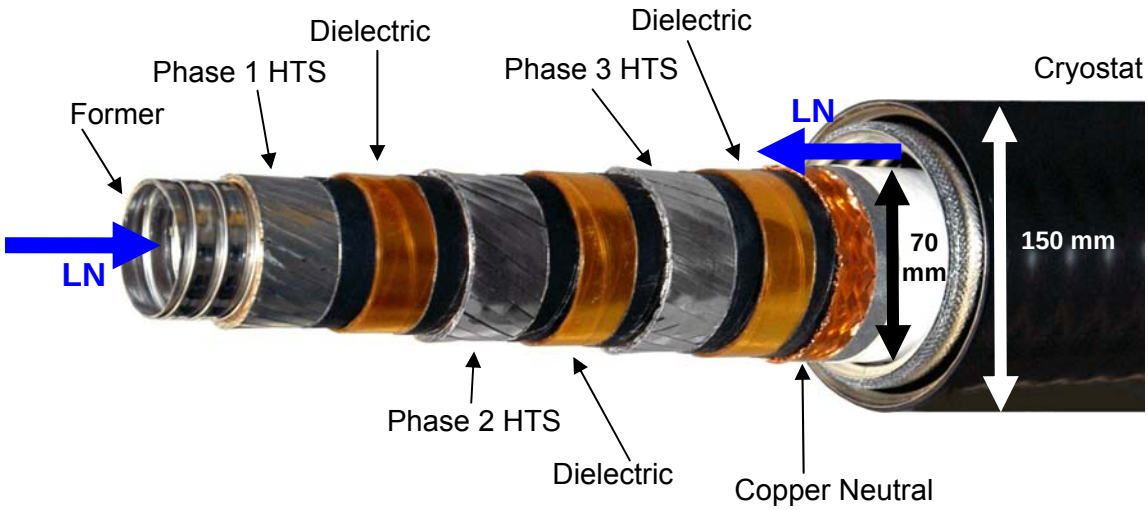

Fig. 9. . Baseline counterflow cooled triaxial HTS cable.

Analysis has also been conducted looking at the counterflow cooling of long length HTS cables. An earlier study by (see J.A. Demko, et. al., *IEEE Trans. on Appl. Supercon*., Mar. 2001), showed that there are finite length limits for counterflow cooled cables to a few hundred meters but certainly less than a km. The reason for the limit is mostly due to the interstream conductance as discussed in Edney, (*Cryogenics*, December 1967). Edney's work assumes there is a refrigerator at each end of the cable recooling the flow and neglects axial conduction along the cable which is also significant in determining the axial temperature profile.

Analysis of the baseline cable configuration for a 2 km cable system was conducted. In order to obtain the temperature profiles, the pressure drop calculations were not performed. This is because of the extremely high flowrates required to maintain reasonable operating temperatures.

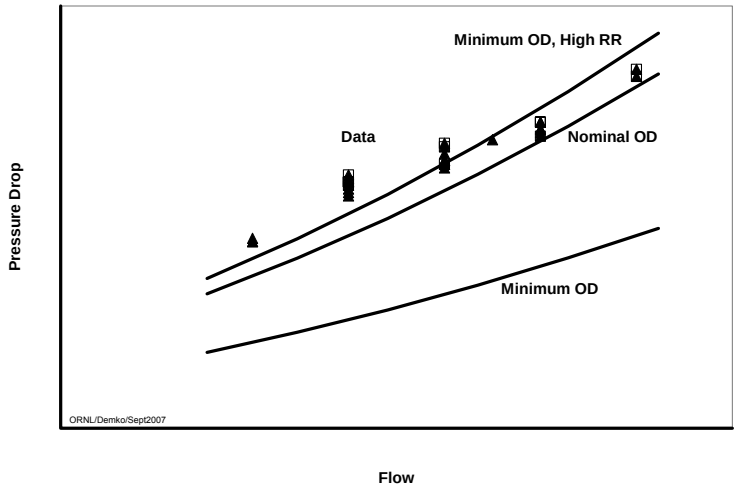

Fig. 10. . Pressure drop comparison of measurements in a 50-meter cryostat containing a dummy cable with calculations assuming different geometric properties.

For the baseline case, the maximum temperature will be at the far end of the cable, as shown in the typical temperature profile given in Fig. 11. If the interstream conductance can be eliminated, a temperature profile as shown in Fig. 12 can be obtained. The cable can be cooled at a substantially reduced flowrate.

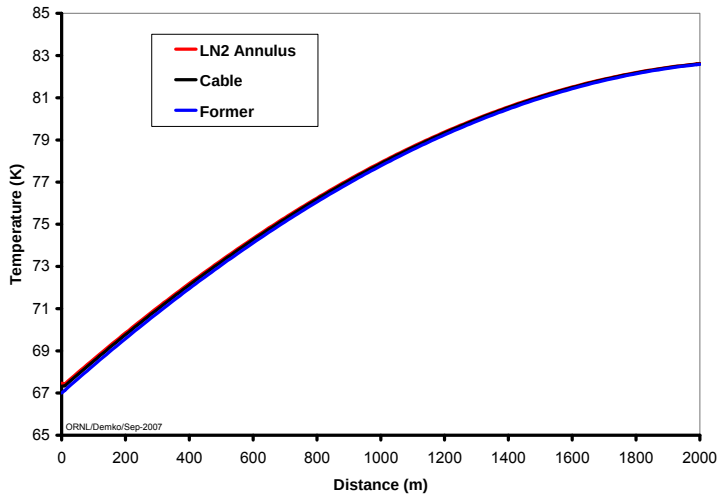

Fig. 11. . Temperature distribution along a 2-km triaxial HTS cable for the baseline counterflow design case at a flow of 8000 g/s.

Calculations of the required flow to maintain a maximum cable temperature are shown in Fig. 12 for a baseline triaxial cable design similar to the AEP design, and assuming that the interstream conductance is eliminated. The pressure drop is proportional to the flowrate squared. From the calculations in Fig. 13, the ratio of pressure drops for the two cable systems with a maximum cable temperature around 73 K is 2500. Typical cable systems of shorter length have pressure drops less than 1 bar, indicating that the pressure drop of a 2-km counterflow cooled cable with the baseline design scales according to the flowrate squared to over 2000 bars. This is

an unreasonable operating pressure since typical system components are not rated for those pressures. Some means to block the interstream conductance is required.

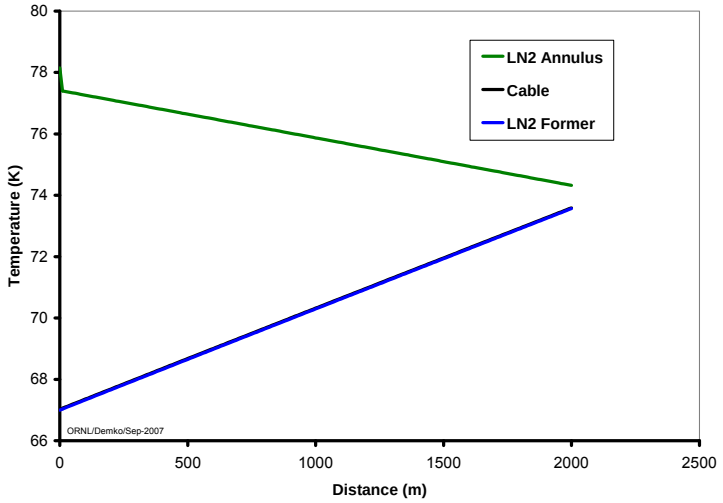

Fig. 12. . Temperature profiles along an HTS cable with no interstream thermal conductance at a flow of 325 g/s.

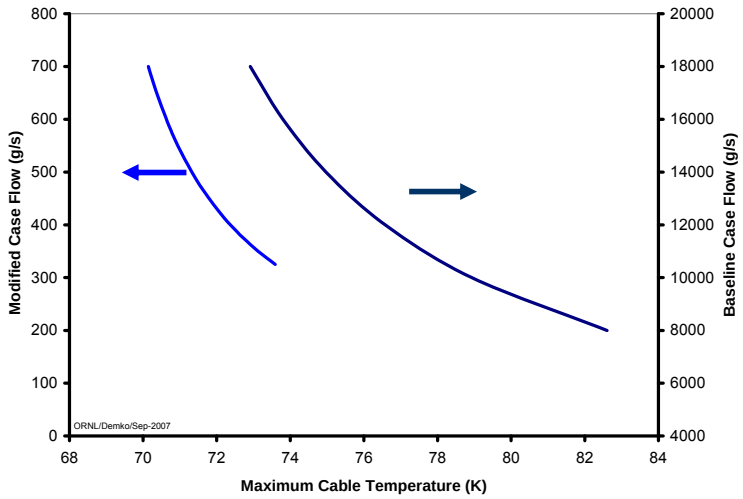

Fig. 13. Flowrate of liquid nitrogen required in a 2 km triaxial HTS cable system for a specified maximum temperature in the baseline case or with no interstream thermal conductance blocked.

Long length counterflow cooled HTS cable projects, like the 1.7 km long Entergy HTS cable, require that an accurate assessment be made to calculate the pressure drop and cooling characteristics. Using the baseline configuration will result in pressure drops that cannot be contained within the pressure rating of the existing system. To decrease the pressure drop, and system pressure, to a practical level, the flow passage dimensions can be significantly increased, or design modifications can be made to the cable to inhibit the interstream conductance. Additional testing is needed to calibrate and validate the calculations for long length cable systems. Substantial overdesign and higher cable system construction costs will result if this issue is not addressed.

To resolve this issue a cryogenic test loop is required since only limited data is available for model validation and calibration. A previous test was conducted on a 5-meter counterflow cooled

coaxial HTS cable as reported by Demko [*Adv. Cryo. Engr.* 1999] but the interstream conductance effects are not significant in this situation because of the low aspect ratio, and also because the temperature profile was dominated by termination heat loads.

7) Qualification of insulation design of 35-kV class model cable

Electrical insulation requirements were determined for a 35-kV class model cable. Based on statistical data for impulse breakdown in model cable and data on impulse breakdown as a function of insulation thickness (Figure 14), a model cable was fabricated using newly designed stress cones. High voltage tests were performed on the model cable immersed in liquid nitrogen in the ORNL large high voltage cryostat (Figure 15). Testing included partial discharge, AC withstand and impulse (positive and negative waveforms). Table 1 lists the various tests that were performed. The model cable passed these tests completing the milestone for qualification of a 35-kV class model cable.

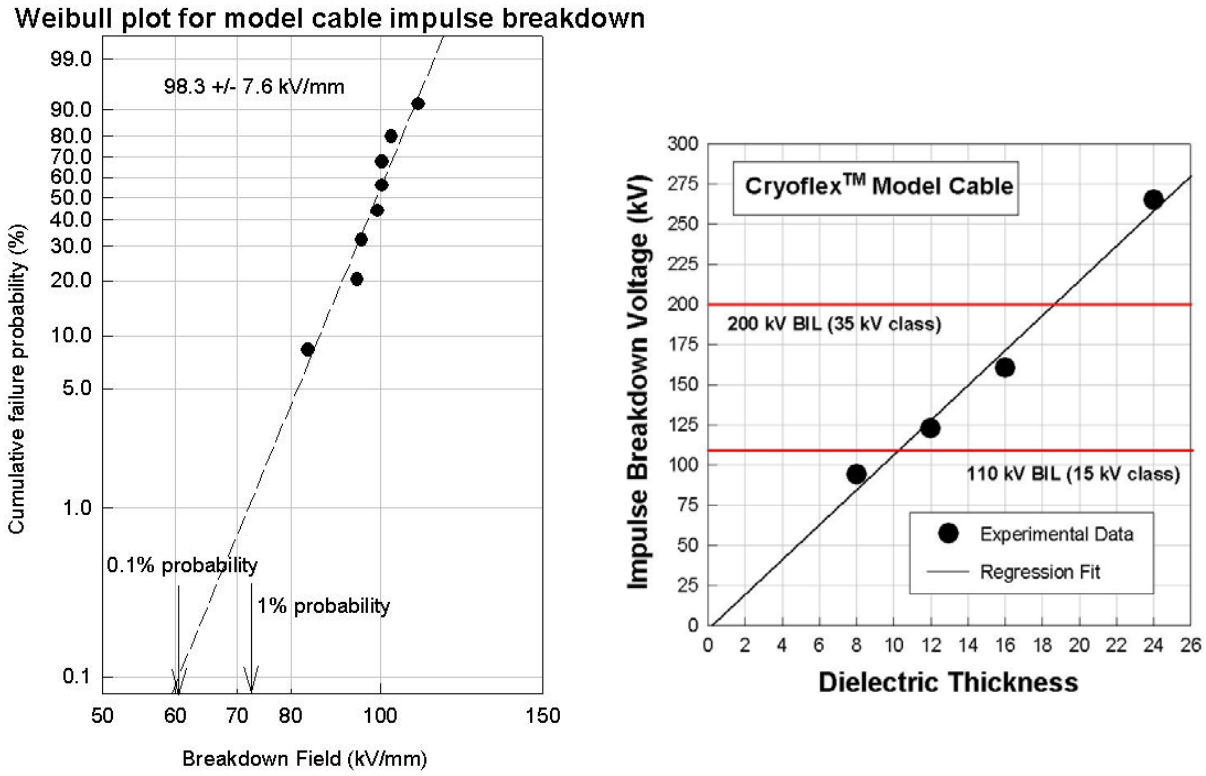

Fig. 14. (left) Weibull statistical plot of impulse breakdown of model cables; (right) Plot of impulse breakdown as a function of dielectric thickness in liquid nitrogen.

Fig. 15. (left) Technician holding model cable prior to immersion into large high voltage cryostat. (right) AC withstand setup showing the large HV cryostat in the background.

Table 1: Test sequence for high voltage qualification of 35-kV model cable.

1	PD test to 1.5 times Um = 52.5 kVrms:	Passed
2	AC withstand at 2.5 times Um = 87.5 kVrms for 15 minutes:	Passed
3	Positive lightning impulse (1.2/50 usec) conditioning at 50%, 65%, 80% of BIL (BIL= 200 kV) (according to IEEE Std 82-2002):	Passed
4	Ten (10) positive impulses at BIL = 200 kV:	Passed
5	Negative impulse conditioning at 50%, 65%, 80% of BIL:	Passed
6	Ten (10) negative impulses at BIL = 200 kV:	Passed
7	Recheck PD to 1.5 times Um:	Passed
8	AC withstand at 2.5 x Um = 87.5 kVrms for 15 minutes (Dielectric Integrity Verification, section 5.3.5 of I EEE 82-2000) [ensures BIL test did not damage]:	Passed

8) Preliminary study being performed to evaluate the feasibility of HTS DC cables to power supercomputers and data centers.

The implementation of the next generation, peta-flop-scale supercomputer at Oak Ridge National Laboratory (ORNL) is already underway. Consistent with that planning is the corresponding facility engineering to support these planned upgrades. One of the major problems with the planned upgrades in computer processing speeds is the corresponding need for increased electrical power and interior cooling for the facility. The electrical power for the next generation supercomputer i.e. the Cray –Baker and beyond (Cray-Marble and Cray-Granite), all will require a 48 V dc input to the processor board. At this relatively low voltage level, this translates to an

ever increasing amount of feeder current to handle the enormous electrical power load. At these low dc voltage and high current levels, the corresponding conventional copper and/or aluminum electrical bus required to carry this enormous power is massive in size and weight. For facility planning purposes, the approximate electrical input power requirements that have been estimated for these next generation supercomputers are: a) 3 MW for the Cray-Jaguar, b) 7-10-mW for the Cray-Baker, and c) up to 30 MW for the Cray-Granite and Cray-Marble. In reviewing this proposal, it should be clarified that there is presently (February 2007) an existing ~ 7.3 MW of electrical power available to building 5600 supplied by three (3) separate electrical feeds rated at: 2 MW, 2 MW, and 3.3 MW, respectively. Therefore, to obtain the necessary 30 MW in the final installation, an additional 23.7 MW of electrical power will need to be added to the facility by year 2010. It is these additional 23.7 MW of electrical power that is addressed in this proposal. For the purposes of this proposal, we have rounded the required electrical power value to ~ 24 MW.

In this application, a superconducting electrical bus (cables) operating with a large dc current level has the potential to significantly reduce the size, weight, and energy consumption over a corresponding conventional copper/aluminum bus. The Applied Superconductivity Group (ASG) has been tasked with looking at various options of supplying large amounts of electrical power via a high-current, low voltage dc bus. An initial study was performed and four different options were identified. These four options are:

1) Conventional ac power baseline: Option 1
2) DC power at 48 V and 500 kA: Option 2
3) DC power at 1.2 kV and 20 kA with converter: Option 3
4) DC power at 410 V at 58.5 kA without converter: Option 4.

The advantages and disadvantages of the HTS dc cable to the conventional solution are listed below.

Advantages

- Interface to the supercomputer internal power supply at 410 V dc enhances efficiency by ~ 3 % (for the 24 MW load only)→ 720 kW reduction in heat load to the facility
- Zero electrical ac bus losses resulting in a ~ 2 % higher transmission efficiency →429 kW reduction in heat load (Option 4 cryogenic system)
- Significantly lighter weight
- Significantly smaller cross sectional area of the HTS electrical bus
- Significantly smaller facility footprint
- Zero magnetic fringe field (co-axial design→ see Figure 4)
- Transmission loss independent of length allowing remote placement of source power feed
- Reduced arc-flash hazard inside supercomputer facility

Disadvantages

- HTS wire presently is over 2-5-times more expensive→ selling for ~ $50-150/kA-m compared to conventional copper for ~ $25-30/kA-m
- DC HTS cable needs to be cooled to an operating temperature of ~ 70-77 K and therefore requires a cryogenic cooling system. This adds additional capital cost and an electrical power penalty which must be factored into the overall annual operating costs

The constraints of the electrical power problem addressed is this study are:

- This study address the addition of 23.7 MW (~ 24 MW for calculation purposes) to building 5600

- A 13.8 kV ac transformer located external to the ORNL supercomputer facility (building 5600) will supply the electrical power from the new ORNL sub-station.
- The planned upgrade in electrical power will scale from ~ 7.3 MW in calendar year 2007 up to 30 MW by calendar year 2010 (see Figures 1a and 1b).
- The electrical power feed to the processing boards of the Cray Supercomputer requires a 48 V dc input at < 3 % ripple.
- The rectification of the 13.8 kV ac to dc feed is located approximately 100 m from the ORNL supercomputer facility.
- The cryogenic system necessary to operate the HTS based electrical bus is located external to the ORNL facility and co-located with the 13.8 kV ac to dc rectification.
- For the superconducting bus option, each electrical termination, i.e. the transition from the 77 K region to the room temperature region, occupies ~ 16 ft^2 per termination.

Status of milestones:

- Develop overcurrent model for 2G wire (DC). (July 31, 2007): **Met July. 2007.**
- Qualify new Cryoflex dielectric insulation in 15 kV and 35 kV class model cables with appropriate high voltage testing for each class. (Sept. 30, 2007): **Met Sept. 2007.**
- Evaluation of HTS cable system architectures for long length systems. (Sept. 30, 2007): **Met Sept. 2007.**

Interactions:

Work involves close and regular collaboration with Ultera (Southwire & nkt cables).

Subtask 4.2: Development of high-voltage HTS power transformer.
S.W. Schwenterly, D.R. James, I. Sauers, A.R. Ellis

Objectives:
High-temperature superconducting utility power transformers offer prospects for improved efficiency, smaller size and weight, lessened environmental hazard, better overload tolerance, and longer lifetime in comparison with conventional power transformers. The current U.S. utility power transformer inventory is aging and will soon require replacement, offering a large potential market for advanced superconducting transformers. ORNL is collaborating with Waukesha Electric Systems (WES) and a utility partner to continue development of HTS power transformers. Objective of this project is to perform R&D on issues necessary to extend the transformer operation to higher voltages required for compatibility with the existing power grid. A commercially viable HTS transformer will have to operate at voltages in the range of 138 kV and above, and withstand 650-kV impulse.

Highlights:
1) Completed assembly of HTS transformer high voltage test cryostat.
Assembly of the 30 inch (762 mm) cryostat was completed in December. The large volume of the test chamber will permit high voltage testing of practical components such as model coils, leads, surface insulation, standoffs, etc. as well as large LN2 gaps where there is little data at the higher voltages. Shown in the figures are the internal components and the completed assembly ready for testing. The design allows for changing the electrode test gap from zero up to 6 inches (152.4 mm) in the vertical direction in situ, i.e. the gap can be changed in liquid nitrogen (LN2) without having to warm up the system and remove the electrode assembly. This feature will greatly speed up the data taking process for LN2 gaps. There are also provisions for rotating the high voltage lead which will allow multiple samples to be tested in situ.

The system is equipped with multiple sensors, transfer lines and pressure relief system for continuous monitoring and operation. The bushing is rated for 550 kV BIL (Basic Impulse Level). The pressure will be set between 1 and 2 bar absolute which will prevent bubbles from forming which can reduce insulation strength.

The system was first pressurized to a few psig and checked for leaks. Following those tests the chamber was pumped down and checked for leaks under vacuum. Good vacuum was obtained. The

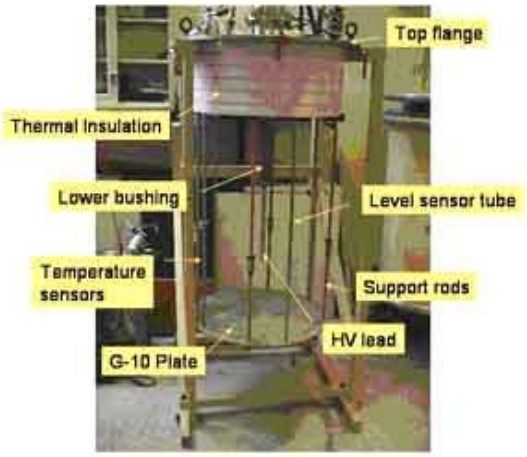

Fig. 1. Lower assembly which will be inside the dewar. High voltage electrodes will be attached to the HV lead. Test fixtures will be supported by the G-10 plate.

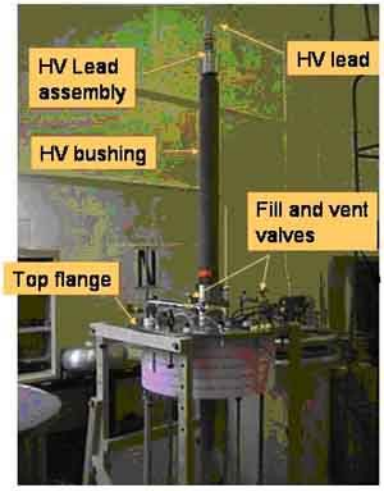

Fig. 2. Upper assembly showing the HV bushing and cyrogenic fill valves and lines.

cryostat was then filled with liquid nitrogen. Operation of the level sensor and multiple temperature sensors at different heights inside the cryostat were verified as was pressure stability in the range from 0 to 9 psig. The temperatures in the test region of the dewar were found to be quite stable with time which will allow adequate time for high voltage testing of components and variable gaps. Gap settings can be changed externally without opening the pressure chamber of the cryostat. The partial discharge characteristics of the bushing were tested up to 145 kVrms and found to be consistent with earlier tests done in air and with the bottom end of the bushing immersed in LN2. Tests have begun late in the quarter on AC breakdown voltages of sphere to plane gaps in LN2 as a function of gap and pressure from 0 to 9 psig.

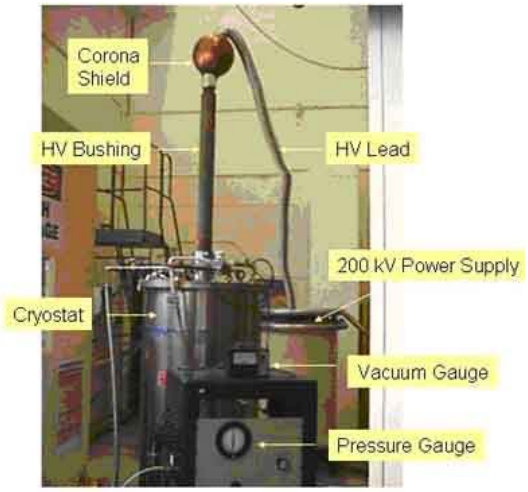

Fig. 3. Completed 30-inch test cryostat with 200 kV high voltage power supply and bushing.

2) HTS Program CPS Control Milestone met - Complete 30-in test dewar and carry out HV tests.

Initial measurements on ac breakdown in liquid nitrogen (see figure 4) were performed in the new 30 inch (762 mm) diameter dewar that was reported in the FT2007 1Q Progress Report. Successful testing of this large volume dewar in Feb. 2007 satisfies the control milestone, and represents an enhanced capability at ORNL for device demonstration testing. Data obtained in this equipment will be used in the design of high voltage insulation for superconducting transformers under a collaborative agreement with Waukesha Electric Systems.

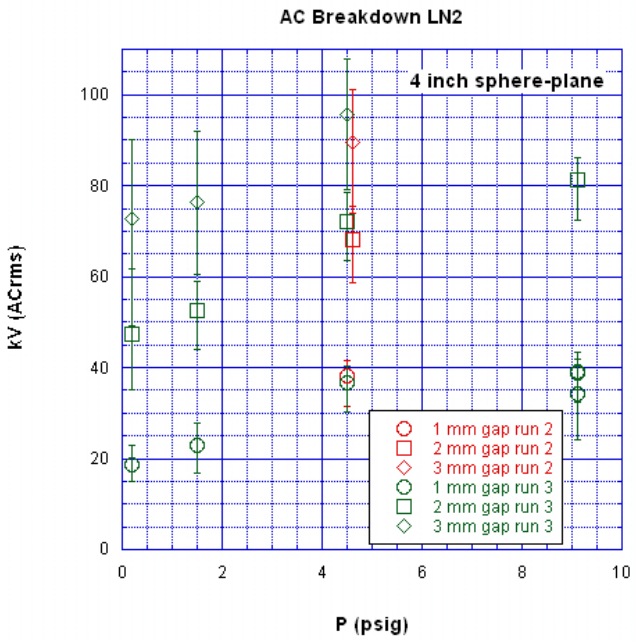

Fig. 4. AC breakdown in pure liquid nitrogen gaps for sphere-plane electrode geometry.

The electrode geometry was a 4 inch (101.6 mm) diameter stainless steel sphere for high voltage to a grounded plane. The finish on the sphere was a typical industrial grade. The bushing arrangement allows for changing the gap in place with the electrodes still immersed in LN2 which greatly speeds up data acquisition. The breakdown voltage generally increased slightly with increasing pressure of LN2 as expected. A 3-mm gap at 9.1 psig was not run due to exceeding the ac voltage rating of the high voltage bushing. The symbols are the average value of at least 10 breakdowns and the error bars are the minimum and maximum breakdown values.

3) High-voltage "dummy" test coil being fabricated.

S.W. Schwenterly visited the Waukesha Electric Systems (WES) plant during March 19-21 to finalize designs and test plans for a new high-voltage test coil that will be wound by WES. This coil will be made with copper dummy conductor, and will closely simulate the geometry proposed for the high-voltage winding of the 24-MVA, 115/13.09-kV transformer that is the goal of our current SPE proposal. Conductor for the coil has been insulated with WES's proprietary synthetic material. The coil will contain multiple samples to allow determination of breakdown voltage statistical distributions. It will be immersed in liquid nitrogen for the tests. An existing dewar at ORNL is being refurbished for the tests and will be shipped to WES. Tests will be carried out at WES with both full-wave and chopped-wave impulse voltages as well as 60-Hz ac voltages. WES personnel are making impulse voltage distribution calculations on the 24-MVA design for comparison with the test results. On other design issues, a new potential supplier has been identified for the composite dewars that will be required for the transformer.

4) Testing of tape insulation for HTS transformers.

A proposed synthetic tape wrapped on copper tape (as a surrogate for HTS tape) has been tested in open bath liquid nitrogen in a crossed tape arrangement which has previously been described. Results indicate that butt gaps tend to lower the breakdown strength.

A total of 48 measurements have been made and are plotted in a Weibull probability plot shown in Figure 5. The plot appears to be linear with the exception of the two lowest points at 10.7 and 15.4 kVrms. These two data points do not appear to be consistent with the rest of the data suggesting that another breakdown mechanism was involved such as the presence of a bubble trapped under the tape. If these two points are removed and the probabilities are recalculated and then replotted, the data becomes linear as shown in Figure 6. The data follows a Weibull distribution from the highest breakdown value to the lowest.

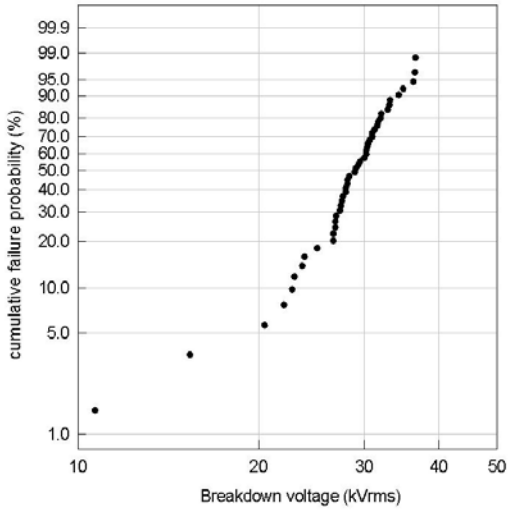

Fig. 5. Breakdown data on synthetic tape wrapped on copper in a crossed tape geometry in liquid nitrogen.

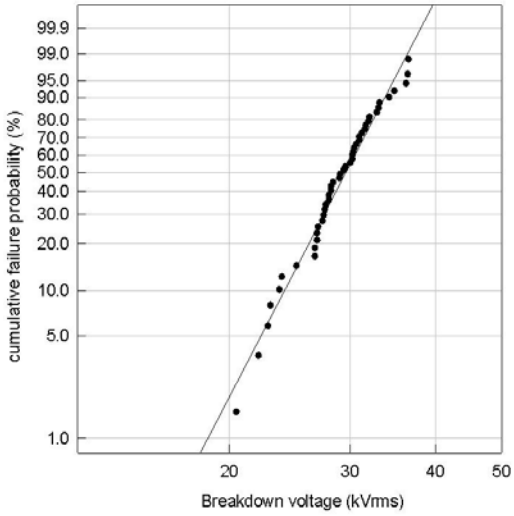

Fig. 6. Breakdown data from Figure 5 replotted without the two lowest breakdown values.

After breakdown the tapes were examined for the breakdown location relative to a butt gap on either tape. The data were then divided into three groups: (1) no butt gap on either tape, (2) a butt gap on one of the tapes and (3) a butt gap on both tapes. The data were organized according to the breakdown location and replotted, shown in Figure 7. The mean values for the three types of breakdown locations are given in Table I, indicating that the butt gaps tend to lower the breakdown strength.

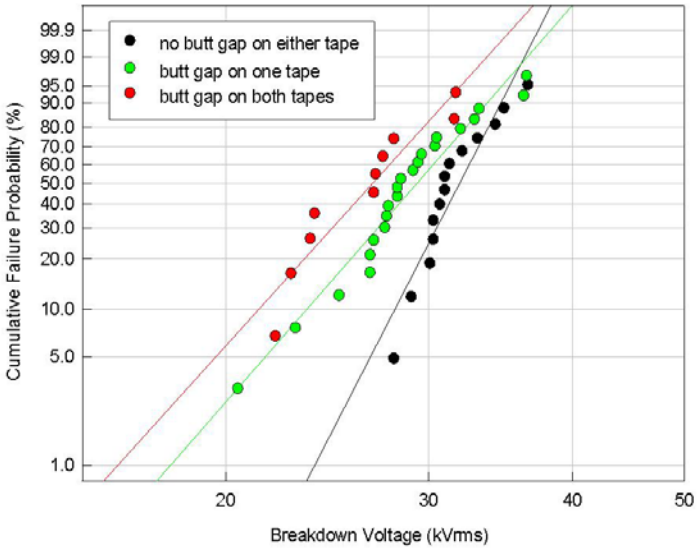

Fig. 7. Effect of butt gap on breakdown probability distribution

Table I. Mean breakdown values according to location

Breakdown location	Mean value (kVrms)	Standard deviation (kVrms)
No butt gap	31.6	2.4
Butt gap on one tape	28.9	3.8
Butt gap on both tapes	26.5	3.4

Status of milestones:

- Complete 30-in test dewar and carry out HV tests. (July 31, 2007**): Met Feb. 23, 2007**.
- Complete cryogenic cooling, ac loss and HTS coil design aspects of transformer conceptual design and engineering analysis. (Sept. 30, 2007): **On going**

Interactions:

Close collaboration with Waukesha Electric Systems (WES) continues in this project. S.W. Schwenterly visited Waukesha during November 6-10 for working meetings on technical details related to ongoing work. E.F. Pleva from WES visited ORNL in early December for technical discussions. Tom Golner of WES visited ORNL in November to discuss electrical insulation issues for the both the HTS transformer and Gridworks compact transformer projects.

Subtask 4.3: Baldor Reliance Electric CRADA: HTS Industrial Motor.
Chris Rey, Paul Fisher, R.C. Duckworth, Tim Kadri

Objectives:
High-temperature superconducting motors offer prospects for improved efficiency, smaller size and weight, and better overload tolerance in comparison with conventional motors. HTS motors will have half the losses of conventional motors of the same rating. Applications will be for motors above 1000 horsepower for utility and industrial customers. A 5000 hp HTS motor could save a single customer $50,000 in energy costs per year. About 1/3 of U. S. electrical energy generated is used to power motors of this rating and above. Potential energy savings for the U. S. alone, if HTS motors fully penetrate the marketplace, could be high as $1B per year. Objective of this collaborative work with Reliance Electric is to develop HTS motors and address issues such as the use of 2G wire in rotor field coil winding, quench characterization and detection, and stable cryogenic operation.

Highlights:
1) Apparatus to test HTS wires at low temperatures, high currents and high magnetic fields at various angles has been constructed and tested.
A simple but elegant test apparatus was designed and fabricated in order to study the critical current (I_c) behavior of 2G YBCO tape. The test apparatus was designed to probe the following parameter space of the 2G YBCO tape:

- High Currents (0 → > 300 A) → upgrade to 580 A
- B-field dependence (0-5 T)
- Temperature dependence (30 K → 85 K)
- Angular dependence (0˚ → 90˚)
- Reasonable length scales (0 - 10 cm)
- Statistical significant sampling
- Splice characterization

Shown in Figure 1 is a full-view picture of the test apparatus used to test the 2G YBCO tape. The measurement portion of the test rig was attached to a Cryomech AL-330 cryocooler, which was used to cool the 2G YBCO tapes. The test apparatus was designed to measure the I_c of five (5) discrete segments of YBCO tape originally cut from one continuous piece length. A close-up (end view) of the test apparatus is shown in Figure 2 below. Each of the five separate 2G YBCO tapes was mounted on five (5) separate measurement platforms. The five measurement platforms were oriented at the following angles with respect to the external applied magnetic field (B-field): 0˚, 30˚, 45˚, 60˚, and 90˚. During operation, the test apparatus (shown in Figs. 1 and 2) was lowered into a vacuum cryostat which was surrounded by a NbTi solenoid magnet capable of reaching magnetic fields up to 5 T.

Fig. 1. Front-view of test apparatus used to measure I_c of 2 G YBCO tapes vs. magnetic field and orientation angle (θ).

Initial tests were performed at 83 K in order to study the I_c vs. B and θ at a temperature close to T_c and in the low current carrying capacity regime of the 2G YBCO tape. Initial measurements were performed on 4-mm wide, copper-stabilized YBCO tape fabricated by SuperPower. Test results shown in Figure 3 are a plot of the critical current (I_c) vs. B-field for five different field orientations at 83 K. Results show that at 83 K, the YBCO tape has an anisotropic I_c in which the I_c for B-fields parallel to the axis of the tape are ~ 3-4 times larger than the I_c with a B-field perpendicular to the axis of the tape. For the remaining angles in between 0˚ and 90˚, the I_c shows a weak dependence on B-field orientation, in which a slight decrease in I_c is observed as the external applied B-field has a smaller parallel component (i.e. a more perpendicular component).

Future plans for worked performed from July through the close of the SPI effort in September 2007 include: a) presentation of results at the annual DOE Peer review in August 2007, b) testing more samples from multiple vendors, c) investigate splice configurations vs. B, T, and θ, d) lower temperatures, and e) coordinate testing w/ NIST for mechanical behavior.

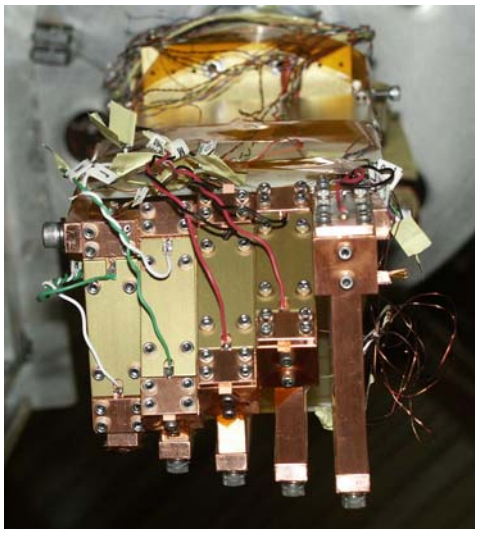

Fig. 2. End-view of test apparatus used to measure I_c of 2 G YBCO tapes vs. magnetic field and orientation angle (θ).

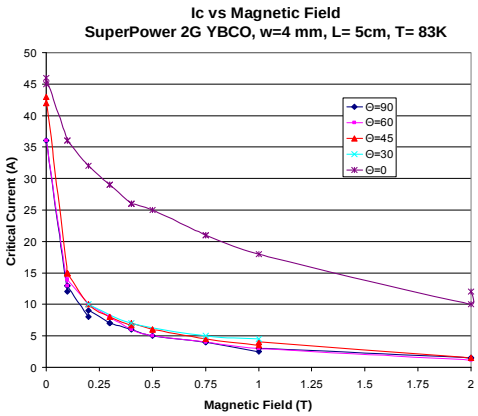

Fig. 3. I_c vs. B-field for five (5) separate field orientations at T=83 K.

2) Electrical Splice Resistance Measurements of 1G and 2G HTS Tapes

Oak Ridge National Laboratory (ORNL), in support of the Superconducting Partnership Initiative (SPI) with Reliance-Baldor has been investigating the electrical splice resistance of both first-generation (1G) Bi-2223 powder-in-tube tape (PIT) and second-generation (2G) YBCO coated conductor (CC). The overall purpose of the experimental investigation was to study the splice resistance of 1G Bi-2223 tape and 2G YBCO coated conductor for HTS motor/generator applications as a function of: a) surface preparation condition, b) flux type, c) solder type, d) sheath materials, e) operating temperature, f) thermal cycle, and g) magnetic field. For brevity purposes only the 2G YBCO data will be presented.

Lap Joint Construction

The 2G YBCO coated conductor (CC) was fabricated by SuperPower. The 2G CC's were approximately 4 mm wide and 0.1 mm thick with a 35 μm thick Cu plating on all four sides the CC. The I_c of the 2G CC was ~ 86 A (77K, self-field) with an n-value ~ 20-40.

There are several different configurations for splice joints such as: lap joints, butt joints, "praying hands" joints, and shim joints where resistive metals or superconducting materials are

overlapped between two adjacent HTS tapes. This study has been limited thus far to the common lap joint type, in which one HTS tape is laid flat over the second HTS tape. The interface region, the "overlap distance" is a key factor in determining the magnitude of the splice resistance. To measure the electrical splice resistance, current is passed from one HTS conductor through the splice joint and through the second HTS conductor. The voltage is measured across the lap joint with a pair of voltage taps that span the entire joint.

Apparatus

To measure the statistical spread in the electrical splice resistance, a series of seven (7) lap joints were fabricated using similar preparation and fabrication techniques (see Fig. 4). Reasonable care, typical of that found in a laboratory type setting, was taken in the preparation of these lap joints to control preparation parameters such as: a) overlap distance, b) surface preparation and cleaning, c) flux type and amount, d) solder type and amount, and e) solder temperature. An eighth voltage tap pair containing "no lap joint" was also included in the series electrical connection. This eighth voltage tap served as a control sample in order to study the effects of the lap joint splice resistance versus the electrical resistance of the HTS tape itself. These eight (8) voltage tap pairs (VT1 → VT8) were then electrically connected in a series configuration and wrapped around a 6061-T6 anodized aluminum (Al) "hub" (see Fig. 5). The anodized coating provided the electrical isolation from the Al hub. The Al hub could then be attached directly to the cold finger of a CryoMech Al-330 cryocooler or submerged in an open bath of LN2. To date all tests have been performed at both room temperature and in pool boiling LN2 at 77 K. In the future, temperature dependent tests are planned for the temperature range from 30 K to 80 K.

Figure 4: Simple sketch of splice configuration showing seven "lap joints" in series.

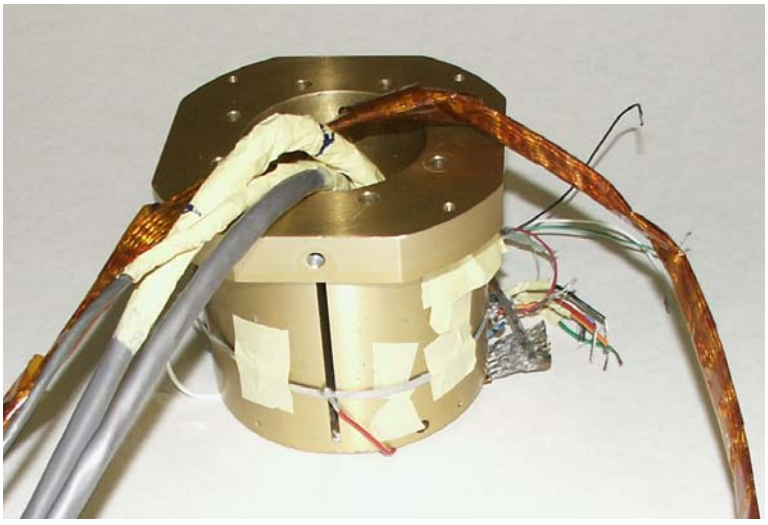

Figure 5. Al 6061 anodized "hub" used to measure the splice resistance of the 1G Bi-2223 and 2G YBCO samples. The Al hub can be attached to a cryocooler or directly submerged in LN2.

Results

The splice fabrication, experimental apparatus, and measurement technique used in both 1G and 2G splice joints were similar. Two YBCO CC's were soldered together with a 0.25 inch overlap distance, using a rosin core Sn(60)-Pb(40) solder with an ethyl alcohol surface cleaning both before and after tinning. The primary difference between the two fabrication methods was care was taken with the 2G CC to keep track of which sides of the CC were being soldered. In this report, we only present data taken in which the two sides of HTS material face one other (i.e. so-called "HTS-to-HTS"). Future studies are planned in which "HTS-to-substrate" splice measurements are studied.

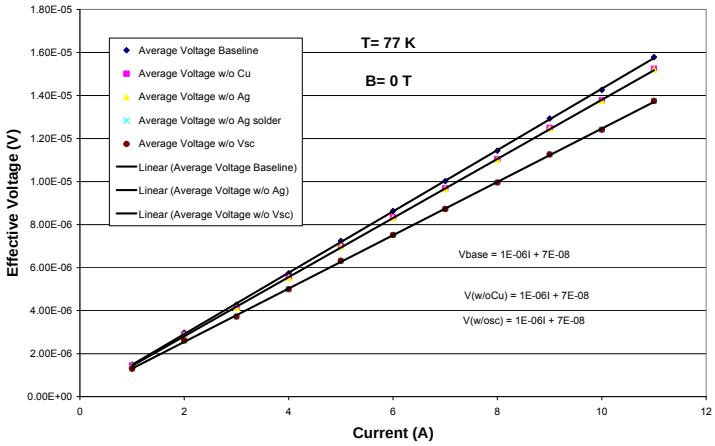

Figure 6a. V_{eff} vs. current (low currents) for a copper clad 2G YBCO CC lap joint with a 0.25 inch overlap at 77 K and B= 0 T. The slope of the baseline curve represents the total splice resistance. The 2G YBCO was fabricated by SuperPower.

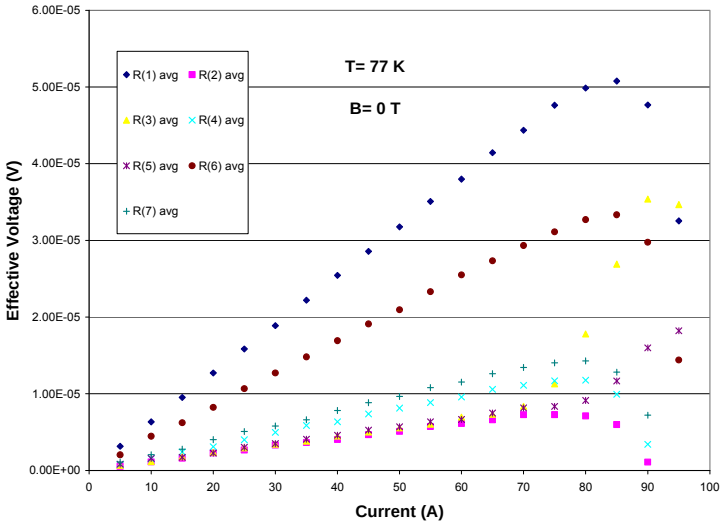

Figure 6b. V_{eff} vs. current (high currents) for a copper-clad, 2G YBCO CC lap joint with a 0.25 inch overlap at 77 K and B= 0 T. The slope of the baseline curve represents the total splice resistance. Note, the non-linear behavior due to the subtraction of the resistance of the YBCO at higher currents.

Shown in Fig. 6a (upper) is a plot of V_{eff} versus current (low currents) for a 2G YBCO CC. The slope of the curve represents the total splice resistance including the contributions from the copper cladding R_{sheath} and the resistance of the superconductor (R_{sc}). The lower points have been corrected by subtracting off the contributions from both R_{sheath} and R_{sc}. When the slope of this curve is multiplied by A_c, the contact resistance (in Ω-cm^2) can be obtained. At these low currents levels < 10 A, the points are far more linear than at the higher current levels where the resistance of the YBCO plays a greater role. Shown in Fig. 6b (lower) is a plot of the V_{eff} versus current for high currents up to 90 A. Note, the non-linear behavior at currents approaching and above the I_c of the sample (I_c ~ 86 A). This is most likely caused by the simple subtraction of the resistance of the superconductor (represented by Eq. 1) not being valid in this regime. Shown in Figs. 7 and 8 are the V_{eff} versus current graphs at 77 K for applied B-fields of 1 T and 2 T.

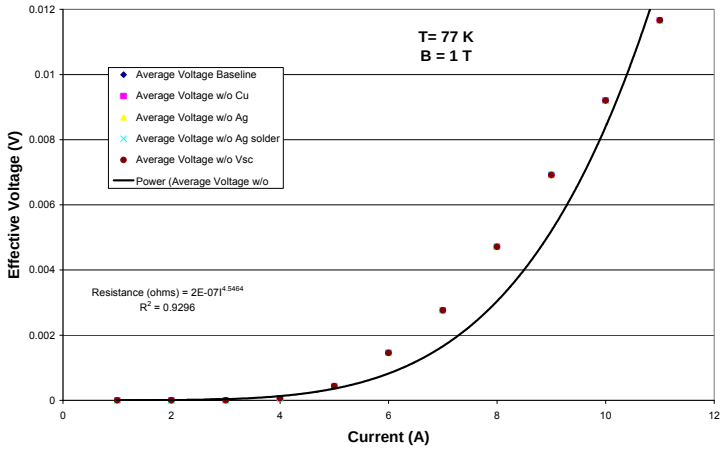

Figure 7. V_{eff} vs. current (low currents) for a Cu clad 2G YBCO lap joint with a 0.25 inch overlap at 77 K and B=1 T. The slope of the curve represents the total splice resistance. Note, that all of the points even after subtraction of the normal metal components are indistinguishable.

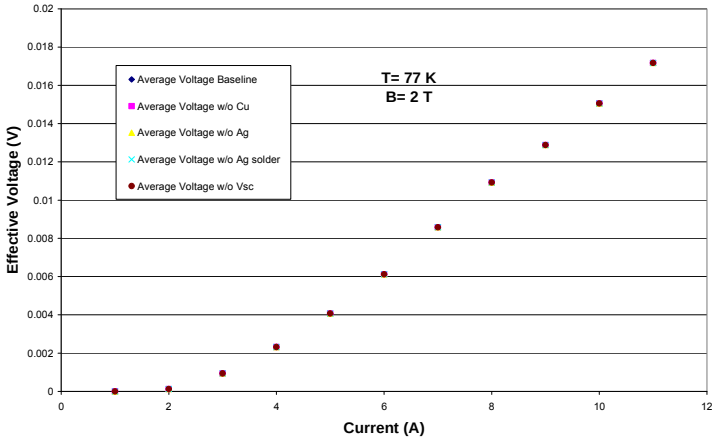

Figure 8. V_{eff} vs. current (low currents) for a Cu clad 2G YBCO lap joint with a 0.25 inch overlap at 77 K and B=2 T. The slope of the curve represents the total splice resistance. Note, that all of the points even after subtraction of the normal metal components are indistinguishable.

Conclusion

ORNL has been investigating the splice resistance in lap joints fabricated with both 1G PIT tapes and 2G YBCO coated conductor as a function of: a) surface preparation condition, b) flux type, c) solder type, d) sheath materials, e) operating temperature, f) thermal cycle, and g) magnetic field. Results indicate that in the 1 G Bi-2223 tapes R_{splice} degrades only slightly (~ 0.5 %) with multiple thermal cycles as long as care is taken to avoid ballooning at the ends of the PIT tape. No degradation was observed in the 2G CC within the accuracy of the measurement. As expected, surface preparation and solder type play a role in determining both the magnitude and variations among splice resistance, but the most significant role is played by the magnitude of the applied transport current and what fraction of I_c the joint will experience during operation. This is particularly evident in the measurements taken in applied B-fields. Measurements performed on the 1G Bi-2223 tapes show a lower splice resistance than the 2G YBCO CC by factors of 3-9. It is not yet known why there is such a large difference in these values. It is known that splices made to the substrate side (i.e. non-HTS) of 2G CC are considerably higher than those made directly to the HTS side. Although care was taken by the researchers to distinguish and keep track of these different sides on the CC, there is often extremely poor labeling on the tapes themselves.

In addition, ORNL is collaborating with the National Institute of Standards and Technology in Boulder, CO in studying the mechanical behavior of splice resistance as a function of tensile stress.

Status of milestones:

- Conduct research to characterize DC loss (voltage drop vs. current, temperature, magnetic field, and magnetic field direction) in 2-G HTS tapes. (Sept 30, 2007): **Met June 2007.**

Interactions:

Work includes close collaboration with Baldor Reliance Electric. Results are communicated to Baldor to assist in their motor development and planning activities.

Subtask 4.4: Fault current limiter CRADA with SuperPower.
D.R. James, A. R. Ellis, I. Sauers, E. Tuncer

Objectives:
ORNL has teamed with SuperPower, Inc. (SP) on the development of a superconducting fault current limiter (FCL). This is an enabling device that can significantly mitigate fault currents and prevent costly equipment damages. It promises to positively impact electric power transmission/ distribution reliability and security by introducing a new element in the grid that and provide lower cost solutions for grid protection. Purposes of the project are to assist in the development of FCL by performing high voltage (HV) R&D on specified FCL internal components and providing technical design support.

Highlights:
1) Test set up being prepared for HV qualification of bushing.
Preparations are being made for high voltage qualification testing of a bushing to be used in liquid nitrogen (LN2). SuperPower is furnishing the bushing and team members from SuperPower will come to ORNL in April to conduct the tests in conjunction with ORNL staff.

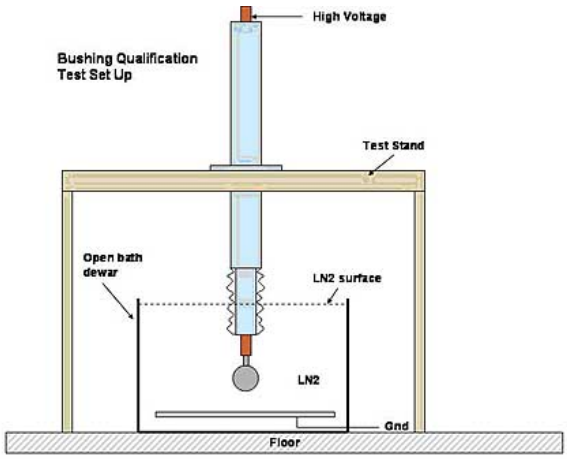

Fig. 1. Test set up for qualification testing of a bushing to be used in LN2.

A schematic of the basic test set up is shown in figure 1. Tests to be done include partial discharge, AC withstand, and positive and negative lightning impulse (1.2 μs rise/50 μs fall time) withstand. The impulse voltage level will be the standard BIL (Basic Impulse Insulation Level) of 650 kV for this class of bushing. To verify performance of the bushing, tests will be done in air at room temperature to establish a baseline. The tests will then be done in LN2 and repeated again in air and results compared. Electric field calculations and preliminary testing have been done to verify the type of termination and air gaps needed for the withstand tests. High voltage tests will also be conducted on a mockup of the fault current limiting elements provided by SuperPower. These tests will also be performed in an open LN2 bath.

2) Performed high voltage test of 138-kV bushing fro FCL.
A high voltage bushing which is planned to be used on the SuperPower HTS fault current limiter, has been tested at ORNL in both ambient air and in open bath liquid nitrogen. Tests included AC withstand, partial discharge and impulse (BIL) withstand. The bushing successfully passed multiple testings.

The bushing was furnished by SuperPower and shipped to ORNL. Previous calculations and impulse testing in air by ORNL determined the gaps and spacings needed to withstand lightning impulse voltages of 650 kV of both polarities. This is the first time this laboratory has

performed testing at this voltage level. Based on this information, a non-conducting stand was designed and built of wood to hold the bushing in a vertical orientation which allowed a 60 inch (1.52 m) sphere to earthed-plane gap to be set. A lifting beam was purchased which allowed the bushing to be hoisted with a large 50 cm corona ring on the top lead. For the lower termination in air, two 22 inch (55.9 cm) diameter aluminum hemispheres were obtained and welded to form a sphere (Figure 2). The stand was also designed with a lower position which allowed the bottom part of the bushing to be immersed in an open bath of LN2 (Figure 3). In this case a 6 inch (152.4 mm) diameter stainless steel sphere was used with a 6 inch gap to a grounded plane at the bottom of the dewar. Much smaller gaps can be used in LN2 since the dielectric strength of LN2 is much higher than that of air.

Fig. 2. Wayne Ordon of SuperPower inspects a 22 inch (55.9 cm) diameter aluminum sphere used as a bushing termination for air withstand tests. A large air gap of 60 inches (1.52 m) was required to prevent flashover when qualifying at 650 kV impulse voltages.

Drew Hazelton and Wayne Ordon of SuperPower came to ORNL to participate in the tests which were done from April 16 – 20. The testing order followed was the same as the manufacturer. The bushing passed 5 successive negative lightning impulse voltages at 654 kV which verified the manufacturers factory tests. Partial discharge was tested up to 100 kVrms which was the limit of the equipment and found to be 1.1 pC at 99.9 kVrms. The bushing then passed a 60 sec withstand test at 200 kVrms which was the maximum voltage of the power supply. Partial discharge tests were successfully repeated which completed the air tests.

The open dewar was installed and bushing repositioned at the lower gap. A thermocouple was mounted on the bushing to monitor cooldown. Slow continuous addition of LN2 to the dewar allowed the bushing to cool down slowly and fill the bath after several hours.

Lig. 3. Left to right, Drew Hazelton and Wayne Ordon of SuperPower and Alvin Ellis of ORNL examine the lower end of the bushing immersed in LN2. Ice formation occurs on the sheds just above the surface of the LN2.

The bushing again passed 5 consecutive negative lightning impulse shots at 653 kV in LN2. The partial discharge tests were repeated again to 100 kVrms where the level was less than 5 pC and hence passed the test. An open circuit test of the partial discharge system without the bushing indicated that most of the partial discharge detected was coming from the detector system and not the bushing. The 200 kVrms withstand test for 60 seconds was again passed as was a repeat of the partial discharge test. The tan delta and capacitance measurements were performed before and after each series of voltage measurements and found to be consistent. Impulse tests were again repeated in LN2 the next day with 5 consecutive negative withstands at 655 kV. The polarity was switched to positive and 5 consecutive withstands were obtained at

655 kV. Partial discharge was also successfully repeated. Hence overnight immersion in LN2 did not adversely affect performance.

The bushing was allowed to warm up slowly over 48 hours and the high voltage tests were repeated in air at room temperature. The bushing successfully passed five negative impulses at 664 kV peak. The partial discharge test was passed at less than 1.7 picocoulomb at 100.6 kVrms. The bushing then passed a 60 second withstand test at 200.4 kVrms ac which was followed by a second partial discharge test which passed at 2.6 picocoulomb at 100.3 kVrms. Based on these tests, we do not believe the bushing was degraded by immersion in LN2 and is a viable candidate for use.

These successful tests also demonstrated the ability to test large 138 kV class bushings to the 650 kV BIL level in the ORNL High Voltage facility.

3) HV testing on FCL assembly mockup performed.

Under routine conditions, the HTS Fault Current Limiter (FCL) will be operated at full line voltage and hence its assembly must be designed to withstand the high electric fields between its components and the grounded tank. Hence, it is necessary to perform high voltage tests on scale models to validate the design (Figure 4). During this quarter such tests were conducted at ORNL on a mockup supplied by SuperPower. Partial discharge, ac breakdown voltage, and impulse breakdown voltage were done first in air for comparison to results in liquid nitrogen. For these initial tests, only impulse breakdown was performed in liquid nitrogen in an open bath. These results will provide useful design guidelines for the full scale system.

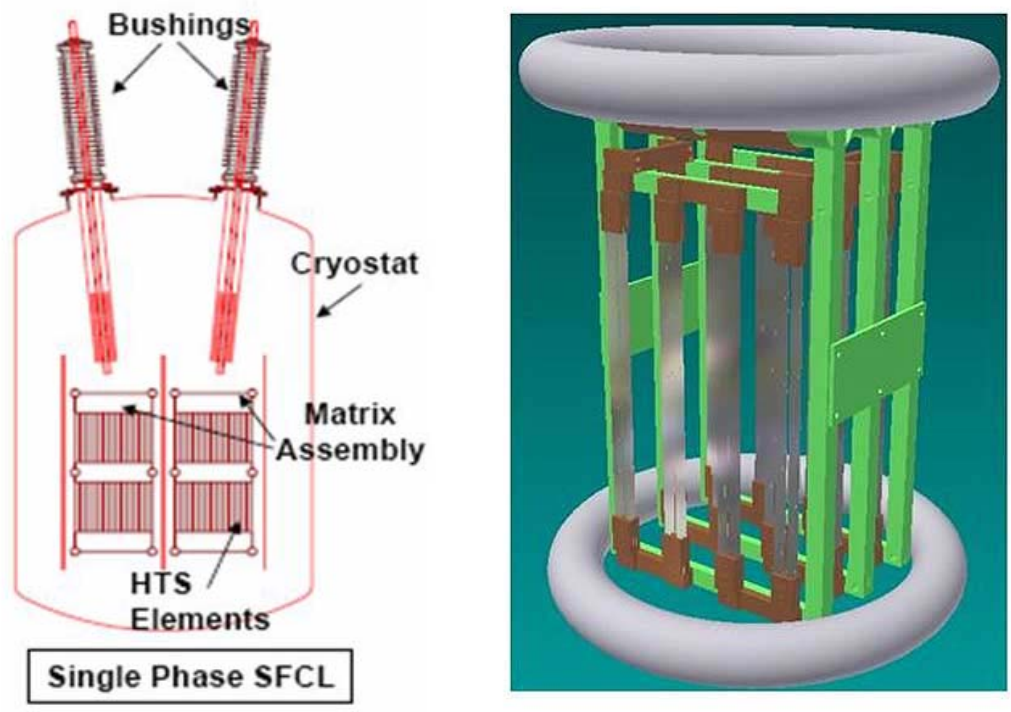

Figure 4. (Left) Conceptual drawing of the HTS Fault Current Limiter. (Right) Sketch of the mockup of the FCL matrix assembly for testing in an open bath.

Following successful testing of a 145-kV bushing at ORNL in the previous quarter, high voltage tests were initiated on a mockup of the proposed FCL which was assembled by SuperPower and delivered to ORNL. The mockup model consists of components closely resembling an actual FCL including corona rings, simulated HTS elements, conductors, supports, coils and connections. The high voltage tests performed included partial discharge (PD) onset, ac breakdown, and impulse breakdown. The mockup was suspended in an open dewar with a grounded plate on the bottom and grounded cylindrical side walls (Figure 5). Tests were performed in air first to identify any potential problems and to compare with results for the mockup fully immersed in liquid nitrogen in an open bath at 77 K. Measurements in air were obtained as a function of spacing between the various components and the side wall for different orientations of the mockup. Initial impulse breakdown in LN2 have been obtained for voltages up to 480 kV. The breakdown data allows statistical evaluation using a Weibull distribution of failure probability. These results will help to determine the clearances needed in the actual device and estimate the failure probability for design purposes.

Figure 5. (Left) Alvin Ellis sets the gap between the side wall and a component of the FCL mockup in an open liquid nitrogen bath. The mockup is suspended in the bath which allows changing of the gap and isolation from the bottom of the tank. (Right) Open bath showing the high voltage connections for ac partial discharge testing.

Status of milestones:

- Participate in DOE Readiness Review to develop 2G matrix elements. (Feb. 28, 2007): **Met Dec 2006.**
- Complete HV testing of SFCL matrix sub-assemblies at ORNL. (Sept 30, 2007): **Met Sept. 2007.**

Interactions:

ORNL has been working closely with SuperPower on the design of SFCL. There were frequent discussions and exchanges in preparation for the HV bushing test. SuperPower staff came to ORNL to participate in the above HV bushing tests in open bath liquid nitrogen.

Subtask 4.5: Cryogenic dielectric R&D and design rules.
I. Sauers, E. Tuncer, D.R. James, A. R. Ellis, M. Pace

Objectives:

Cryogenic dielectrics, like cryogenic cooling systems, is an enabling technology for HTS grid applications. Conventional dielectrics have grown with the grid over the last 120 years to higher voltage levels, now approaching 1 MV in some cases, and high component reliabilities with proven materials. Utilities expect comparable reliability for new technologies and this puts a high expectation on the performance of HTS devices. To meet the expectation, there is an increasing need for cryogenic dielectric data on liquid nitrogen and other materials, such as fiberglass reinforced plastics (G10) at longer gaps where currently the data available in the literature is sparse. Partial discharge, surface flashover, ac and impulse breakdown data are needed with sufficient statistical information to design large scale systems with adequate safety factors. In this work we focus on characterizing generic cryogenic dielectric properties, including aging studies, on existing materials, as well as developing generic design rules that can be used by the high voltage engineer in designing HTS cables, transformers, fault current limiters, and terminations.

Highlights:

1) Breakdown of Cryoflex compared with PPLP in liquid nitrogen.

We have re-examined the breakdown strength of Cryoflex by evaporating electrodes on sheets of cryoflex. Results of multiple measurements were compared with PPLP (polyprolyene paper laminate) using the same electrode arrangement in liquid nitrogen (LN2). Significantly higher breakdown strengths were confirmed for Cryoflex.

Four materials were tested: old embossed Cryoflex (o-CFe), old unembossed Cryoflex (o-CFu), new embossed Cryoflex (n-CFe), and PPLP. The number of measurements made for each material are 12, 16, 17, and 18 respectively. Data shown in figure 1 represents the mean

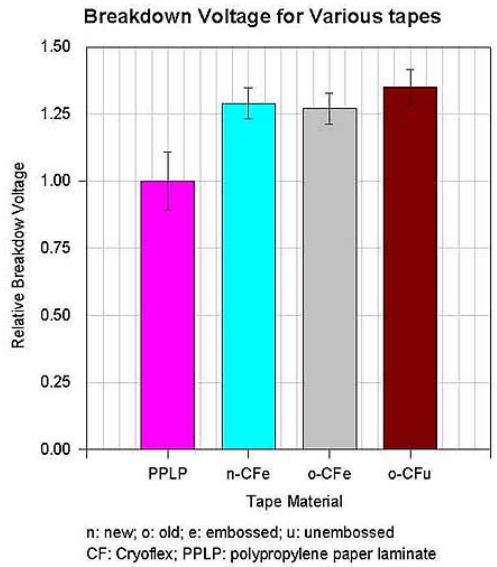

Fig. 1. Mean breakdown voltage for PPLP, n-CFe, o-CFe, and o-CFu

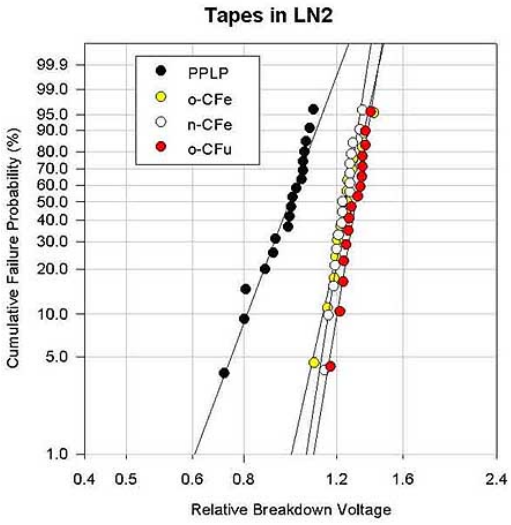

Fig. 2. Weibull plots of breakdown voltage distributions of different tape materials in LN2

breakdown values normalized to that of PPLP, with standard deviations indicated by the error bars. All of the Cryoflex samples show a 25-30% improvement in strength over PPLP. This is consistent with previous breakdown measurements of model cables insulated with PPLP and o-CFe where the insulation consists of the tape/LN2 combination and where the Cryoflex insulated model cable has a 19% higher breakdown strength than PPLP. Weibull distributions of the data reveal the superior performance of all Cryoflex materials. When the data is extrapolated to a 1% probability of breakdown the difference in breakdown voltage between the different forms of Cryoflex is about 40% higher than PPLP (Fig. 2).

2) New cell design led to improved measurement setup for electrical properties of cryogenic dielectric materials.

The measurement setup for electrical properties of materials was improved with a new cell design, which is used in the cryocooler. Initial tests on the unfilled polyvinyl alcohol (PVA) showed good temperature stability in the cell. Previously, large temperature gradients were observed on film samples. Dielectric properties of the PVA was measured between 15 K and 350 K with 5 K steps.

3) Dielectric test setup for insulated tapes completed.

Test apparatus has been developed to perform dielectric tests of insulated tapes in liquid nitrogen (LN2). Figures 3 and 4 show the experimental set up in which one of the tapes is arranged perpendicular to three tapes for multiple measurements without having to remove the tapes from the liquid nitrogen bath. Each tape is wrapped with five layers of dielectric strips, so the total number of strips of electrical insulation between the two tapes is 10 layers. Each strip layer is nominally 0.003" (0.076 mm) giving a total of 0.76 mm of insulation between the two tapes. An average of 6 measurements yielded a breakdown strength of 30.9 ± 5.4 kVrms/mm in open bath (1 bar) liquid nitrogen.

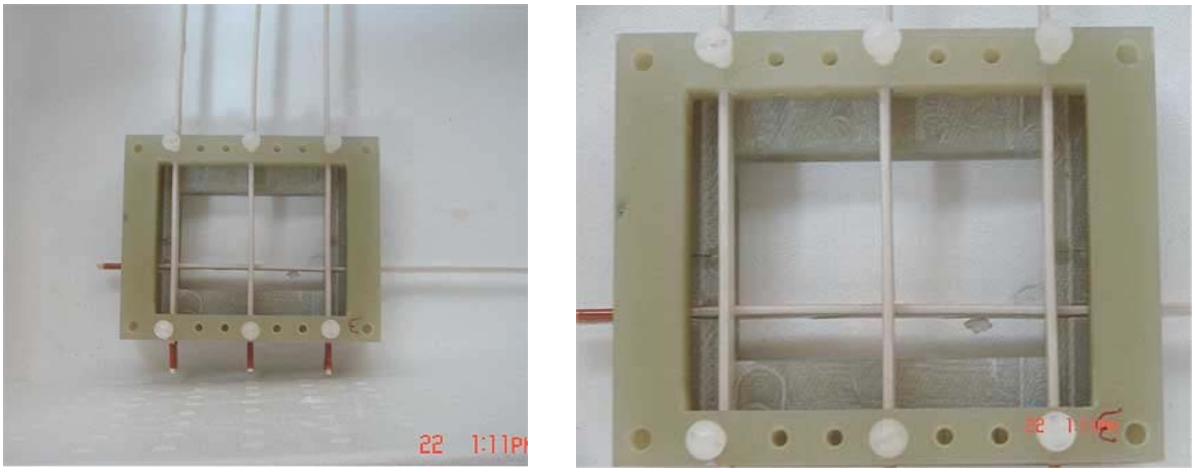

Fig. 3. Experimental setup for measuring breakdown of insulated tape in open bath liquid nitrogen. In the photos the horizontal tape is at ground potential and each of the vertical tapes are ramped at high voltage until breakdown while the other tapes are floating.

Fig. 4. Tape assembly in Styrofoam dewar, connected to voltage divider.

4) AC breakdown in liquid nitrogen

Liquid nitrogen (LN_2) is commonly used both as a coolant and electrical insulation in high temperature superconductor (HTS) equipment for power applications. Hence it is necessary to know the electrical breakdown characteristics of LN_2 under a variety of practical conditions. Measurements on ac breakdown in liquid nitrogen were performed in a stainless steel dewar of 30 inch (762 mm) diameter which could be pressurized from 1 to 2 bar absolute (Figure 5). The high voltage electrode was a 4 inch (101.6 mm) diameter stainless steel sphere to a grounded plane. The finish on the sphere was a typical industrial grade which might be used in practice. A sliding seal at the top of the bushing allows the high voltage lead to be moved up and down for changing the gap in place with the electrodes still immersed in LN2 which greatly speeds up data acquisition. The breakdown voltage increased linearly with gap over the limited range studied which is expected for this electrode geometry since the electric field is approximately uniform for gaps small compared to the sphere radius. Larger gaps were not studied since the phase-to-ground voltage rating of the bushing could not be exceeded.

It is important to understand the statistics of the breakdown values since equipment must designed such that the predicted failure probability is quite low, for example 1%. A Weibull distribution is frequently used as a model for the failure probability in breakdown measurements where the failure mechanism is thought to be due to a "weakest link" or defect. This distribution is given as:

$$F(V) = 1 - \exp[-(V/V_{63.2})^b] \qquad (1)$$

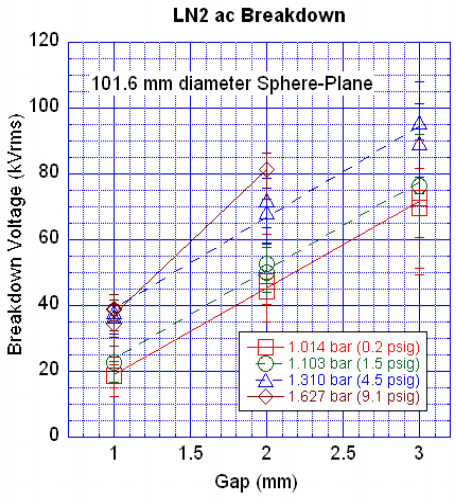

Fig. 5. AC breakdown data for liquid nitrogen as a function of gap for 101.6 mm (4 inch) sphere to plane electrode geometry. The symbols are the average value of at least 10 breakdowns and the error bars are the minimum and maximum breakdown values.

where $F(V)$ is the cumulative failure probability and $V_{63.2}$ is the breakdown voltage with probability of 63.2%. On a Weibull plot, b is the so-called shape parameter or slope of the straight line fit to the data. If the data fit a straight line well, then it can be assumed that the breakdown values follow a Weibull distribution. Figure 6 shows the liquid nitrogen ac breakdown values for the 101.6 mm (4 inch) sphere-to-plane gap for a pressure of 1.014 bar (0.2 psig) for gaps of 1, 2, and 3 mm. From such plots the breakdown voltage for a 1% failure probability can be estimated. This data can be used for design purposes in a number of applications. For example a 2 mm gap for this geometry and pressure should hold off about 26 kVrms with a 1% failure probability. Additional work is needed on the statistics of impulse breakdown in liquid nitrogen gaps, especially at higher voltages.

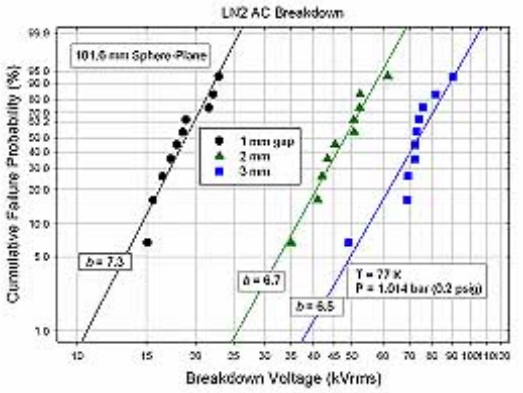

Fig. 6. Liquid nitrogen gap ac breakdown voltages plotted as a Weibull distribution of failure probability. The electrode geometry was 101.6 mm (4 inch) sphere-to-plane at a pressure of 1.014 bar (0.2 psig). The b values are the Weibull shape parameter and slope of the linear fit.

5) AC breakdown data for fiberglass reinforced plastics (FRP) in liquid nitrogen

Another commonly used material for HTS applications is fiberglass reinforced plastic (FRP). Among these materials G10 is often used for structural purposes, but because the material is often in a region of high electrical stress, it must serve as a dielectric. Very little data is available in the literature, necessitating research in finding the dielectric strength under various conditions in order to develop design rules (i.e. thicknesses, spacings and safety margins for the particular voltage application).

The G10 composites are composed of laminates of glass fiber cloths. In the breakdown tests laminate directions parallel and perpendicular to the applied electric field direction were chosen as the material is not isotropic. Two different thicknesses for each laminate thickness were tested. The results are summarized in the following table.

sample	***thickness***	***Voltage [kVrms]***	***Field [kV/mm]***	***Threshold***
Sheet[a]	29 mil (0.725mm)	32.5±4.1	44.8±5.6	27.7 kV/mm
Sheet[a]	125 mil (3.125mm)	70.4±5.7	22.5±1.8	19.3 kV/mm
Rod[b]	40mil (1mm)	23.6±0.8	23.6±0.8	19.6 kV/mm
Rod[b]	80mil (2mm)	35.8±2.0	17.9±1.0	12.9 kV/mm

a Sheet samples were cut from a flat G10 piece. Laminates are perpendicular to field.

b Samples cut from rods. These samples have laminates parallel to the field direction.

6) Evaluation of LN2 breakdown in terms of stressed volume and electrode area.

Although there is a substantial amount of data in the literature on high-voltage breakdown in liquid nitrogen, there are design and scaling issues relating to stressed volume and electrode area

which has indicated that the breakdown strength decreases with increased volume and area. To date there are no well defined rules that can be applied, especially when considering safety factors using the Weibull distribution of breakdown. Therefore work is currently underway to analyze breakdown data in LN2 in terms of stressed volume and area for sphere-plane electrode geometry.

7) Cryogenic Dielectrics web site.

A web site has been created for cryogenic dielectrics (Figure 7). The web site will make breakdown data in materials commonly used for high temperature superconducting applications available to design engineers and researchers. The site currently contains a data base of breakdown data for liquid nitrogen, a commonly used cryogen and dielectric for HTS applications.

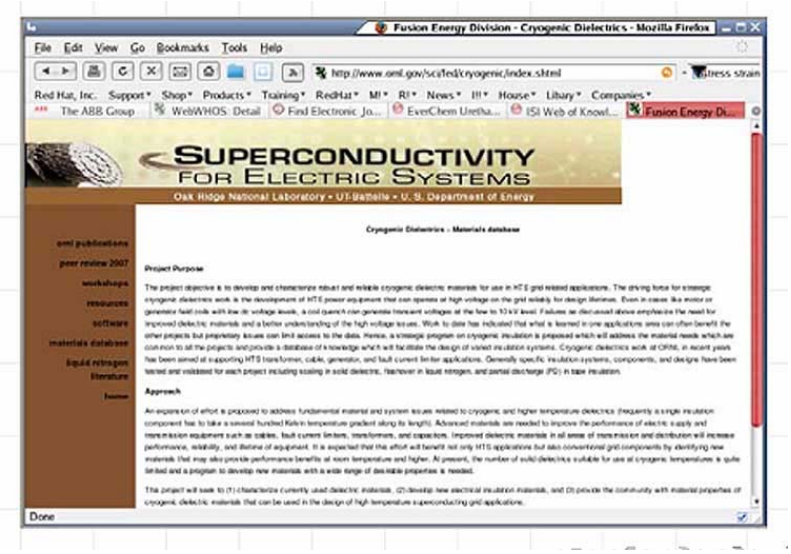

Figure 7 Screen shot of cryogenic dielectrics homepage

8) Collaboration with CAPS/FSU

Collaboration with the Center for Advanced Power Systems (CAPS) at Florida State University has been initiated with a September 17-18 visit of ORNL staff to CAPS in Tallahassee, FL where a small cryogenic dielectrics program is being initiated. During this first visit, specific areas of investigation were identified which will lead to sharing of dielectric samples for characterization at both ORNL and CAPS.

Status of milestones:

- Quantify ac and impulse breakdown in LN2 as function of gap and electric field profile. (Aug 31, 2007): **Met June 2007.**
- Quantify breakdown strength and partial discharge characteristics of solid G10 in cryogenic environment. (Sept 30, 2007): **Met Sept. 2007.**

Interactions:

Results are communicated to the appropriate industry partners to assist in their development and planning activities.

Subtask 4.6: SPI/SPE Readiness Reviews.
M. J. Gouge

Objective:
Several previous HTS demonstration projects had technical failures that precluded successful demonstration on the electric grid. These failures could have been avoided or circumvented if objective technical reviews were performed at critical go/no-go junctures. Recognizing this, the Program initiated a Readiness Review process that has contributed greatly to the success of the remaining demonstration projects. The goal of the reviews is to enhance the probability of successful completion of demonstration projects by focusing on early identification and resolution of technical issues. Reviews are conducted by a small group of experts independent of the demonstration project teams with emphasis on an objective technical in-depth review.

Highlights:

- A report was issued in March 2007 to DOE-OE and SuperPower, Inc. (SP) documenting the December 18, 2006 Superconductivity Partnership with Industry (SPI) Project Readiness Review conducted at SP as part of a more general "DOE/EPRI project re-engagement" meeting.
  It had been nearly 18 months since the previous readiness review and the basic fault limiting technical approach had changed as well as several key project staff and major participants. SuperPower placed the Matrix Fault Current Limiter (MFCL) project in a "reduced effort" status following a readiness review in the summer of 2005. The program remained in that status until mid-2006. At that time a newly reconstructed, SuperPower-led team established a new project technical baseline using second generation (2G) HTS tape-based elements as replacements for the bulk BSSCO matrix elements used in the MFCL device. The project name was revised slightly to Superconducting Fault Current Limiter (SFCL) project. Readiness reviewers were Mike Gouge (ORNL) and Bill Hassenzahl (AEA).

- A web-site was implemented with lessons-learned from the prior SPI projects and general design guidance. It is located at: *http://www.ornl.gov/hts_readiness_reviews*. In FY 2008 this web-site will be upgraded to include more lessons-learned from prior SPI projects, some general design guidance on high voltage, vacuum, etc. and a forum where SPE participants can post comments or questions and get feedback. A paper was written and presented at the 2007 Cryogenic Engineering Conference entitled "Vacuum-Insulated, Flexible Cryostats for Long HTS Cables: Requirements, Status and Prospects." The abstract is given below.

- Several high temperature superconducting (HTS) cable demonstration projects have begun operation on the electric grid in the last few years with the liquid nitrogen-cooled, three-phase cable contained in one or more vacuum-insulated, flexible cryostats with lengths up to ~600 meters. These grid demonstration projects are realistic prototypes of the anticipated commercial market which will require superconducting cable lengths in the multiple kilometer range with the vacuum-jacketed cryostats in underground ducts providing acceptable thermal insulation for up to decades. The current state-of-the art for flexible cryostats (installation constraints, heat loads with a good and degraded vacuum,

impact of cable bends, getter performance and lifetime, weld and accessory reliability) is discussed. Further development needed to meet the challenging commercial HTS cable application is outlined.

- A new program solicitation on superconducting power equipment resulted in five new projects, with selection in June 2007. In early FY 2008 the selected projects will begin (2 cable and 3 FCL projects). Contact has been made with the leaders of the three FCL projects on timing for an initial review of the projects. The team's organization/resources will be reviewed to ensure sufficient capability to address the technical challenges.

Status of milestones:

- Organize SPI/SPE session at 2007 Wire Development Workshop. (Jan. 31, 2007): **Met Jan. 2007**.
- Conduct readiness review of SFCL project with revised matrix design (2G tape). (Feb. 28, 2007): **Met Dec 2006**.
- Conduct initial readiness reviews of new SPE projects to ensure realistic deliverables and competent teams. (Sept. 30, 2007): **Ongoing.**

Section 5: Technical R&D and Support (Sub-Contracts)

Laboratory-coordinated activities involving the R&D of 2G wires and technical support of the HTS program.

Subtask 5.1: American Superconductor Corp. 2G wire development subcontract.
M.W. Rupich (American Superconductor)

Objective:

AMSC is currently commissioning a manufacturing line for the production of 2G HTS wire based on the MOD-YBCO/RABiTS™ technology. AMSC's process is presently capable of producing 2G wire with a performance level nearing that required for initial commercial and military HTS wire-based applications. However, in order to meet the DOE and commercial cost/performance targets for broad market acceptance, it is necessary to further increase the critical current of the 2G wire, optimize the wire architecture and properties for specific applications and reduce the 2G wire manufacturing cost. The objective of this subcontract is to accelerate the development of a low-cost manufacturing process for 2G wire by (1) improving the process rates and yields of the continuous processing technologies, (2) enhancing the critical current of the YBCO layer, (3) and developing 2G wire architectures suitable for commercial and military applications.

Highlights:

- *1) Critical current of AMSC's 344 superconductors exceeds 100 A at 77K, self-field*
  - 117 A performance was achieved in a 70 meter length of standard 344 superconductors produced on AMSC's pilot manufacturing line.
  - Average critical current (77k, self-field) of AMSC's production wire reaches the 80 – 100 A level.
- *2) 1.4 μm YBCO films qualified for insertion into AMSC's baseline production*
  - 150 A (375 A/cm-w) achieved in 5-meter qualification runs of 344 superconductors.
  - 1.4 μm hybrid Y(Dy)BCO/YBCO process slated for standard production in CY2007.
- *3) Improved manufacturing processes and rate enhancements provide path to volume production of 344 superconductors with commercial-level electrical performance.*
  - Enhanced production rates and process modifications developed for full-scale production equipment will enable an annual production capacity of 720 km of 344 superconductors in December 2007.
  - Processing rates consistent with achieving commercial cost targets with 10-cm strips have been demonstrated.
- *4) AMSC's 2G scale up on track for production capacity of 720 km/year in December 2007*
  - 100% of production scale equipment installed
  - 75% of processes qualified
- *5) Additional rate enhancements increase capacity of slowest steps in production process.*
  - Improvements in texture anneal and decomposition rates increase capacity to beyond 720 km/yr target for 344 supercondiuctors.

- *6) Prototype 344 Superconductor with LZO solution buffer showed good I_c.*
  - Slot die coated MOD LZO buffer replaced PVD YSZ layer
  - 8 meters-long prototype 344 superconductor showed good average I_c of 70 A at 77K s.f., with maximum and minimum sectional I_c of 84 A and 56 A, respectively.
- *7) AMSC's 344 superconductors with stainless steel lamination used in successful Fault Current Limiter (FCL) demonstrations.*
  - Siemens and AMSC demonstrated the first successful test of a 2MVA FCL produced with 344 superconductors with a stainless steel laminate in February 2007
  - Hyundai demonstrated an 8.3 MVA FCL, manufactured with AMSC's 344 superconductors. The unit achieved an AC withstand voltage of 143kV, nearly three times the 50kV targeted performance.
- *8) AMSC's 344 superconductors used in successful cable test.*
  - Nexans fabricated and successfully tested a cable built with AMSC's 344 superconductors
  - Cable specifications include:
    - 138 kV – 1820 A @ 74 K, 30 meters, 2-layer conductor – 33 tapes 2G wire (1-layer screen 1G wire)

Technical progress:

- *1) Improved texture in RABiTS template leads to increased Jc in YBCO films*
  - Mechanism controlling texture enhancement in Y_2O_3 seed layer was identified. Standard (4-cm) RABiTS template produced in AMSC's pilot line with the enhanced texture supported J_c's of 5 MA/cm^2 in a 0.8 μm thick Y(Dy)BCO film..
- *2) Performance of 344 superconductors nears commercial level*
  - A critical current of 117 A (minimum) was achieved in a 70 meter length of 344 superconductors produced in AMSC's pilot manufacturing line. This performance level, achieved in a 0.8 μm YBCO film, is approaching the 120 A level required for early commercial applications.
  - A critical current of 150 A was demonstrated in a 5 meter length of 344 superconductors fabricated with a 1.4 μm YBCO layer.
  - R&D samples have achieved critical currents exceeding 550 A/cm-width providing a path to a critical current of over 200 A in 344 superconductors.
- *3) Process Improvements*
  - Modification of the pilot slitting line has reduced variability between alternating cuts, resulting in higher overall produce performance and increased product yield.
  - A modified oxygenation process, introduced into pilot manufacturing line, has enhanced the in-field performance of 344 superconductors and significantly reduced processing time.
  - Improvements of texture anneal process increased processing capacity (344 superconductor equivalent) to ~2Mm/yr.
  - A modified decomposition process demonstrated in R&D equipment that increases process capacity (344 superconductor equivalent) to ~ 1Mm/yr for 1.4 μm thick HTS

Status of milestones:

- 20 – 100 meter length of 344 superconductor wire with a critical current exceeding 100 A at 77K, self-field (July 31, 2007).
  - **Met January 2007** - 117 A (77K, self-field) over 70 m of 344 superconductor.
- 100 meter lengths of 344 superconductor with an Ic exceeding 120 A at 77K, self-field.
  - **On track for December 2007**.
  - 150 A demonstrated in 5 meter qualification wires

Subtask 5.2: SuperPower Inc. 2G wire development subcontract.
V. Selvamanickam (SuperPower)

Objective:
SuperPower is now in a position to produce good quality 2G wire in "pilot-scale" mode with performance level that satisfies most HTS demonstration applications. To meet the DOE and practical commercial application cost/performance target, however, it is necessary to further improve the HTS transport properties. Further, it is important to refine the conductor structure and fabrication processes to reduce the conductor cost. The purpose of this project is to accelerate the development of commercial long-length high-performance IBAD/MOCVD 2G wire.

Highlights:
1) Research-grade MOCVD/IBAD 2G wire from SuperPower exceeds 700 A/cm performance.
High 2G wire I_c is necessary for many HTS power applications as well as a lower cost/performance ratio. SuperPower has been very successful in increasing 2G wire I_c using its proprietary Metalorganic Chemical Vapor Deposition (MOCVD) process. Recently, very high I_c samples have been obtained at SuperPower using its continuous reel-to-reel manufacturing equipment. These research-grade samples are approximately 3.5 microns thick, and are deposited in 5 successive passes on SuperPower's IBAD-MgO/LMO templates. Transport measurements showed that these wires possess I_c's in excess of 700 A/cm-width. More importantly, detailed measurements indicated that overall I_c continuous to increase with HTS thickness, thereby suggesting that much higher wire I_c's may be obtained by simply adding more HTS passes. Effort continues to further increase individual layer and overall wire I_c's. The thick film MOCVD process has been evaluated in longer R&D lengths up to approximately 10 m. Critical current values of nearly 600 A/cm in meter lengths and nearly 500 A/cm over 11 m have been achieved.

2) Research-grade MOCVD/IBAD 2G wire from SuperPower exceeds 740 A/cm performance across entire 12 mm sample width.
High 2G wire I_c is necessary for many HTS power applications as well as a lower cost/performance ratio. SuperPower has been very successful in increasing 2G wire I_c using its proprietary Metalorganic Chemical Vapor Deposition (MOCVD) process. Previously, we reported critical currents exceeding 700 A/cm-width in MOCVD films that were approximately 3.5 microns thick, deposited in 5 successive passes on SuperPower's IBAD-MgO/LMO templates. Now, we have developed a new precursor composition that enabled critical currents of 740 A/cm-width (measured across the full 12mm sample width) in a film that was 2.8 micron thick, deposited in 4 passes (Fig. 1). This critical current value corresponds to a J_c level of 2.65 MA/cm^2 which was the

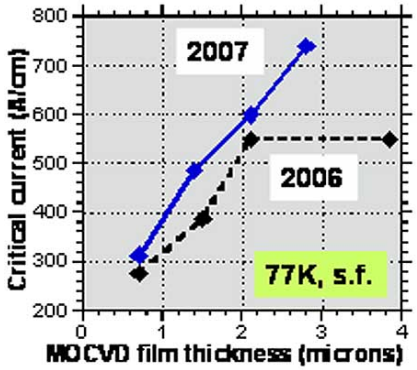

Fig. 1. Critical currents of SuperPower MOCVD films as functions of film thickness (number of passes). I_c 's were measured across entire 12 mm sample width.

level that we used to achieve in 0.7 micron thick films only two years ago. Critical current measurement on this sample at ORNL after patterning showed values in excess of 800 A/cm-width.

3) Record long-length performances achieved by SuperPower at high production rates.
SuperPower has invested significant amount of resources on the optimization and scale-up of its MOCVD-IBAD 2G wire, with particular emphases on wire performance, uniformity length and throughput. As a result, substantial progress has been made with many record long-length performances achieved at high production rates. Among these are a 103-meter length with end-to-end I_c greater than 300 A/cm, a 203-meter length with minimum I_c of 227 A/cm, and a 427-meter length with minimum I_c of 191 A/cm. In January 2007, SuperPower produced a 595-meter 2G wire with minimum I_c of 173 A/cm. This is the longest 2G wire yet manufactured in the world with a record 102,935 A-m performance (Fig. 2). This is the first time that the 100,000 A-m milestone has been surpassed, and is almost hobbled the performance of SuperPower's nearest competitor. Most importantly, these long length wires were manufactured at high rates, the slowest step having a speed of 45 m/h (135 m/h equivalent production rate for 4 mm-width wire). Even at these high production rates, there are no degradations in the performance and the wire uniformity. Another important accomplishment was achievement of tape speeds of 100 m/h or more over 300 m of 12 mm wide wire (equivalent to 300 m/h of 4 mm wide wire) in deposition of buffer layers atop IBAD MgO using all reactive sputtering processes, while maintaining texture values of 6 to 8 degrees.

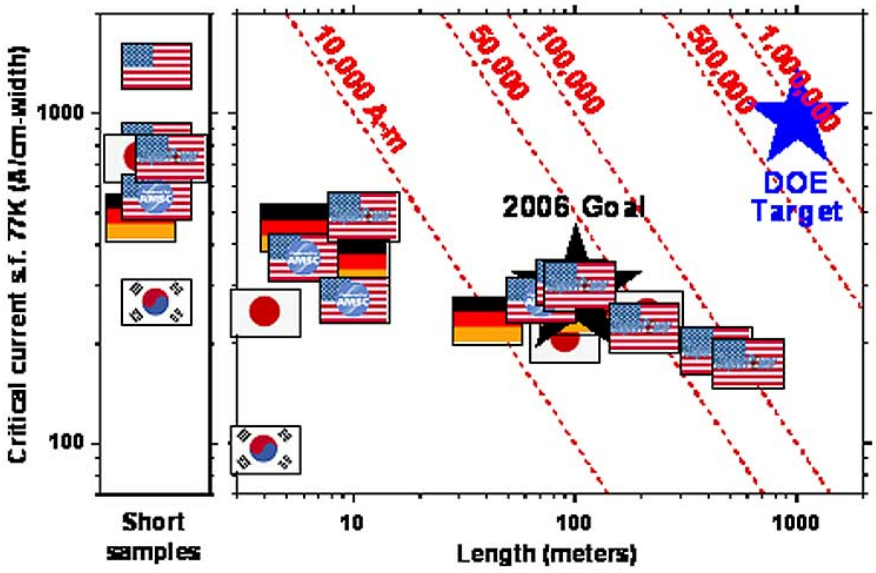

Fig. 2. Worldwide long length performance of 2G wires using technical substrates.

4) Significant enhancements in production rates.
SuperPower has invested significant amount of resources on the optimization and scale-up of its MOCVD-IBAD 2G wire, with particular emphases on wire performance, uniformity, length and throughput. As a result, substantial progress has been made with many record long-length performances achieved at high production rates. We have previously reported several achievements of long-length 2G wire produced at high speeds, the slowest step (MOCVD)

having a speed of 135 m/h of 4 mm-width wire. Now, we have increased the speed of the MOCVD process to 180 m/h of 4 mm wide wire. At the same time, we maintained a high critical current level of 285 A/cm in a 1 micron thick HTS film produced at this high rate. Figure 3 shows the advancements made in the last year in increasing the speed of the MOCVD process. Next, we produced a 130 m long 2G wire with all processes at high speeds (IBAD MgO at 360 m/h, homo-epi MgO at 345 m/h, LMO at 345 m/h, and MOCVD at 180 m/h, all values for 4 mm wide wire). A minimum critical current of 201 A/cm was achieved over 130 m with a 3.5% uniformity in Ic (see Fig. 4). The speeds listed above correspond to annual production capacities of 1400 km/year for the IBAD, homo-epi MgO, and LMO processes and 720 km/year for MOCVD, even assuming that only 45% of time in a year is available for deposition.

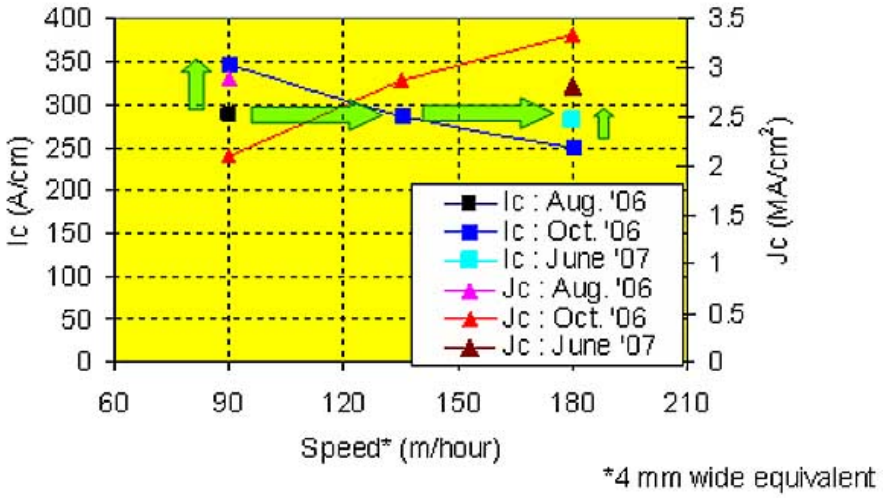

Fig. 3. Increase in production speed of MOCVD process while maintaining high Ic performance

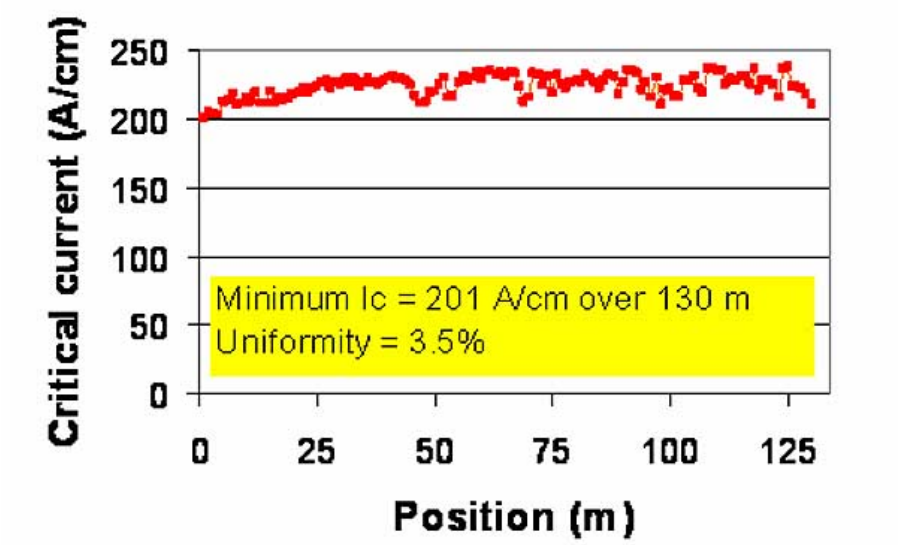

Fig. 4. Uniform high Ic in long length 2G wire produced at high rates.

Table 1: Long-length 2G wire with all processes at high production rates

Process	Month	IBAD MgO	Homo-epi MgO	LMO	MOCVD YBCO
Speed of 4 mm wide tape (m/h)	Oct. '06	360	240	240	135
	June '07	360	345	345	180
Production capacity (km/yr) (if 45% of time/year is available for deposition)		1,440	1,380	1,380	720

5) 2G wire substrate length barrier.

SuperPower has invested significant amount of resources on the optimization and scale-up of its MOCVD-IBAD 2G wire, with particular emphases on wire performance, uniformity, length and throughput. As a result, substantial progress has been made with many record long-length performances achieved at high production rates. Last Quarter, we reported the achievement of high-performance uniform 2G wire that was manufactured using high rates for all the production steps:. The 130 m long 2G wire with all processes at high speeds (IBAD MgO at 360 m/h, homo-epi MgO at 345 m/h, LMO at 345 m/h, and MOCVD at 180 m/h, all values for 4 mm wide wire) has a minimum critical current of 201 A/cm with a 3.5% uniformity in I_c. In this Quarter, we report on the production of fully-buffered IBAD-MgO substrates that exceeded the 1 kilometer 2G substrate length barrier for the first time. Several substrates in excess of 1 kilometer were manufactured. It can be seen from Table 1 and Fig. 5 that these substrates are highly textured, with in-plane texture uniformity as low as 2.1%.This achievement brings us one step closer to kilometer-length 2G wire manufacturing.

Table 2: In-plane texture and uniformity of SuperPower's kilometer-length 2G IBAD-MgO substrates.

Tape	Length (m)	In-plane texture (deg)			Uniformity
		Avg.	Min.	Max	
1	1,001	6.79	6.20	7.84	6.2 %
2	1,343	6.33	5.80	7.16	3.3 %
3	1,346	6.85	6.00	7.35	2.1 %
4	1,372	6.20	5.83	6.68	2.2 %

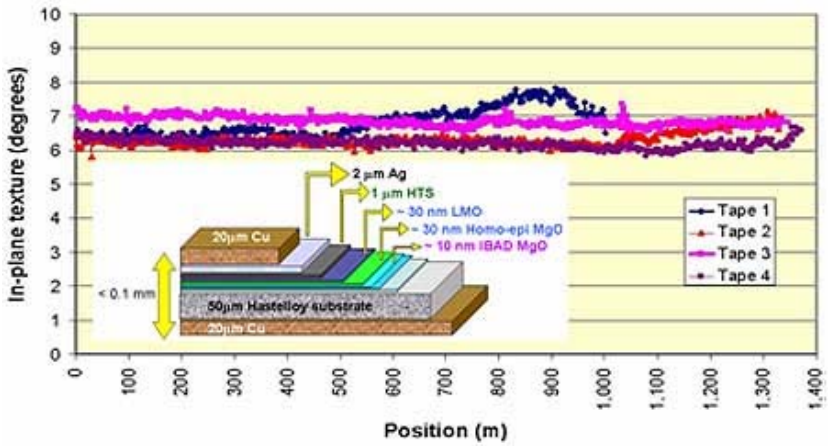

Fig. 5. In-plane texture as a function of length in SuperPower's kilometer-length 2G IBAD-MgO substrates.

Status of milestones:

- Short sample 2G wire with I_c of 750 A/cm. (July 31, 2007): **Met July 2007**.
- Short sample 2G wire with a J_e of 30 kA/cm^2 at 77 K, 1 T (without copper stabilizer) (July 31, 2007): **On going**. *Presently at 20 kA/cm^2 level which exceeded Title III target.*

Subtask 5.3: NIST-Boulder electromechanical studies for superconductor development subcontract.

J.W. Ekin, N. Cheggour, Danko van der Laan (NIST-Boulder)

Objective:

Substantial advances have been achieved in the development and fabrication of 2G wires, particularly in the area of critical current performance. For these wires to be broadly employed in practical applications, however, both the electromechanical responses and the mechanical integrity of 2G wires under operational stresses in cryogenic environment must be determined and understood. In addition, these factors will vary with wire geometry and will therefore influence the conductor design and fabrication. Objective of this project is to perform the electromechanical research needed to develop 2G wires for electric power-grid and high magnetic-field applications. Critical performance feedback will be provided to companies and organizations developing the conductors and demonstration projects.

Highlights:

1) Substantial improvement in 2G wire delamination strength.

HTS/buffer delamination in 2G wires will result in catastrophic failure. This failure mode has been of particular concern in wires that have been slit. We have been collaborating with wire manufacturers to improve the delamination strength under transverse tension. Data feedback is critical to the present wire production scale-up process. Recent results have shown that an improved quality control during 2G wire production significantly raises the delamination strength, even when the conductors are slit. More delamination testing is underway to verify this finding. Also, conductors with new geometries to improve the delamination strength are being prepared by industry and will be tested at NIST once they are received.

HTS/buffer delamination in 2G wires will result in catastrophic failure. This failure mode has been of particular concern in wires that have been slit. We have been collaborating with wire manufacturers to improve the delamination strength under transverse tension. Data feedback is critical to the present wire production scale-up process. The significant increase in delamination strength of slit MOCVD-IBAD YBCO coated conductors that was reported in our 3rd quarterly report has been confirmed. In addition, conductors with a thick YBCO coating, and those with a filamentized YBCO layer for low AC loss, will be tested shortly.

2) Modeling the axial strain effect on critical current

The effect of axial tensile and compressive strain on the critical current of YBCO coated conductors has been studied extensively. We have successfully completed the engineering modeling of the strain effect in self-field of conductors with YBCO layers ranging from 0.8 to 3.0 μm. The effect can be described with a simple expression for both MOD-RABiTS and MOCVD-IBAD coated conductors.

3) Modeling in-plane bending on critical current.

We have been studying the critical current vs. in-plane bending strain in order to obtain engineering design data for power cable bending limits. The database has been extended with results on YBCO coated conductor with thick YBCO layers. We were successful in modeling the

critical current vs. in-plane bending of YBCO coated conductors with a YBCO layer thickness ranging form 0.8 to 3.0 μm. The model uses the axial strain distribution over the width of the YBCO layer and the response of the critical current to axial strain to calculate the critical current when the conductor is bend in-plane.

Technical progress:

1) New electromechanical test configurations for 2G wires.

We converted the experimental setup for the determination of axial compressive and tensile strain effects, as well as in-plane bending effects on 2G wires. The setup has been automated and can be operated without requiring the use of a servo-hydraulic test system. The data is needed by the wire developers to set strain limits for engineering designs. We will use this setup to study new wire configurations, such as conductors with thick YBCO layers and YBCO layers that are striated for low AC loss applications.

2) Commence modeling of "hard" bending on critical current.

We have been studying the critical current vs. hard-bending strain in order to obtain engineering design data for power cable bending limits. The database has been extended with results on YBCO coated conductor with thick YBCO layers. We have begun the modeling of the hard bending effect on critical current, to predict this effect from data obtained from tensile and compressive strain on critical current.

3) Stress-strain characterization of 2G wire joints.

Due to finite wire length, most practical HTS applications will contain solder joints. Failure at these critical nodes will render the device inoperable. Therefore, it is necessary to determine and understand the joint characteristics at room and cryogenic temperatures to avoid failure during winding, field-splicing, installation and operation. We have designed a new experiment to measure both the joint resistivity and the coated-conductor critical-current as a function of stress at 76 K. Various joints, made by ORNL and by NIST using different types of solders, were tested at NIST. We measured differences in joint resistivity between samples before stress is applied. Depending on the joint preparation, a large increase in resistivity is measured at relatively low stress levels. Procedures for joints preparation are needed to ensure that the joint resistivity does not deteriorate with stress. We will extend the testing of coated conductor joints to joints that are prepared by SuperPower and by American Superconductor.

4) Stress-strain characterization of dielectrics.

Dielectrics are needed for electric power applications to prevent high-voltage breakdown under operation. Since the dielectric material is applied directly to the YBCO coated conductor, it has to withstand the axial strain that the conductor experiences during winding and under operation. NIST designed a new setup to measure the stress-strain characteristics of polyvinyl alcohol dielectrics that were produced by ORNL. The results at room temperature show that the overall strength of the dielectrics is largely enhanced when they are filled with nano-particles and that their sensitivity to strain depends on the applied strain rate. We will continue the stress-strain measurements on dielectrics and will modify our experiment to be able to test at cryogenic temperatures.

Status of milestones:

- Complete delamination-strength measurements at 76 K on a total of 30 slit 2G wire samples with new geometries, fabricated by AMSC and SuperPower. (July 31, 2007): **Met July 2007.**
- Complete measurements of critical-current vs. hard-bending strain at 76 K on a total of 6 2G wire samples, fabricated by AMSC and SuperPower. (Sept. 30, 2007): **Met July 2007.**

Interactions:

We maintain substantial interactions with industry and organizations by independent testing of their HTS wires. Results are communicated to the appropriate partners to assist in their development and designing activities.

Subtask 5.4: NIST-Gaithersburg subcontract to investigate HTS phase relationships.
W. Wong-Ng, L.P. Cook, I. Levin (NIST-Gaithersburg)

Objective:

In order to maximize the performance and provide for cost-effective means to fabricate 2G wires, accurate data on the phase equilibria of mixed lanthanide HTS compounds and their behavior as applied to thin films is required. The main objective of this work is to provide critical phase equilibrium data on the single-phase regions of mixed lanthanide HTS phases under conditions that match 2G wire processing. These phases fall in the systems Ba-R-R'-Cu-O, where R and R' are selected lanthanides and Y. The data will enable improvement of the superconducting properties of 2G wires through enhanced flux-pinning, leading to expeditious and cost-effective market entry. Another objective is to determine a parallel set of Ba-R-Cu-O phase diagrams as applied to films. Since phase assemblages in thin films could differ from those predicted by the bulk phase equilibria, availability of phase relations for Ba-R-Cu-O films will be critical for the further development of 2G wires.

Highlights:

- By mixing the smaller lanthanides Y with the larger Sm in the $Ba_{2-x}(Sm_{1+x-y}Y_y)Cu_3O_{6+z}$ superconductor, both flux-pinning and melting properties can be tailored and optimized. Following the determination of the single-phase region of the solid solution $Ba_{2-x}(Sm_{1+x-y}Y_y)Cu_3O_{6+z}$ under various processing conditions so as to provide data for intrinsic flux pinning applications, we have succeeded determining the phase equilibria in the vicinity of the $Ba_{2-x}(Sm_{1+x-y}Y_y)Cu_3O_{6+z}$ phase. We found that this solid solution (in the BaO-poor region) is in equilibrium with CuO, $BaCuO_2$, $(Y,Sm)_2Cu_2O_5$, $(Sm,Y)_2CuO_4$, $Ba(Sm,Y)_2CuO_5$, and $BaCu_2O_2$ under 100 Pa p_{O2} at 810 °C. This information also identifies possible phases for flux pinning application, an important area for coated conductor development.

- Phase relationships of the thin film Ba-Y-Cu-O system and the Ba-(Nd,Eu,Gd)-Cu-O system have been determined under 0.1% O_2 at 735 °C. These films were prepared using the BaF_2 *ex situ* techniques (e-beam evaporation and trifluoroacetate (TFA) approach). Results of high temperature x-ray diffraction indicated different phase relationships in the vicinity the high-temperature superconductor Y213 and Gd213 in films relative to bulk because of the absence of the green phase (BaY_2CuO_5 and $BaGd_2CuO_5$, respectively). Possible reasons for different phase relationships in bulk and thin film materials include strain, texturing, and kinetics that are determined by the substrate, film thickness, and the processing conditions. Using the combinatorial thin film synthesis approach with oxides as targets, we confirmed the difference in phase relationships and established that the presence of 'fluorine' is not the cause for the difference.

- Phase relationships of $Ba_2RCu_3O_{6+x}$ (where R=lanthanides or mixed lanthanides) on films provide guidelines for coated conductor processing. We have used the mixed lanthanide films in the system Ba-(Nd,Eu,Gd)-Cu-O to demonstrate the difference between phase relations in films and in bulk. We have also successfully prepared combinatorial films using

the RABiTS substrate provided by AmSC and used these to construct the $BaCuO_2$-Y_2O_3-CuO diagram for films. We confirmed the absence of the green phase, BaY_2CuO_5, which leads to different phase relations around $Ba_2YCu_3O_{6+x}$ in films.

- A paper concerning the understanding of melting temperature of $Ba_2RCu_3O_7$ (R= Nd, Sm, Gd, Y, and Er) has been submitted. The conventional Debye temperature, customarily estimated using an isotropic approximation, fails to account for the trend of melting temperatures for the $Ba_2RCu_3O_7$ high T_c superconductors, as a function of the ionic radius of R^{3+}, or r(R^{3+}). We overcame this problem by calculating the 'improved' Debye temperatures using the mean sound velocity along the *c*-axis of $Ba_2RCu_3O_7$ that features an anisotropic layered structure.

Technical progress:

1) Phase equilibria of the Ba-Sm-Y-Cu-O system

In addition to completing the single-phase region determination of the solid solution $Ba_{2-x}(Sm_{1+x-y}Y'_y)Cu_3O_{6+z}$ under different processing conditions so as to provide data for intrinsic flux pinning applications, we have succeeded investigating the phase diagram in the BaO-poor region of the complex Ba-Sm-Y-Cu-O system under 100 Pa p_{O2} at 810 °C. Phase relationships surrounding the $Ba_{2-x}(Sm_{1+x-y}Y'_y)Cu_3O_{6+z}$ single phase in the complex multi-component BaO-Sm_2O_3-Y_2O_3-CuO_z system, including solid solution studies of various related phases have been studied in detail. We found that this solid solution (in the BaO-poor region) is in equilibrium with CuO, $BaCuO_2$, $(Y,Sm)_2Cu_2O_5$, $(Sm,Y)_2CuO_4$, $Ba(Sm,Y)_2CuO_5$, and $BaCu_2O_2$.

Currently we are continuing to collaborate with ORNL and AFRL to use selected samples of this $Ba_{2-x}(Sm_{1+x-y}Y_y)Cu_3O_{6+z}$ region with Sm/Y ratio of 0.667/0.333 to correlate with superconducting properties. The targets have been prepared at NIST and have been delivered to AFRL for film deposition on single crystal substrates. Once they have succeeded the deposition process, the targets will be delivered to ORNL for film deposition on RABiTS.

2) Phase Relationships Determination in the Ba-R-Cu-O System

We successfully determined the phase relationships of the Ba-Y-Cu-O, Ba-(Nd,Eu,Gd)-Cu-O, Ba-Nd-Cu-O and Ba-Gd-Cu-O systems in film form. At 735 °C and 100 Pa p_{O2}, high-temperature x-ray diffraction experiments showed that while $BaNd_2CuO_5$ ('brown-phase' structure) can be prepared in film form using the trifluoroacetate (TFA) solution methods on $SrTiO_3$ substrates, $BaGd_2CuO_5$ and $Ba(Nd_{1/3}Eu_{1/3}Gd_{1/3})_2CuO_5$ ('green-phase' structure) cannot. As a result of the absence of the 'green phase' in films, $Ba_2(Nd_{1/3}Eu_{1/3}Gd_{1/3})Cu_3O_{6+x}$ is in equilibrium with the 'brown phase', and a compatibility line is found between $Ba_2GdCu_3O_{6+x}$ and Gd_2O_3 in the BaO-poor region of the Ba-Gd-Cu-O diagram, a configuration different from that of the bulk phase diagram.

We are continuing to advance our understanding of the phase relationships of the thin film Ba-Y-Cu-O system in the vicinity the high-temperature superconductor Y213 using the combinatorial thin film synthesis approach with oxides as targets and RABiTS as the substrate (provided by AmSC). Similar to the films prepared using the "BaF_2" process, we also confirmed the absence of the green phase BaY_2CuO_5. Because of this absence, phase relations around $Ba_2YCu_3O_{6+x}$ are different from the bulk for the combinatorial route as well. Possible reasons for different phase relationships in bulk and thin film materials include strain, texturing, and kinetics

that are determined by the substrate, film thickness, and the processing conditions. We continue to study the cause of the differences with particular focus on the effect of fluorine and other differences in processing conditions.

Status of milestones:

- Complete initial determination of single-phase regions for selected mixed lanthanides (July 31, 2007): **Met July 2007.**
- Complete initial study on processing relationships among phases in selected Ba-R-Cu-O systems as applied to films (Sept. 30, 2007): **Met July 2007.**

Interactions:

We continue to interact with ORNL and AFRL on phase equilibria and property studies of $Ba_{2-x}(R_{1+x-y}R'_y)Cu_3O_{6+z}$; with BNL on modeling of phase transitions and melting of $Ba_2RCu_3O_{6+z}$ phases; with ORNL and AmSC on phase relationships of Ba-Y-Cu-O and Ba-R-Cu-O films. (we have completed a Ba-Y-Cu-O diagram for films on RABiTS provided by AmSC); and with Superpower on the determination of the interaction of $Ba_2YCu_3O_{6+z}/LaMnO_3$, where $LaMnO_3$ is a potential buffer layer.

Subtask 5.5: University of Houston MOD processing and pinning subcontract.
K. Salama (Univ. Houston)
Status of milestones:

- Under negotiation.

Subtask 5.6: Energetics technical support subcontract.
B. Marchionini (Energetics)
Status of milestones:

- Compile and distribute to DOE the results from the Annual Peer Review Meeting: **Met Sept. 2007.**

Subtask 5.7: TMS technical support subcontract.
P. Herz (Technology & Management Services, Inc)
Status of milestones:

- Complete remaining web-design tasks: **Met Feb. 2007.**

Subtask 5.8: Bob Lawrence & Associates outreach subcontract.
Bob Lawrence (Bob Lawrence & Associates)
Status of milestones:

- Publish periodic Superconductivity Update Newsletter for HTS outreach: **Met Sept. 2007.**

Subtask 5.9: Navigant HTS Technology and market Assessment subcontract.
David Walls (Navigant)
Status of milestones:

- Complete initial HTS Market Assessment report. **Met Aug. 2007.**

APPENDIX A

Planned ORNL FY 2007 Foreign Travel:

Name	Destination	Date	Purpose
Isidor Sauers	Vancouver, Canada	Oct. 13 – Oct. 18, 2006	Attend and host 2007 Conference on Electrical Insulation and Dielectric Phenomena (CEIDP).
Parans Paranthaman	Tsukuba, Japan	Nov. 2 - Nov.7, 2006	Attend 20th Int'l Symposium on Superconductivity (ISS07) & visit research centers.
Amit Goyal	Jeju Island, Korea	Nov. 6 – Nov. 12, 2006	Attend Int'l Workshop on Coated Conductors for Applications (CCA07) & visit research centers.

End of FY 2007 ORNL Superconducting Technology Program Annual Report
for the
Office of Electricity Delivery and Energy Reliability